

Copyright  
by  
Divya Thakur  
2009

**Tracking Control for Nanosatellites**

by

**Divya Thakur, B.S.**

**THESIS**

Presented to the Faculty of the Graduate School of  
The University of Texas at Austin  
in Partial Fulfillment  
of the Requirements  
for the Degree of

**MASTER OF SCIENCE IN ENGINEERING**

THE UNIVERSITY OF TEXAS AT AUSTIN

May 2009

## Tracking Control for Nanosatellites

APPROVED BY

SUPERVISING COMMITTEE:

---

Belinda G. Marchand, Supervisor

---

Maruthi R. Akella

## Acknowledgments

I have been extremely fortunate to be surrounded by people who have inspired and supported me throughout my research endeavors. To the person I owe the most gratitude is my advisor, Dr. Belinda G. Marchand, for believing in me and allowing me to freely pursue my research interests. Through her mentoring, she has imparted in me the focus, strength, and motivation to truly succeed in a research environment. I thank her for offering her expertise and wealth of knowledge to guide my research in the right direction, and for her all her patience throughout my academic and research experience.

I would also like to thank Dr. Maruthi R. Akella for the opportunity to learn from one of the leading experts in the controls field. My experiences through learning from Dr. Akella as an undergraduate and graduate student played a pivotal role in shaping my interests in graduate school.

I would like to thank the members of Dr. Marchand's research group (past and present), Chad Smith, Stuart Stanton, and Sara Scarritt for making this a truly gratifying and memorable experience through all its trials and tribulations. I am especially indebted to Stuart Stanton for providing his guidance and expertise through many trying periods of my research and academic endeavors. His remarkable insight into complex problems and challenging questioning have been instrumental in shaping my academic and research outlook.

I would also like to give special thanks to my fellow GNC colleague, Srikant Sukumar, for his endless patience and willingness to lend his ear and immense knowledge and expertise of control systems. To my colleague and friend, Brian Bradford, I thank you for your unconditional support and the inspiration you provide me with everyday. Your steadfast nature has been my anchor through thick and thin. And finally, I would like to thank my parents for their moral support and encouragement throughout my studies. Without them, this would never have been possible.

# Tracking Control for Nanosatellites

Divya Thakur, M.S.E.

The University of Texas at Austin, 2009

Supervisor: Belinda G. Marchand

Often, it is the case that spacecraft mass properties are not completely determined in the course of pre-flight testing. This results in dynamic uncertainty with regard to attitude controller performance as the spacecraft inertia parameters cannot be reliably determined. In this study, several control regimes are analyzed for nanosatellite attitude and angular rate tracking in the presence of arbitrarily large inertia matrix uncertainty. A tracking controller is formulated using partial feedback linearization and Lyapunov's indirect method. In addition, a nonlinear tracking control law based on Lyapunov's direct method is developed. Both control algorithms are robust to small inertia perturbations, but the performance subsequently degrades with large inertia uncertainty. A non-certainty equivalence adaptive controller is presented that maintains consistent performance of the nanosatellite in the face of inertia uncertainty of arbitrary magnitude. The adaptive control delivers precise reference attitude and angular rate tracking and is a far better alternative to non-adaptive controllers that are only mildly robust to inertia uncertainty.

# Table of Contents

<b>Acknowledgments</b>	<b>iv</b>
<b>Abstract</b>	<b>vi</b>
<b>List of Figures</b>	<b>ix</b>
<b>Chapter 1. Introduction</b>	<b>1</b>
1.1 Background . . . . .	3
1.2 Research Motivation . . . . .	7
1.3 Thesis Organization . . . . .	8
<b>Chapter 2. Mathematical Background</b>	<b>10</b>
2.1 Dynamical Model . . . . .	10
2.1.1 Coordinate Reference Frames . . . . .	11
2.1.2 Direction Cosine Matrix . . . . .	13
2.1.3 Euler Parameters . . . . .	15
2.1.4 Euler's Rotational Equations of Motion . . . . .	17
2.2 Tracking Error Dynamics . . . . .	22
2.3 Concepts of Stability . . . . .	29
2.4 Vector Norms and $\mathcal{L}_p$ Spaces . . . . .	35
2.5 Summary . . . . .	37
<b>Chapter 3. Linear Control Theory</b>	<b>38</b>
3.1 Tracking Control . . . . .	38
3.2 Control Design Based on Feedback Linearization . . . . .	40
3.3 Lyapunov's Indirect Method . . . . .	42
3.3.1 Linearization of Autonomous Systems . . . . .	43
3.3.2 Linearization of Non-Autonomous Systems . . . . .	44
3.3.3 Stability Analysis Using Lyapunov's Indirect Method . . . . .	45

3.3.4	Stability of Slowly Time-Varying Systems . . . . .	47
3.4	Control Design Based on Lyapunov's Indirect Method . . . . .	48
3.5	Lyapunov's Direct Method . . . . .	54
3.5.1	Stability Analysis using Lyapunov's Direct Method . . . . .	59
3.5.2	Robustness to Plant Perturbations . . . . .	62
3.6	Control Magnitude Constraints . . . . .	63
3.7	Design Examples . . . . .	67
3.8	Summary . . . . .	77
<b>Chapter 4.</b>	<b>Nonlinear Control Design Based on Lyapunov's Direct Method</b>	<b>79</b>
4.1	Nonlinear Tracking Control Using Filter Variables . . . . .	79
4.2	Control Magnitude Constraints . . . . .	84
4.3	Design Examples . . . . .	84
4.4	Summary . . . . .	91
<b>Chapter 5.</b>	<b>Nonlinear Adaptive Control Design</b>	<b>93</b>
5.1	Introduction to Adaptive Control . . . . .	94
5.1.1	Direct Adaptive Control . . . . .	94
5.1.2	Persistence of Excitation . . . . .	99
5.1.3	Indirect Adaptive Control . . . . .	102
5.1.4	Non-Certainty Equivalence Adaptive Control . . . . .	107
5.2	Non-CE Adaptive Control Design for Spacecraft Tracking . . . . .	108
5.2.1	Stability Analysis . . . . .	113
5.3	Design Examples . . . . .	116
5.4	Summary . . . . .	124
<b>Chapter 6.</b>	<b>Conclusions</b>	<b>126</b>
	<b>Bibliography</b>	<b>128</b>
	<b>Vita</b>	<b>133</b>



## List of Figures

2.1	Orthogonal Base Vectors . . . . .	12
2.2	Body-Fixed Frame . . . . .	14
2.3	Rigid Body Motion . . . . .	18
2.4	Stability in the Sense of Lyapunov . . . . .	32
2.5	Uniform Asymptotic Stability of an Equilibrium . . . . .	34
3.1	Illustration of a Lyapunov Function . . . . .	56
3.2	Direct Implementation of Optimal Saturated Term . . . . .	65
3.3	Saturation Functions Signum and Tanh . . . . .	66
3.4	Nonlinear Tracking Control Law Simulation for a PE Reference Trajectory . . . . .	73
3.5	Nonlinear Tracking Control Law Simulation for a non-PE Reference Trajectory . . . . .	77
4.1	Lyapunov Control Law via Filter Construction: Simulation for a PE Reference Trajectory . . . . .	88
4.2	Lyapunov Control Law via Filter Construction: Simulation for a Non-PE Reference Trajectory . . . . .	91
5.1	A Model Reference Adaptive Control System . . . . .	95
5.2	Simulation of a Model Reference Adaptive Controller with Constant Reference Input . . . . .	101
5.3	Simulation of a Model Reference Adaptive Controller with Sinusoidal Reference Input . . . . .	102
5.4	Indirect Adaptive Control System . . . . .	103
5.5	Non-CE Adaptive Control Law Simulation for a PE Reference Trajectory . . . . .	120
5.6	Non-CE Adaptive Control Law Simulation for a non-PE Reference Trajectory . . . . .	124

# Chapter 1

## Introduction

Traditional satellite design process is entirely focused on a highly customized, mission-driven objective for the satellite bus. The unique design of a satellite bus requires exhaustive testing, verification and redesign. However, such an iterative design procedure is associated with increased costs and lengthy development timelines. For example, the time required from mission conception to launch and on orbit commissioning for a telecommunications satellite typically ranges from 3-6 years<sup>1</sup>. Furthermore, inherent in the design process is the technological risk associated with deploying nonstandard equipment.

Recent interest in minimizing the design to launch time frame for service and tactical satellites motivates an operationally responsive space paradigm. The responsive space approach is to employ small satellites that are cost-effective and can be developed and integrated on a shortened schedule. The small satellites could effectively be launched on-demand, allowing them to carry out immediate diagnostic and service missions for larger disabled satellites or to investigate time-sensitive science phenomena. In addition, a small satellite could serve as a low-cost testbed for new technology demonstration.

Responsive space advocates transformation from a mission-specific satellite design process to a generic plug-n-play (PnP) environment<sup>2</sup> that supports rapid

turnaround times from design to launch readiness. PnP implements a modular approach to satellite bus design and integration using commercial component-ready modular panels. This approach has been widely utilized in industry and has been particularly successful with manufacturers of automobiles and personal computers. Research in PnP design process is being actively funded by industry as well as government agencies such as Air Force Research Laboratories (AFRL) and Air Force Office of Scientific Research (AFOSR). Of particular interest is the University Nanosatellite Program (UNP), a national competition hosted by AFRL that promotes innovative small satellite design that supports responsive space endeavors.

The UNP competition is held at two year cycles, during which participating Universities develop a nanosatellite that is consistent with the stringent mission requirements set forth by the program<sup>3</sup>. A nanosatellite refers to an artificial satellite with mass in the range of 1 kg to 10 kg. The shortened time frame prevents exhaustive dynamic testing of the nanosatellite, which may introduce errors in the system model due to inertia matrix uncertainty or sensor misalignment<sup>4</sup>. Furthermore, actuators such as thrusters and reaction wheels may be subject to constraints on their operating range. For example, actuators operating at their maximum capacity are said to be saturated<sup>5</sup>. Control saturation is an important design consideration for nanosatellites which often employ miniaturized systems with minimal propulsive capability.

The University of Texas at Austin is an active participant in the UNP competition. The University has designed a third generation nanosatellite, Texas 2 Step, to demonstrate autonomous rendezvous and close proximity operations un-

der severe mass, power and budget constraints<sup>3</sup>. The baseline mission is to launch two nanosatellites in a stacked configuration and to perform a scheduled separation. Once the chaser drifts to within 2 – 3 km of the target, it initiates autonomous rendezvous. The chaser nanosatellite is equipped with cold gas thrusters assumed to have full three axis control. If the chaser is required to track the attitude and angular velocity of the target for proximity operations, a sophisticated attitude and angular rate tracking controller is essential in order to provide high precision performance.

The nanosatellite attitude and angular rate tracking control law needs to deliver excellent performance while staying within the control torque limits. Cold gas thrusters typically provide thrusting capability on the order of 1 – 2 N, which may correspond to torque values of 0.2 – 0.5 N · m in each of the three axes. Most importantly, however, the control system must be able to accommodate uncertainties in the plant structure as the shortened design time frame limits dynamical testing prevalent in traditional satellite design.

## 1.1 Background

The attitude control of rigid spacecraft is a widely studied subject, and several stabilizing feedback controllers are available in existing literature<sup>5–7</sup>. Specifically, spacecraft attitude control applications with practical design considerations such as arbitrarily large inertia matrix uncertainty has been the focus of extensive research efforts over the years<sup>4,7–12</sup>. Among these, adaptive control is able to adjust to uncertain parameters using an online identification (estimation) mechanism. Adaptive control is traditionally classified into two categories: indirect adaptive

control and direct or model-reference adaptive control. A more recent approach to designing adaptive controllers is called immersion and invariance (I&I) control<sup>10</sup>.

Wen and Delgado<sup>7</sup> develop several reference attitude and angular velocity tracking control algorithms. These include a model independent control law, a model based tracking controller, and an indirect adaptive tracking controller based on the certainty-equivalence (CE) principle. In CE based adaptive control theory, the controller parameters are computed from plant parameter estimates that are updated periodically and treated as if they were the true plant parameters<sup>13</sup>. In Wen and Delgado<sup>7</sup>, the control formulations are based on both the error quaternion as well as error angular velocity feedback. In contrast to this approach, Costic et al.<sup>8</sup> presents a purely error quaternion-based adaptive tracking control formulation for a rigid spacecraft with inertia uncertainty. The proposed adaptive output feedback control strategy is independent of angular velocity measurements but is still developed in the classical CE-based framework.

A vast majority of existing adaptive attitude-control formulations for stabilizing spacecraft attitude tracking dynamics is based upon the classical CE principle. However, CE based adaptive controllers can suffer from performance degradation if the underlying reference signal does not satisfy certain persistence of excitation conditions<sup>13-15</sup>. Seo and Akella<sup>11,12</sup> introduce a novel noncertainty-equivalence adaptive attitude-tracking control method that overcomes this limitation and delivers superior performance to the classical CE-based adaptive control scheme. The controller in Seo and Akella is based in the immersion and invariance<sup>10</sup> adaptive framework and is able to recover ideal (no parametric uncertainty) system dynamics, a

feature that is not available with CE-based control formulations.

The design of nonlinear control systems that account for control saturation is a subject of extensive research in existing literature. However, theoretical treatment for adaptive spacecraft control in the presence of control saturation limits is fairly limited. Most adaptive control law solutions with saturation consideration are addressed in the model reference adaptive control framework. Břsković et al.<sup>16</sup> considers the design of a globally stable adaptive tracking control algorithm in the presence of control input saturation and parametric uncertainty. The control algorithm in Břsković et al.<sup>16</sup> is based on variable structure control design, which ensures asymptotic convergence of the angular velocity error. In this work, asymptotic convergence of the attitude error is achieved through careful selection of certain design parameters. An approximate sign function is introduced by Břsković et al.<sup>16</sup> to avoid the discontinuous nature of the variable structure approach. However, a theoretical proof that guarantees system stability using the smooth saturation function is not provided. Wallsgrove and Akella<sup>17</sup> address the lack of a rigorous theoretical proof and propose a smooth attitude stabilization control law containing hyperbolic tangent functions that remains within saturation constraints and guarantee convergence of angular velocity error. In the study by Wallsgrove and Akella<sup>17</sup>, asymptotic convergence of the attitude errors is not ensured, although judicious selection of design parameters may increase the likelihood that the attitude error converges to zero.

Robinett et al.<sup>18</sup> developed a feedback control system that remains stable under saturation constraints. The saturation control law is obtained by minimizing a

performance index, which is essentially the first derivative of the Lyapunov function. The control law is shown to be effective in numerical simulations, although the saturation function employed in this formulation has a discontinuous nature near the saturation boundary. In this thesis, a similar Lyapunov optimal control strategy is adopted to account for saturation in the non-adaptive control regimes. However, the discontinuous saturation function proposed in Robinett et al.<sup>18</sup> is replaced by an approximate hyperbolic tangent saturation function that smoothes the transition from saturated to unsaturated behavior.

Káráson and Annaswamy<sup>19</sup> address model reference adaptive control of linear time-invariant plants in the presence of control saturation by modifying the error signal to remove the effects of the control deficiency. However, nonlinear non-autonomous plants are not addressed. In contrast, Tandale et al.<sup>20</sup> presents a heuristic structured adaptive dynamic inversion control subject to control torque limits. The controller formulation proposed in Tandale et al.<sup>20</sup> employs pseudo control hedging to prevent parameter drift by modifying the reference trajectory. However, no mathematical proof is provided to determine whether the spacecraft trajectory converges to the original reference state. Unlike the heuristic approach of Tandale et al.<sup>20</sup>, Leonessa et al.<sup>21</sup> develops a direct adaptive tracking control for multivariable nonlinear systems and provides a mathematical proof that asserts asymptotic stability for the spacecraft. The proposed framework modifies the adaptive control signal to the reference system dynamics to ensure asymptotic stability of error dynamics under actuator amplitude and rate constraints.

## 1.2 Research Motivation

Often, it is the case that spacecraft mass properties are not completely determined in the course of pre-flight testing. This is especially of concern in a plug-and-play satellite environment in which the conception to launch time frame is significantly shorter. Among other things, this results in dynamic uncertainty with regard to attitude controller performance during operation.

In this study, several control regimes are analyzed for nanosatellite attitude and angular rate tracking in the presence of arbitrarily large inertia matrix uncertainty. Specifically, the performance of adaptive and non-adaptive control regimes are examined. Control amplitude constraints are incorporated into the non-adaptive controller formulations using a commonly employed saturation function.

The tracking controllers are designed using the University of Texas student nanosatellite, Texas 2 Step, as the experimental platform. The Texas 2 Step mission is to demonstrate autonomous rendezvous and proximity operations. The spacecraft is assumed to be equipped with cold-gas thruster actuation system that enables full three-axis control. The main objective is to enable the nanosatellite to accurately track a reference trajectory in the presence of arbitrarily large inertia matrix uncertainty. Physical limitations of the actuation system are only addressed by the non-adaptive control systems as adaptive control systems typically assume full control authority.



### 1.3 Thesis Organization

Chapter 2 begins with the rigid body dynamics for a rotating rigid vehicle in space. A thorough description of the attitude kinematics and rotation equations of motion is provided. Then, the error dynamics are developed for a spacecraft that is to track the attitude trajectory of an unactuated (passive) target through controlled maneuvers. The control objective is stated and additional mathematical background regarding dynamic system stability is provided to allow the reader to follow the stability analyses in subsequent chapters.

Chapter 3 provides the basic concepts of tracking control design. A tracking controller that is dependent on the model structure is designed using concepts from feedback linearization and linear control theory. Lyapunov's indirect method and Lyapunov's direct method are introduced for stability analysis. The tracking controller is modified to account for actuator saturation constraints. Numerical simulations are provided to demonstrate the performance of the unsaturated and saturated control design with and without uncertainties in the inertia parameter. The controller is robust to small inertia perturbations but the performance subsequently degrades with large inertia uncertainty.

In Chapter 4, a reference attitude and angular velocity tracking control law based on Lyapunov's direct method is presented. First order stable filters are implemented in aiding the construction of the controller. The resulting control law is dependent on the model structure and delivers high tracking performance while preserving the constraints on torque expenses. The performance subsequently degrades with large uncertainties in the inertia parameters.

Chapter 5 begins with a brief introduction to adaptive control. The two types of classical adaptive control methods, namely direct and indirect adaptive control, are described with examples. The concept of persistence of excitation and its important role in parameter estimation is explained with the aid of numerical simulations. Based on the results of Seo and Akella<sup>11</sup>, a non-certainty equivalence adaptive controller is designed to maintain consistent performance of the nanosatellite with arbitrary uncertainty in its inertia parameters.

## Chapter 2

### Mathematical Background

In this chapter, the dynamical model for the spacecraft tracking problem is developed. Rigid body kinematics are derived using an appropriate set of attitude coordinates to express the orientation of the spacecraft, while Euler's rotational equations of motion are developed starting from the basic concept of rigid body angular momentum. In addition, a brief overview of the mathematical concepts of system stability is provided in order to allow the reader to follow the development of control systems in subsequent chapters.

#### 2.1 Dynamical Model

The dynamical model for the attitude of a rotating rigid body in space describes the evolution of the vehicle orientation and angular velocities. There are many commonly accepted attitude representations to describe the orientation of a rigid body<sup>5,22</sup>. However, some are prone to geometrical and mathematical singularities at certain rotational displacements<sup>5</sup>. Singular representations are unsuitable for onboard spacecraft control systems. An ideal representation is one that allows a full range of motion without limiting the operational limit of the spacecraft control system. For this investigation, Euler parameters are selected to represent the orientation of the body. Euler parameters, also known as quaternions<sup>5</sup>, provide a

nonsingular attitude description and are well suited for spacecraft applications.

The attitude kinematical equations mathematically describe the time evolution of a rigid body’s orientation in space. These equations are independent of the external forces acting on the rigid body. The impact of forces and their imparted moments is addressed in Euler’s rotational equations of motion<sup>5,22</sup>. The rotational equations describe the three degree of freedom rotational motion of a body that may be under the influence of gravitational and other external forces.

### 2.1.1 Coordinate Reference Frames

Three reference frames are necessary for appropriately modeling the dynamics of the spacecraft rendezvous problem: the inertial reference frame,  $\mathcal{N}$ , the commanded reference frame,  $\mathcal{R}$ , and the body-fixed reference frame,  $\mathcal{B}$ . A general right-hand set of three mutually orthogonal unit vectors denoted by  $\{ \hat{i}_1, \hat{i}_2, \hat{i}_3 \}$ , where the  $\hat{\phantom{x}}$  symbol denotes a vector of unit magnitude, can be employed as basis vectors of any coordinate system  $\mathcal{J}$ . Basis vectors<sup>22,23</sup> are linearly independent and any vector  $\mathbf{x}$  associated with that coordinate frame can be expressed as a unique linear combination of  $\hat{i}_1, \hat{i}_2$ , and  $\hat{i}_3$  as

$$\mathbf{x} = x_1\hat{i}_1 + x_2\hat{i}_2 + x_3\hat{i}_3. \quad (2.1)$$

The scalar components are usually collected into a  $3 \times 1$  matrix  $\mathbf{x}$  as

$$\mathbf{x} = \begin{bmatrix} x_1 \\ x_2 \\ x_3 \end{bmatrix}, \quad (2.2)$$

which is also referred to as a “column vector”, or simply a “vector.” Equation (2.2) is the representation of the vector defined in Equation (2.1) with respect to the basis

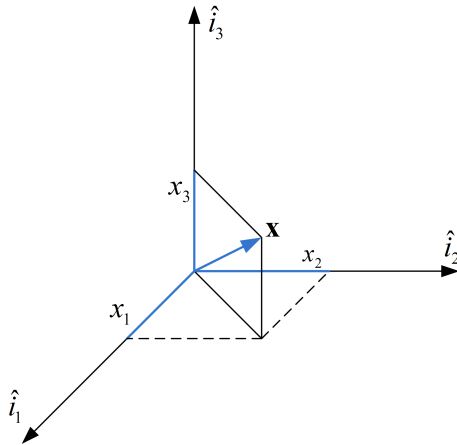


Figure 2.1: Basis of a coordinate system.<sup>22</sup>

vectors  $\{ \hat{i}_1, \hat{i}_2, \hat{i}_3 \}$ .

Equation (2.1) can also be written as a product of two matrices, one containing the scalar components  $x_1$ ,  $x_2$ , and  $x_3$  and the other containing the basis vectors. That is,

$$\mathbf{x} = \begin{bmatrix} x_1 & x_2 & x_3 \end{bmatrix} \begin{bmatrix} \hat{i}_1 \\ \hat{i}_2 \\ \hat{i}_3 \end{bmatrix}, \quad (2.3)$$

where the nonstandard  $3 \times 1$  matrix representation of the basis vector set  $\{\hat{\mathbf{i}}\}$  is sometimes referred to as a *vetrix*<sup>5,22</sup> since its elements are unit vectors rather than scalar quantities.

Using the above approach, each of the reference frames  $\mathcal{N}$ ,  $\mathcal{R}$  and  $\mathcal{B}$  can be uniquely described using a set of three orthogonal unit vectors collected into a  $3 \times 1$  column matrix of vectors. That is,

$$\{\hat{\mathbf{n}}\} \equiv \begin{bmatrix} \hat{n}_1 \\ \hat{n}_2 \\ \hat{n}_3 \end{bmatrix} \quad \{\hat{\mathbf{r}}\} \equiv \begin{bmatrix} \hat{r}_1 \\ \hat{r}_2 \\ \hat{r}_3 \end{bmatrix} \quad \{\hat{\mathbf{b}}\} \equiv \begin{bmatrix} \hat{b}_1 \\ \hat{b}_2 \\ \hat{b}_3 \end{bmatrix}, \quad (2.4)$$

where  $\{\hat{\mathbf{n}}\}$ ,  $\{\hat{\mathbf{r}}\}$  and  $\{\hat{\mathbf{b}}\}$  represent the unit vector triads or basis vectors for the reference frames  $\mathcal{N}$ ,  $\mathcal{R}$  and  $\mathcal{B}$  respectively. For the problem at hand, the inertial reference frame is defined as the Earth-Centered Inertial (ECI) frame. The ECI frame,  $\mathcal{N}$ , originates at the center of the Earth and is inertially fixed in space. The fundamental plane of rotation of the ECI frame is the Earth’s mean equator. The unit vector  $\hat{n}_1$  points in the vernal equinox direction, while  $\hat{n}_3$  is aligned with the mean rotation axis of the Earth. Finally,  $\hat{n}_2$  completes the right-handed triad. The desired attitude is naturally stated in its own reference frame, referred to as the commanded reference frame,  $\mathcal{R}$ . It is described with respect to the ECI frame and may be aligned with the inertial reference frame.

The  $\mathcal{B}$  frame basis vectors are assumed to be aligned with the principal axes of the spacecraft (Figure 2.2). This assumption is consistent with the spacecraft configuration for FASTRAC (Formation Autonomy Spacecraft with Thrust, Relnav, and Crosslink) which is used as a testbed for the proposed control system. The inertia tensor,  $\mathbf{J}$ , that approximates the nanosatellite is given by<sup>3</sup>,

$$\mathbf{J} = \begin{bmatrix} 0.656 & 0 & 0 \\ 0 & 0.656 & 0 \\ 0 & 0 & 0.986 \end{bmatrix} \text{ kg}\cdot\text{m}^2. \quad (2.5)$$

### 2.1.2 Direction Cosine Matrix

The direction cosine matrix (DCM),  $\mathbf{C}$ , is a  $3 \times 3$  proper orthogonal matrix (that is,  $\det(\mathbf{C}) = 1$  and  $\mathbf{C}^{-1} = \mathbf{C}^T$ ) used to map one reference frame to another. For example, the unit vector triad  $\{\hat{\mathbf{b}}\}$  of the body fixed reference frame is mapped

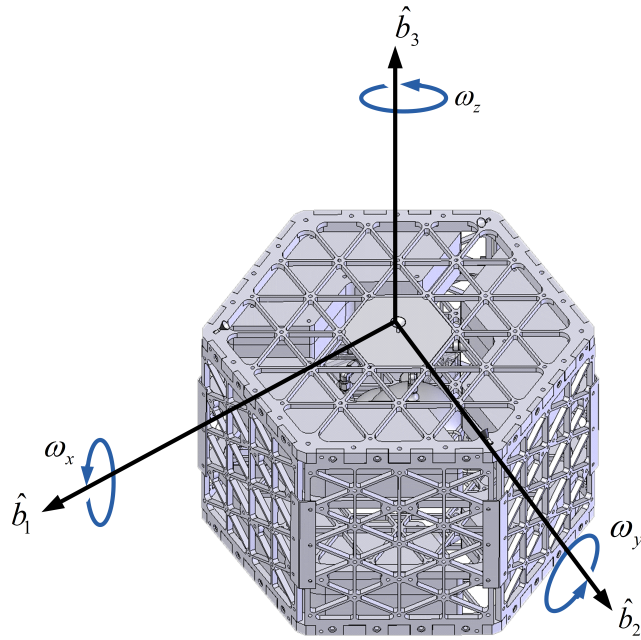


Figure 2.2: Body-fixed frame aligned with the principal axes of the nanosatellite.

from the inertial frame  $\{\hat{\mathbf{n}}\}$  through

$$\{\hat{\mathbf{b}}\} = {}^{\mathcal{B}}\mathbf{C}^{\mathcal{N}}\{\hat{\mathbf{n}}\}. \quad (2.6)$$

Each entry of  ${}^{\mathcal{B}}\mathbf{C}^{\mathcal{N}}$  is obtained through the projection of the set of  $\{\hat{\mathbf{b}}\}$  vectors onto the  $\{\hat{\mathbf{n}}\}$  vectors as

$${}^{\mathcal{B}}\mathbf{C}^{\mathcal{N}}_{ij} = \hat{b}_i \cdot \hat{n}_j, \quad (2.7)$$

where the superscript  $\mathcal{N}$ , on the right hand side of  ${}^{\mathcal{B}}\mathbf{C}^{\mathcal{N}}$ , indicates the current reference frame and the superscript  $\mathcal{B}$ , on the left hand side, indicates the desired or final reference frame achieved through the coordinate transformation.

### 2.1.3 Euler Parameters

The attitude coordinates can also be stated in terms of Euler's principal rotation vector and principal rotation angle. Euler's principal rotation theorem states that the orientation of a rigid body can be arbitrarily changed by performing a single rigid rotation of the body through an angle  $\Phi$  about an axis  $\hat{\mathbf{e}}$  that is fixed to the body and stationary in inertial space<sup>5,7</sup>. The angle  $\Phi$  is known as the principal angle and the axis of rotation,  $\hat{\mathbf{e}}$ , known as the principal axis or Euler axis, is an eigenvector of  $\mathbf{C}$  corresponding to a unit eigenvalue. Thus the matrix  $\mathbf{C}$  satisfies<sup>5</sup>

$$\mathbf{C}\hat{\mathbf{e}} = \hat{\mathbf{e}}, \quad (2.8)$$

where  $\hat{\mathbf{e}} \in \mathbb{R}^3$  is a unit vector, that is,

$$\hat{\mathbf{e}}^T \hat{\mathbf{e}} = 1. \quad (2.9)$$

The Euler axis and rotation angle are non-unique in sign and the sets  $(\hat{\mathbf{e}}, \Phi)$  and  $(-\hat{\mathbf{e}}, -\Phi)$  both represent the same orientation. The principal rotation angle  $\Phi$  captures the shortest rotation about  $\hat{\mathbf{e}}$  and is non-unique since a rotation of  $\Phi - 2\pi$  produces the same orientation. Given the direction cosine matrix  $\mathbf{C} = [C_{ij}]$ , the principal rotation angle,  $\Phi$  is computed from

$$\cos(\Phi) = \frac{1}{2}(C_{11} + C_{22} + C_{33} - 1). \quad (2.10)$$

The principal axis,  $\hat{\mathbf{e}}$ , is given by

$$\hat{\mathbf{e}} = \begin{bmatrix} e_1 \\ e_2 \\ e_3 \end{bmatrix} = \frac{1}{2 \sin \Phi} \begin{bmatrix} C_{23} - C_{32} \\ C_{31} - C_{13} \\ C_{12} - C_{21} \end{bmatrix}. \quad (2.11)$$



Note that, for a zero angle rotation ( $\Phi = 0$ ), a mathematical singularity exists in Equation (2.11). Therefore, the principal rotation vector is not suitable for small angle rotations or when the reference state is inertially fixed of zero rotation since the control application would require working close to the singular attitude of  $\Phi = 0$ .

In order to globally represent the attitude coordinates of the spacecraft without singularities, the minimal four Euler parameter (or the unit quaternion) representation is sought. The Euler parameter vector  $\mathbf{q}(t) \in \mathbb{R}^4$  is defined in terms of the Euler rotation angle,  $\Phi$ , and principal axis,  $\hat{\mathbf{e}}$ , and is written as

$$\mathbf{q} = \begin{bmatrix} q_0 \\ \mathbf{q}_v \end{bmatrix} = \begin{bmatrix} \cos(\frac{\Phi}{2}) \\ \hat{\mathbf{e}} \sin(\frac{\Phi}{2}) \end{bmatrix}. \quad (2.12)$$

From Equation (2.9) it follows that  $\mathbf{q}$  must satisfy the unit norm constraint,

$$q_0^2 + \mathbf{q}_v^T \mathbf{q}_v = 1. \quad (2.13)$$

The unit norm constraint states that all possible rotational motions of a rigid body must correspond to a trajectory on the surface of a four-dimensional unit sphere. Although the unit quaternion is globally non-singular, it is non-unique and given a certain attitude,  $-\mathbf{q}$  and  $\mathbf{q}$  represent the same orientation. The sign ambiguity stems from the non-uniqueness of the principal rotation elements themselves, and is easily resolved by choosing a sign on the initial conditions of the quaternion trajectory and remaining consistent throughout the associated quaternion propagation. The Euler parameter kinematic differential equation may be expressed in the form

$$\dot{\mathbf{q}} = \frac{1}{2} \mathbf{E}(\mathbf{q}) \boldsymbol{\omega}, \quad (2.14)$$

where the  $4 \times 3$  matrix  $\mathbf{E}(\mathbf{q})$  is defined as

$$\mathbf{E}(\mathbf{q}) = \begin{bmatrix} -\mathbf{q}_v^T \\ q_0 \mathbf{I} + [\mathbf{q}_v \times] \end{bmatrix}. \quad (2.15)$$

In Equation (2.15),  $\mathbf{I}$  is the  $3 \times 3$  identity matrix. Note that Equation (2.14) may equivalently be expressed as

$$\begin{aligned} \dot{q}_0 &= -\frac{1}{2} \mathbf{q}_v^T \boldsymbol{\omega}, \\ \dot{\mathbf{q}}_v &= \frac{1}{2} q_0 \mathbf{I} + [\mathbf{q}_v \times]. \end{aligned}$$

The direction cosine matrix,  ${}^{\mathcal{B}}\mathbf{C}^{\mathcal{N}}(\mathbf{q})$ , can be parameterized in terms of the quaternion  $\mathbf{q}^{5,24}$ , that is,

$${}^{\mathcal{B}}\mathbf{C}^{\mathcal{N}}(\mathbf{q}) = (q_0^2 - \mathbf{q}_v^T \mathbf{q}_v) \mathbf{I} + 2 \mathbf{q}_v \mathbf{q}_v^T - 2 [\mathbf{q}_v \times]. \quad (2.16)$$

where  $[\mathbf{q}_v \times]$  is the matrix representation of the linear cross-product operation  $\mathbf{q}_v \times$  and is given by the skew-symmetric vector-cross product matrix operator<sup>7</sup>

$$[\mathbf{q}_v \times] = \begin{bmatrix} 0 & -q_{v3} & q_{v2} \\ q_{v3} & 0 & -q_{v1} \\ -q_{v2} & q_{v1} & 0 \end{bmatrix}. \quad (2.17)$$

Furthermore, the quaternion kinematic differential equation of Equation (2.14) can be stated in terms of the direction cosine matrix,  ${}^{\mathcal{B}}\mathbf{C}^{\mathcal{N}}(\mathbf{q})$ , as<sup>5</sup>

$$\frac{d}{dt} {}^{\mathcal{B}}\mathbf{C}^{\mathcal{N}}(\mathbf{q}) = -\boldsymbol{\omega} \times {}^{\mathcal{B}}\mathbf{C}^{\mathcal{N}}(\mathbf{q}). \quad (2.18)$$

#### 2.1.4 Euler's Rotational Equations of Motion

Consider the rigid body to be a system of particles  $p_i$  of mass  $m_i$ , as illustrated in Figure 2.3. The vector  $\mathbf{R}_i$  represents the position of  $p_i$  relative to the

inertial origin  $O$ . Now consider the frame  $\mathcal{B}$  originating at the center of mass,  $C$ , of the rigid body. The rigid body, and hence the frame  $\mathcal{B}$ , rotates relative to  $\mathcal{N}$  with some angular velocity  $\boldsymbol{\omega}$ . The vector  $\mathbf{R}_c$  denotes the position vector of  $C$  relative

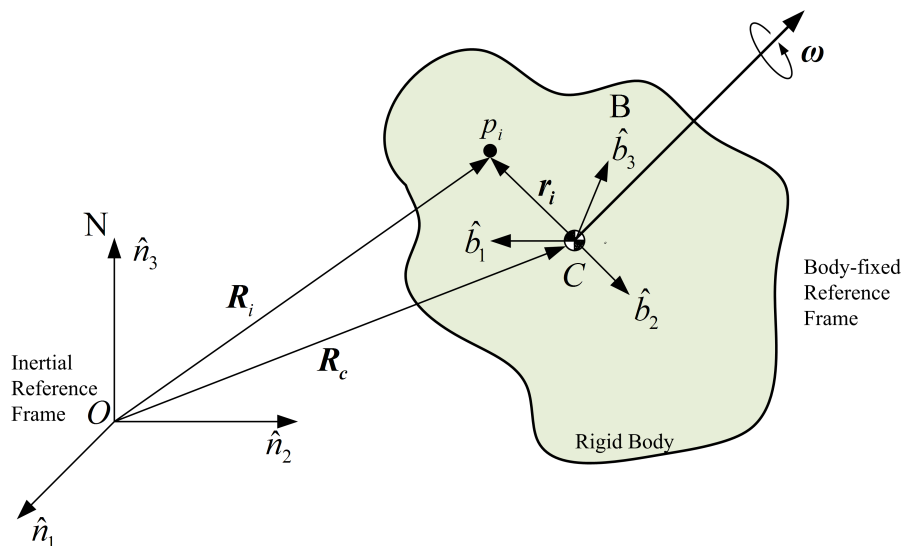


Figure 2.3: Rigid body motion relative to a body-fixed reference frame  $\mathcal{B}$  originating at the center of mass.<sup>22</sup>

to  $O$ . Let  $\mathbf{r}_i$  denote the position vector of  $p_i$  relative to  $C$ . The position of  $p_i$  may subsequently be expressed as

$$\mathbf{R}_i = \mathbf{R}_c + \mathbf{r}_i. \quad (2.19)$$

The vector  $\mathbf{r}_i$ , expressed in terms of  $\mathcal{B}$  frame coordinates, is given by

$$\mathbf{r}_i = x_i \hat{b}_1 + y_i \hat{b}_2 + z_i \hat{b}_3. \quad (2.20)$$

The inertial velocity of  $p_i$  is thus determined as

$${}^{\mathcal{N}} \frac{d}{dt} \mathbf{R}_i = {}^{\mathcal{N}} \frac{d}{dt} \mathbf{R}_c + \frac{d}{dt} \mathbf{r}_i, \quad (2.21)$$

where the superscript  $\mathcal{N}$  indicates an inertial derivative. The kinematic transport theorem implies that

$${}^{\mathcal{N}}\dot{\mathbf{R}}_i = {}^{\mathcal{N}}\dot{\mathbf{R}}_c + \frac{{}^{\mathcal{B}}d}{dt}\mathbf{r}_i + \boldsymbol{\omega} \times \mathbf{r}_i. \quad (2.22)$$

The second term in the above expression vanishes since the body in Figure 2.3 is a rigid vehicle. Thus, the velocity of  $p_i$  relative to  $\mathcal{N}$  is

$$\dot{\mathbf{R}}_i = \dot{\mathbf{R}}_c + \boldsymbol{\omega} \times \mathbf{r}_i. \quad (2.23)$$

The total angular momentum of the rigid body about  $C$  is expressed as

$$\mathbf{H}_C = \sum_i \mathbf{r}_i \times m_i \frac{{}^{\mathcal{N}}d}{dt}\mathbf{R}_i, \quad (2.24)$$

which combined with Equation (2.23) can be expanded to

$$\mathbf{H}_C = \sum_i \mathbf{r}_i \times m_i \left( \dot{\mathbf{R}}_c + \boldsymbol{\omega} \times \mathbf{r}_i \right). \quad (2.25)$$

Equation (2.25) can be further rearranged to obtain

$$\mathbf{H}_C = \sum_i m_i \mathbf{r}_i \times \dot{\mathbf{R}}_c + \sum_i \mathbf{r}_i \times m_i (\boldsymbol{\omega} \times \mathbf{r}_i). \quad (2.26)$$

Since  $\mathbf{r}_i$  is measured from  $C$ , it follows that  $\sum_i m_i \mathbf{r}_i = 0$  by the very definition of the center of mass. Therefore, the total angular momentum of the rigid body about its center of mass is

$$\mathbf{H}_C = \sum_i \mathbf{r}_i \times m_i (\boldsymbol{\omega} \times \mathbf{r}_i). \quad (2.27)$$

If the particles are infinitesimally close to each other,  $m_i \rightarrow dm = \rho dV$  where  $dm$  denotes the differential mass,  $\rho$  is the material density, and  $dV$  is the differential

volume. Equation (2.27) can now be expressed in terms of infinitesimal small mass elements as

$$\mathbf{H}_C = \int_V \rho \mathbf{r}_i \times (\boldsymbol{\omega} \times \mathbf{r}_i) dV, \quad (2.28)$$

where the subscript  $V$  denotes a volume integral. The vector  $\boldsymbol{\omega}$  is expressed in terms of its components in the  $\mathcal{B}$  frame as

$$\boldsymbol{\omega} = \omega_x \hat{b}_1 + \omega_y \hat{b}_2 + \omega_z \hat{b}_3. \quad (2.29)$$

Upon substituting the above expression and Equation (2.20) into the integrand of Equation (2.28) and evaluating the vector cross products, the angular momentum is expressed component-wise as

$$\mathbf{H}_{Cx} = J_{xx}\omega_x - J_{xy}\omega_y - J_{xz}\omega_z, \quad (2.30a)$$

$$\mathbf{H}_{Cy} = -J_{xy}\omega_x + J_{yy}\omega_y - J_{yz}\omega_z, \quad (2.30b)$$

$$\mathbf{H}_{Cz} = -J_{zx}\omega_x - J_{yz}\omega_y + J_{zz}\omega_z, \quad (2.30c)$$

where the coefficients  $J_{xx}$ ,  $J_{yy}$ , and  $J_{zz}$  are the *principal moments of inertia* given by,

$$J_{xx} = \int_V \rho(y_i^2 + z_i^2) dV, \quad J_{yy} = \int_V \rho(x_i^2 + z_i^2) dV, \quad J_{zz} = \int_V \rho(x_i^2 + y_i^2) dV,$$

while the coefficients

$$J_{xy} = J_{yx} = - \int_V \rho(x_i y_i) dV, \quad J_{xz} = J_{zx} = - \int_V \rho(x_i z_i) dV,$$

$$J_{yz} = J_{zy} = - \int_V \rho(y_i z_i) dV,$$

are the *products of inertia* of the body about the  $\hat{b}_1$ ,  $\hat{b}_2$  and  $\hat{b}_3$  axes. Equations (2.30a-2.30c) can be written in matrix form as

$$\mathbf{H}_C = \mathbf{J}\boldsymbol{\omega}, \quad (2.31)$$

where

$$\mathbf{J} = \begin{bmatrix} J_{xx} & J_{xy} & J_{xz} \\ J_{xy} & J_{yy} & J_{yz} \\ J_{xz} & J_{zy} & J_{zz} \end{bmatrix} \quad (2.32)$$

is the positive definite mass-moment of inertia matrix of the rigid body. For a rigid body, the sum of the external moments about the center of mass of the body equals the rate of change of the total angular momentum of the body relative to its center of mass. That is,

$$\sum \mathbf{M}_C = \frac{d\mathbf{H}_C}{dt}. \quad (2.33)$$

Since, in this study, the only external moment acting on the spacecraft is the control input,  $\mathbf{u}(t)$ , Equation (2.33) can be expressed as

$$\frac{d\mathbf{H}_C}{dt} = \mathbf{u}. \quad (2.34)$$

Through the kinematic transport theorem, the inertial derivative of the body angular momentum vector is

$$\frac{d\mathbf{H}_C}{dt} = \dot{H}_x \hat{b}_1 + \dot{H}_y \hat{b}_2 + \dot{H}_z \hat{b}_3 + \boldsymbol{\omega} \times \mathbf{H}. \quad (2.35)$$

Thus, Equation (2.34) can be written as

$$\mathbf{u} = \frac{d\mathbf{H}_C}{dt} + \boldsymbol{\omega} \times \mathbf{H}_C, \quad (2.36)$$

where the superscript  $\mathcal{B}$  indicates the vector rate of change of  $\mathbf{H}_C$  as seen by an observer in the body-fixed reference frame. This term can be expanded by substituting

Equation (2.31) and carrying out the derivative,

$${}^{\mathcal{B}}\frac{d}{dt}(\mathbf{H}_c) = \frac{{}^{\mathcal{B}}d}{dt}(\mathbf{J})\boldsymbol{\omega} + \mathbf{J} \frac{{}^{\mathcal{B}}d}{dt}(\boldsymbol{\omega}). \quad (2.37)$$

The first term in Equation (2.37) vanishes if  $\mathbf{J}$  is constant. In addition, it is straightforward to show that

$$\dot{\boldsymbol{\omega}} = \frac{{}^{\mathcal{N}}d}{dt}(\boldsymbol{\omega}) = \frac{{}^{\mathcal{B}}d}{dt}(\boldsymbol{\omega}). \quad (2.38)$$

Under these conditions, substituting Equation (2.37) and Equation (2.38) into Equation (2.36) yields

$$\mathbf{u} = \mathbf{J}\dot{\boldsymbol{\omega}} + \boldsymbol{\omega} \times \mathbf{J}\boldsymbol{\omega}, \quad (2.39)$$

or, as more commonly stated

$$\mathbf{J}\dot{\boldsymbol{\omega}} = -\boldsymbol{\omega} \times \mathbf{J}\boldsymbol{\omega} + \mathbf{u}. \quad (2.40)$$

The above equation is the vector form of Euler's rotational equation of motion.

## 2.2 Tracking Error Dynamics

Consider a spacecraft that is to track the attitude trajectory of a passive target through controlled maneuvers. The spacecraft is required to converge on to the target's quaternion attitude description as well as its angular rotation rates within a specified time period and maintain the convergence for all time thereafter. A control law that satisfies this convergence specification needs constant measured updates for the current attitude of the spacecraft and the desired attitude where the spacecraft should be. The control law aims to drive the attitude and angular velocity tracking errors to zero by adjusting the control effort based on measured updates or estimates of the state.

In order to drive the tracking error to zero, the control law needs a complete dynamical description of the error states. It is assumed that the desired or commanded attitude trajectory of the spacecraft is prescribed in the commanded reference frame. Thus, the desired angular velocity,  $\boldsymbol{\omega}_r$  is specified in the reference frame  $\mathcal{R}$  and  $\mathbf{q}_r$  denotes the orientation of  $\mathcal{R}$  with respect to  $\mathcal{N}$ .

The DCM mapping from unit quaternion to proper orthogonal matrix space is given as follows

$$\mathcal{N} \xrightarrow{\mathbf{q}} \mathcal{B} \Rightarrow \{\hat{b}\} = {}^{\mathcal{B}}\mathbf{C}^{\mathcal{N}}(\mathbf{q})\{\hat{n}\}, \quad (2.41)$$

$$\mathcal{N} \xrightarrow{\mathbf{q}_r} \mathcal{R} \Rightarrow \{\hat{r}\} = {}^{\mathcal{R}}\mathbf{C}^{\mathcal{N}}(\mathbf{q}_r)\{\hat{n}\}. \quad (2.42)$$

In the above equations, the symbol above the arrow denotes the quaternion that parametrizes the DCM to achieve the transformation from the reference frame on the left to the reference frame on the right of the arrow. Thus,  $\mathcal{N} \xrightarrow{\mathbf{q}} \mathcal{B}$  indicates that the transformation from  $\mathcal{N}$  to  $\mathcal{B}$  is achieved by projecting the set of  $\{\hat{n}\}$  vectors onto  $\{\hat{b}\}$  through the DCM  ${}^{\mathcal{B}}\mathbf{C}^{\mathcal{N}}(\mathbf{q})$ . The DCM  ${}^{\mathcal{B}}\mathbf{C}^{\mathcal{N}}(\mathbf{q})$  is in turn parameterized in terms of the quaternion vector  $\mathbf{q}$  that describes the attitude of the rigid body relative to the inertial reference frame,  $\mathcal{N}$ . Using this definition for the DCM mapping, the rotation given by  $\mathcal{R} \rightarrow \mathcal{B}$  is obtained by combining the corresponding rotation matrices,  ${}^{\mathcal{B}}\mathbf{C}^{\mathcal{N}}(\mathbf{q})$  and  ${}^{\mathcal{R}}\mathbf{C}^{\mathcal{N}}(\mathbf{q}_r)$ , through matrix multiplication as follows

$$\{\hat{b}\} = \underbrace{{}^{\mathcal{B}}\mathbf{C}^{\mathcal{N}}(\mathbf{q}) \left( {}^{\mathcal{R}}\mathbf{C}^{\mathcal{N}}(\mathbf{q}_r) \right)^T}_{{}^{\mathcal{B}}\mathbf{C}^{\mathcal{R}}(\mathbf{q}_e)} \{\hat{r}\}. \quad (2.43)$$

The combined rotations can be condensed into a single rotation matrix,  ${}^{\mathcal{B}}\mathbf{C}^{\mathcal{R}}(\mathbf{q}_e)$ , where  $\mathbf{q}_e$  denotes the error between the actual quaternion ( $\mathcal{N} \xrightarrow{\mathbf{q}} \mathcal{B}$ ) and desired



quaternion ( $\mathcal{N} \xrightarrow{\mathbf{q}_r} \mathcal{R}$ ) states. The result may be summarized as

$$\mathcal{R} \xrightarrow{\mathbf{q}_e} \mathcal{B} \Rightarrow \{\hat{b}\} = {}^{\mathcal{B}}\mathbf{C}^{\mathcal{R}}(\mathbf{q}_e)\{\hat{r}\}. \quad (2.44)$$

The attitude error quaternion is extracted from the rotation matrix,  ${}^{\mathcal{B}}\mathbf{C}^{\mathcal{R}}(\mathbf{q}_e)$ , using the following inverse transformation relations<sup>5,24</sup>

$$q_{e_0} = \pm \frac{1}{2} \sqrt{C_{11} + C_{22} + C_{33} + 1}, \quad (2.45a)$$

$$q_{e_1} = \frac{C_{23} - C_{32}}{4q_{e_0}}, \quad (2.45b)$$

$$q_{e_2} = \frac{C_{31} - C_{13}}{4q_{e_0}}, \quad (2.45c)$$

$$q_{e_3} = \frac{C_{12} - C_{21}}{4q_{e_0}}, \quad (2.45d)$$

where  $\mathbf{C}(\mathbf{q}_e) \equiv [C_{ij}]$  is the direction cosine matrix associated with  $\mathbf{q}_e$ . In Equation (2.45a), it is clear that a mathematical singularity exists whenever  $q_{e_0} \rightarrow 0$ , a configuration that describes any principal rotation angle error of  $180 \text{ deg}$ <sup>5</sup>. In order to avoid the computational inaccuracies engendered by this mathematical singularity, a computationally robust algorithm developed by Stanley<sup>5,25</sup> is used instead. The four squared quaternion elements are first computed as

$$q_{e_0}^2 = \frac{1}{4} (1 + \text{trace} [\mathbf{C}]), \quad (2.46a)$$

$$q_{e_1}^2 = \frac{1}{4} (1 + 2C_{11} - \text{trace} [\mathbf{C}]), \quad (2.46b)$$

$$q_{e_2}^2 = \frac{1}{4} (1 + 2C_{22} - \text{trace} [\mathbf{C}]), \quad (2.46c)$$

$$q_{e_3}^2 = \frac{1}{4} (1 + 2C_{33} - \text{trace} [\mathbf{C}]), \quad (2.46d)$$

where  $\text{trace} [\mathbf{C}] = C_{11} + C_{22} + C_{33}$ . The quaternion element  $q_{e_i}$  with the largest magnitude is selected, and the remaining quaternion elements  $q_{e_j}$  are obtained by

coupling the selected  $q_{e_i}$  element with the appropriate three of the following six relations<sup>5</sup>:

$$4q_{e_0}q_{e_1} = (C_{23} - C_{32}), \quad (2.47a)$$

$$4q_{e_0}q_{e_2} = (C_{31} - C_{13}), \quad (2.47b)$$

$$4q_{e_0}q_{e_3} = (C_{12} - C_{21}), \quad (2.47c)$$

$$4q_{e_2}q_{e_3} = (C_{23} + C_{32}), \quad (2.47d)$$

$$4q_{e_3}q_{e_1} = (C_{31} + C_{13}), \quad (2.47e)$$

$$4q_{e_1}q_{e_2} = (C_{12} + C_{21}). \quad (2.47f)$$

The error quaternion,  $\mathbf{q}_e$ , is also stated as a quaternion multiplicative error denoted by

$$\mathbf{q} = \mathbf{q}_r \otimes \mathbf{q}_e, \quad (2.48)$$

or equivalently as,

$$\mathbf{q}_e = \mathbf{q}_r^{-1} \otimes \mathbf{q}, \quad (2.49)$$

where the symbol  $\otimes$  denotes quaternion multiplication. Using the rules of quaternion multiplication<sup>24</sup>, it can be shown that

$$\mathbf{q}_e = \begin{bmatrix} q_{0r} & -q_{1r} & -q_{2r} & -q_{3r} \\ q_{1r} & q_{0r} & q_{3r} & -q_{2r} \\ q_{2r} & -q_{3r} & q_{0r} & q_{1r} \\ q_{3r} & q_{2r} & -q_{1r} & q_{0r} \end{bmatrix} \begin{bmatrix} q_0 \\ q_1 \\ q_2 \\ q_3 \end{bmatrix}, \quad (2.50)$$

or by transmutation,

$$\mathbf{q}_e = \begin{bmatrix} q_0 & -q_1 & -q_2 & -q_3 \\ q_1 & q_0 & q_3 & -q_2 \\ q_2 & -q_3 & q_0 & q_1 \\ q_3 & q_2 & -q_1 & q_0 \end{bmatrix} \begin{bmatrix} q_{0r} \\ q_{1r} \\ q_{2r} \\ q_{3r} \end{bmatrix}. \quad (2.51)$$

Notice in both Equation (2.50) and Equation (2.51), the  $4 \times 4$  matrices are each orthogonal<sup>24</sup>.

Now consider the angular velocity tracking error,

$$\boldsymbol{\omega}_e(t) = \boldsymbol{\omega}(t) - {}^{\mathcal{B}}\mathbf{C}^{\mathcal{R}}(\mathbf{q}_e)\boldsymbol{\omega}_r(t). \quad (2.52)$$

In order to obtain the tracking error dynamics, the time derivative of Equation (2.43) is taken as shown below

$$\begin{aligned} \frac{d}{dt} {}^{\mathcal{B}}\mathbf{C}^{\mathcal{R}}(\mathbf{q}_e) &= \left[ \frac{d}{dt} {}^{\mathcal{B}}\mathbf{C}^{\mathcal{N}}(\mathbf{q}) \right] \left[ {}^{\mathcal{R}}\mathbf{C}^{\mathcal{N}}(\mathbf{q}_r) \right]^T + {}^{\mathcal{B}}\mathbf{C}^{\mathcal{N}}(\mathbf{q}) \left[ \frac{d}{dt} \left[ {}^{\mathcal{R}}\mathbf{C}^{\mathcal{N}}(\mathbf{q}_r) \right]^T \right], \\ &= -\boldsymbol{\omega} \times {}^{\mathcal{B}}\mathbf{C}^{\mathcal{N}}(\mathbf{q}) \left[ {}^{\mathcal{R}}\mathbf{C}^{\mathcal{N}}(\mathbf{q}_r) \right]^T - {}^{\mathcal{B}}\mathbf{C}^{\mathcal{N}}(\mathbf{q}) \left[ {}^{\mathcal{R}}\mathbf{C}^{\mathcal{N}}(\mathbf{q}_r) \right]^T [\boldsymbol{\omega}_r \times]^T. \end{aligned} \quad (2.53)$$

Since  $[\boldsymbol{\omega}_r \times]$  is a skew symmetric matrix, it follows that  $[\boldsymbol{\omega}_r \times]^T = -[\boldsymbol{\omega}_r \times]$ . Thus, the equation above is further reduced as follows

$$\begin{aligned} \frac{d}{dt} {}^{\mathcal{B}}\mathbf{C}^{\mathcal{R}}(\mathbf{q}_e) &= -\boldsymbol{\omega} \times {}^{\mathcal{B}}\mathbf{C}^{\mathcal{N}}(\mathbf{q}) \left[ {}^{\mathcal{R}}\mathbf{C}^{\mathcal{N}}(\mathbf{q}_r) \right]^T + {}^{\mathcal{B}}\mathbf{C}^{\mathcal{N}}(\mathbf{q}) \left[ {}^{\mathcal{R}}\mathbf{C}^{\mathcal{N}}(\mathbf{q}_r) \right]^T [\boldsymbol{\omega}_r \times], \\ &= -\boldsymbol{\omega} \times {}^{\mathcal{B}}\mathbf{C}^{\mathcal{R}}(\mathbf{q}_e) + {}^{\mathcal{B}}\mathbf{C}^{\mathcal{R}}(\mathbf{q}_e)[\boldsymbol{\omega}_r \times]. \end{aligned} \quad (2.54)$$

It is recognized that the expression  ${}^{\mathcal{B}}\mathbf{C}^{\mathcal{R}}(\mathbf{q}_e)[\boldsymbol{\omega}_r \times]$  consists of a cross product operation under a three dimensional rigid body rotation<sup>12</sup>. Thus, for any vector  $\mathbf{a} \in \mathbb{R}^3$  we may express the vector cross product as follows

$$\begin{aligned} {}^{\mathcal{B}}\mathbf{C}^{\mathcal{R}}(\mathbf{q}_e)[\boldsymbol{\omega}_r \times]\mathbf{a} &= {}^{\mathcal{B}}\mathbf{C}^{\mathcal{R}}(\mathbf{q}_e)(\boldsymbol{\omega}_r \times \mathbf{a}), \\ &= {}^{\mathcal{B}}\mathbf{C}^{\mathcal{R}}(\mathbf{q}_e)\boldsymbol{\omega}_r \times {}^{\mathcal{B}}\mathbf{C}^{\mathcal{R}}(\mathbf{q}_e)\mathbf{a}. \end{aligned}$$

This identity is used to simplify the expression for  $\frac{d}{dt} [{}^{\mathcal{B}}\mathbf{C}^{\mathcal{R}}(\mathbf{q}_e)]$  in Equation (2.54)

as follows

$$\begin{aligned}
\frac{d}{dt} \left[ {}^{\mathcal{B}}\mathbf{C}^{\mathcal{R}}(\mathbf{q}_e) \right] &= -\boldsymbol{\omega} \times {}^{\mathcal{B}}\mathbf{C}^{\mathcal{R}}(\mathbf{q}_e) + {}^{\mathcal{B}}\mathbf{C}^{\mathcal{R}}(\mathbf{q}_e) [\boldsymbol{\omega}_r \times], \\
&= -\boldsymbol{\omega} \times {}^{\mathcal{B}}\mathbf{C}^{\mathcal{R}}(\mathbf{q}_e) + {}^{\mathcal{B}}\mathbf{C}^{\mathcal{R}}(\mathbf{q}_e) \boldsymbol{\omega}_r \times {}^{\mathcal{B}}\mathbf{C}^{\mathcal{R}}(\mathbf{q}_e), \\
&= - \left[ \boldsymbol{\omega} - {}^{\mathcal{B}}\mathbf{C}^{\mathcal{R}}(\mathbf{q}_e) \boldsymbol{\omega}_r \right] \times {}^{\mathcal{B}}\mathbf{C}^{\mathcal{R}}(\mathbf{q}_e), \\
&= -\boldsymbol{\omega}_e \times {}^{\mathcal{B}}\mathbf{C}^{\mathcal{R}}(\mathbf{q}_e).
\end{aligned} \tag{2.55}$$

Equation (2.55) follows the form of Equation (2.18). Thus, we may write the error quaternion differential equation as

$$\dot{\mathbf{q}}_e = \frac{1}{2} \mathbf{E}(\mathbf{q}_e) \boldsymbol{\omega}_e. \tag{2.56}$$

Differentiating the angular velocity error vector in Equation (2.52) and evaluating along Equation (2.40) and Equation (2.55) we obtain

$$\begin{aligned}
\dot{\boldsymbol{\omega}}_e &= \dot{\boldsymbol{\omega}} - \frac{d}{dt} \left[ {}^{\mathcal{B}}\mathbf{C}^{\mathcal{R}}(\mathbf{q}_e) \boldsymbol{\omega}_r(t) \right], \\
&= \mathbf{J}^{-1} (-\boldsymbol{\omega} \times \mathbf{J} \boldsymbol{\omega} + \mathbf{u}) + \boldsymbol{\omega} \times {}^{\mathcal{B}}\mathbf{C}^{\mathcal{R}}(\mathbf{q}_e) \boldsymbol{\omega}_r - {}^{\mathcal{B}}\mathbf{C}^{\mathcal{R}}(\mathbf{q}_e) \dot{\boldsymbol{\omega}}_r.
\end{aligned} \tag{2.57}$$

For notational convenience, the expression for the angular velocity error dynamics is given by premultiplying the above equation through by  $\mathbf{J}$ . The corresponding time evolution of the error quaternion follows the form of Equation (2.14). The notation of the DCM is abbreviated from  ${}^{\mathcal{B}}\mathbf{C}^{\mathcal{R}}(\mathbf{q}_e)$  to  $\mathbf{C}(\mathbf{q}_e)$  implying that the DCM that is parametrized in terms of the error quaternion is the mapping from the commanded reference frame to the body frame. Thus, the overall attitude tracking error dynamics for a rigid body is given by

$$\dot{\boldsymbol{\omega}}_e = \mathbf{J}^{-1} (-\boldsymbol{\omega} \times \mathbf{J} \boldsymbol{\omega} + \mathbf{u}) + \boldsymbol{\omega} \times {}^{\mathcal{B}}\mathbf{C}^{\mathcal{R}}(\mathbf{q}_e) \boldsymbol{\omega}_r - {}^{\mathcal{B}}\mathbf{C}^{\mathcal{R}}(\mathbf{q}_e) \dot{\boldsymbol{\omega}}_r, \tag{2.58a}$$

$$\dot{\mathbf{q}}_e = \frac{1}{2} \mathbf{E}(\mathbf{q}_e) \boldsymbol{\omega}_e. \tag{2.58b}$$

where Equation (2.58b) may equivalently be expressed as

$$\begin{aligned}\dot{q}_{e0} &= -\frac{1}{2}\mathbf{q}_{e_v}^T \boldsymbol{\omega}_e, \\ \dot{\mathbf{q}}_{e_v} &= \frac{1}{2}(q_{e0}\mathbf{I} + [\mathbf{q}_{e_v} \times]) \boldsymbol{\omega}_e.\end{aligned}$$

The seven state vector of the system, denoted by  $\mathbf{x}$ , is given by

$$\mathbf{x} = \begin{bmatrix} \mathbf{q}_e \\ \boldsymbol{\omega}_e \end{bmatrix}. \quad (2.59)$$

In Equation (2.58a),  $\boldsymbol{\omega}$  can be expressed entirely in terms of  $\boldsymbol{\omega}_e$  and  $\boldsymbol{\omega}_r$  through the relation in Equation (2.52). Therefore, the nonlinear dynamics of  $\mathbf{x}$  are a vector function  $\mathbf{f}$  of the vectors  $\mathbf{q}_e$ ,  $\boldsymbol{\omega}_e$ ,  $\mathbf{u}$ , that is,

$$\dot{\mathbf{x}} = \mathbf{f}(\mathbf{q}_e, \boldsymbol{\omega}_e, \mathbf{u}, t), \quad (2.60)$$

or in terms of the state,

$$\dot{\mathbf{x}} = \mathbf{f}(\mathbf{x}, \boldsymbol{\omega}, \mathbf{u}, t). \quad (2.61)$$

The dependence of  $\dot{\mathbf{x}}$  on time,  $t$ , comes directly from the reference signals  $\boldsymbol{\omega}_r(t)$  and  $\dot{\boldsymbol{\omega}}_r(t)$  which are in general explicit functions of time. For example,  $\boldsymbol{\omega}_r(t)$  may be described by

$$\boldsymbol{\omega}_r(t) = [ \sin t, \quad \cos 2t, \quad \sin t ]. \quad (2.62)$$

The control objective is to track any reference trajectory,  $[\mathbf{q}_r(t), \boldsymbol{\omega}_r(t)]$ , for all initial conditions,  $[\mathbf{q}(0), \boldsymbol{\omega}(0)]$ , assuming full feedback of the signals  $[\mathbf{q}(t), \boldsymbol{\omega}(t)]$  and uncertainty in inertia parameters. That is, a control torque  $\mathbf{u}(t)$  needs to be designed such that

$$\lim_{t \rightarrow \infty} \mathbf{x}(t) = 0, \quad (2.63)$$

while ensuring that the signals  $\boldsymbol{\omega}$  and  $\mathbf{q}$  remain bounded at all times. In this way, a tracking control problem has been converted into a stabilization problem for the error states<sup>7</sup>.

### 2.3 Concepts of Stability

The concept of stability is essential in control design, because unstable dynamic behavior can have detrimental effects on the integrity of a mechanical system. Intuitively, a system can be described as “stable” if it starts in the vicinity of its operating point and stays there for all time thereafter. If the system deviates from the operating point no matter how close it starts, then the system is unstable. This intuitive concept can be quantified using the concepts of Lagrange stability and Lyapunov stability theory. In this section, a brief overview of stability concepts for nonlinear systems is introduced in order to motivate the development of the attitude control laws and their stability proofs.

Consider a nonlinear dynamical system described by

$$\dot{\mathbf{x}} = \mathbf{f}(\mathbf{x}, \mathbf{u}, t); \quad \mathbf{x}(t_0) = \mathbf{x}_0, \quad (2.64)$$

where  $\mathbf{x} \in \mathbb{R}^n$ ,  $\mathbf{x}(t_0) \in \mathbb{R}^n$ . The system described by Equation (2.64) is said to be a non-autonomous system since the system’s state equation depend explicitly on time. A robotic manipulator is an example of a nonautonomous system as it follows a prescribed trajectory to transfer loads and has an inertia matrix that varies with the position of the arm. A system that has no explicit dependence on time is known as an autonomous system and is written as  $\dot{\mathbf{x}} = \mathbf{f}(\mathbf{x}, \mathbf{u})$ .

The objective of this section is to address theoretical concepts of stability for a nonlinear system described by Equation (2.64). Standard mathematical abbreviation symbols that are used extensively throughout the section are defined here:

- $\forall$  “for all”
- $\implies$  “implies that”
- $\exists$  “there exists”

A few simplifying notations are needed in order to proceed.

**Definition 2.1. Open Ball  $\mathbf{B}_r$** <sup>5,13,26</sup>: Let  $\mathbf{B}_r \in \mathbb{R}^n$  denote an open spherical region or a ball defined by  $\|\mathbf{x}\| < r$  for  $r > 0$ , a strictly positive and real number.

**Definition 2.2. Equilibrium State**<sup>5,13,26</sup>: A state vector  $\mathbf{x}_e$  is said to be an equilibrium state for a system described by  $\dot{\mathbf{x}} = \mathbf{f}(\mathbf{x}, \mathbf{u}, t)$  at time  $t_0$  if

$$f(t, \mathbf{x}_e) = 0, \quad \forall t > t_0. \quad (2.65)$$

The simplest form of stability is if the state  $\mathbf{x}(t)$  remains bounded relative to the equilibrium state  $\mathbf{x}_e$ . The initial state  $\mathbf{x}(t_0)$  could lie arbitrarily close to the equilibrium state while  $x(t)$  may still deviate from the equilibrium for  $t > t_0$ . The only assurance that can be provided is that  $x(t)$  will remain within a finite bound,  $\delta$ , of the equilibrium state. This notion of boundedness is known as Lagrange stability<sup>5</sup>.

**Definition 2.3. Lagrange Stability**<sup>5</sup>: *The equilibrium state  $\mathbf{x}_e$  is Lagrange stable (or bounded) if there exists a  $\delta > 0$  such that*

$$\|\mathbf{x}(t) - \mathbf{x}_e\| < \delta \implies \mathbf{x}(t) \in \mathbf{B}_\delta(\mathbf{x}_e), \quad \forall t \geq t_0. \quad (2.66)$$

The statement of stability in Definition 2.3 can be strengthened by making  $\delta$  arbitrarily small. Stability in the sense of Lyapunov (or Lyapunov stability) states that if the initial state is close enough to the equilibrium state, the system is Lyapunov stable if  $\mathbf{x}(t)$  remains arbitrarily close to the equilibrium for all time. The formal definition follows.

**Definition 2.4. Lyapunov Stability**<sup>5,13,26</sup>: *The equilibrium state  $\mathbf{x}_e$  is Lyapunov stable (or stable in the sense of Lyapunov) if for any  $t_0$  and  $\epsilon > 0$ , there exists a  $\delta(t_0, \epsilon)$  such that*

$$\|\mathbf{x}(t_0) - \mathbf{x}_e\| < \delta \implies \|\mathbf{x}(t, t_0, \mathbf{x}_0) - \mathbf{x}_e\| < \epsilon, \quad \forall t \geq t_0. \quad (2.67)$$

The definition states that the equilibrium point is stable if the state trajectory  $\mathbf{x}(t)$  does not escape a ball of arbitrarily specified radius  $\mathbf{B}_\epsilon$ , and in order for this to be true, a ball of radius  $\delta(t_0, \epsilon)$  can be found such that if  $\mathbf{x}(t)$  originates (at  $t = t_0$ ) within  $\mathbf{B}_\delta$  then  $\mathbf{x}(t)$  can be guaranteed to stay within  $\mathbf{B}_\epsilon$  thereafter. This concept is depicted by curve 1 in Figure 2.4 for  $\mathbf{x} \in \mathbb{R}^2$  where  $\mathbf{x}_e = \mathbf{0}$ . Thus, stability is defined in terms of the equilibrium state and not just in terms of the system. If the dependence of  $\delta$  on the initial time is removed, that is,  $\delta = \delta(\epsilon)$ , then  $\mathbf{x}_e$  is said to be **uniformly stable** in the sense of Lyapunov. Uniform stability implies general stability that is unaffected by the initial time  $t_0$ .



Conversely, the system is said to be **unstable** if there exists at least one ball  $\mathbf{B}_\epsilon$ , such that for any  $\delta > 0$  no matter how small, the system may start anywhere within the ball  $\mathbf{B}_\delta$  and eventually leave the ball  $\mathbf{B}_\epsilon$ . This concept is depicted by curve 2 in Figure 2.4. One may think of the vertical down equilibrium position of a pendulum as stable, while the vertical up equilibrium position is unstable as no matter how close the pendulum starts close to the vertical up position, it will never stay there.

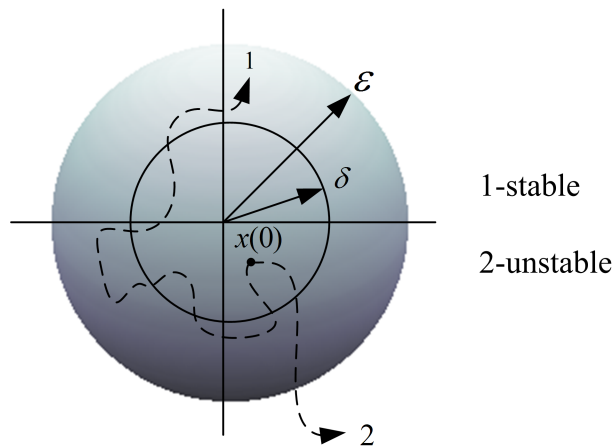


Figure 2.4: Stability in the sense of Lyapunov.

Definition 2.4 guarantees that the motion of the state trajectory remains arbitrarily close to the equilibrium state. However, no guarantees are provided as to whether the state converges to the equilibrium state. A stronger stability statement is made when the trajectory asymptotically converges to the equilibrium state such that  $\|\mathbf{x}(t, t_0, \mathbf{x}_0) - \mathbf{x}_e\|$  approaches zero as  $t \rightarrow \infty$ .

**Definition 2.5. Asymptotic Stability**<sup>5,13,26</sup>: *The equilibrium state  $\mathbf{x}_e$  is said to be asymptotically stable if*

1.  $\mathbf{x}_e$  is Lyapunov stable,
2. there exists a  $\delta(t_0)$  such that

$$\|\mathbf{x}(t_0) - \mathbf{x}_e\| < \delta(t_0) \implies \lim_{t \rightarrow \infty} \|\mathbf{x}(t, t_0, \mathbf{x}_0) - \mathbf{x}_e\| = 0, \quad \forall t \geq t_0. \quad (2.68)$$

The ball  $\mathbf{B}_\delta$  is called a *domain of attraction* of the equilibrium state. The set of all initial conditions  $\mathbf{x}(0)$  such that  $\|\mathbf{x}(t, t_0, \mathbf{x}_0) - \mathbf{x}_e\| \rightarrow 0$  as  $t \rightarrow \infty$  is called *the domain of attraction*.

**Definition 2.6. Uniform Asymptotic Stability**<sup>5,13,26</sup>: *The equilibrium state  $\mathbf{x}_e$  is said to be uniformly asymptotically stable if*

1.  $\mathbf{x}_e$  is uniformly stable,
2. for every  $\epsilon > 0$  and any initial time  $t_0$ , there exists  $\delta_0 > 0$  (independent of  $t_0$  and  $\epsilon$ ) and  $T(\epsilon) > 0$  such that

$$\|\mathbf{x}(t_0) - \mathbf{x}_e\| < \delta \implies \|\mathbf{x}(t, t_0, \mathbf{x}_0) - \mathbf{x}_e\| < \epsilon, \quad \forall t \geq t_0 + T(\epsilon). \quad (2.69)$$

The second condition in Definition 2.6 essentially states that by choosing the initial state,  $\mathbf{x}(0)$ , in a sufficiently small ball at  $t = t_0$ , the subsequent motion of  $\mathbf{x}(t)$  is restricted to lie inside a given cylinder for all  $t \geq t_0 + T(\epsilon)$ <sup>26</sup>. This condition is depicted in Figure 2.5 for  $\mathbf{x} \in \mathbb{R}^2$  and  $\mathbf{x}_e = 0$ .

Asymptotic stability and uniform asymptotic stability guarantee that the state error approaches zero, but cannot predict the rate of convergence<sup>5</sup>. In many engineering applications, it is essential to the system operation to predict how fast

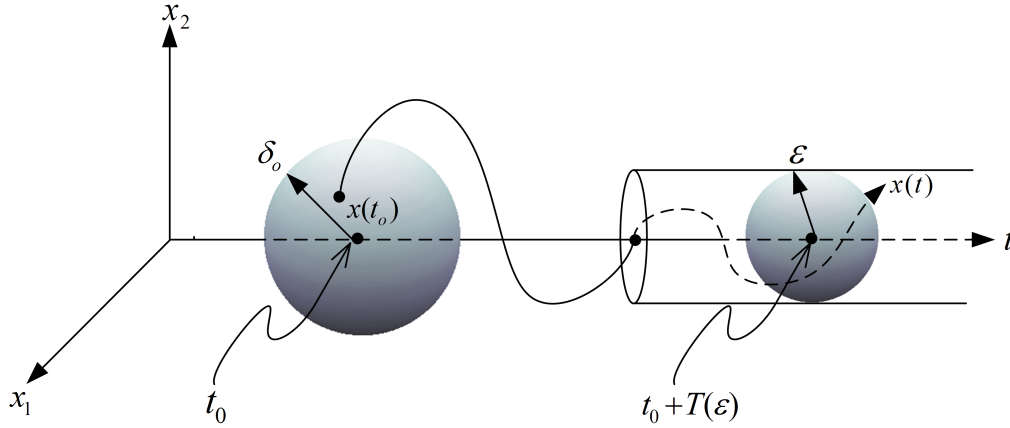


Figure 2.5: Uniform asymptotic stability of an equilibrium.

the system state error decays to zero. This introduces the concept of exponential stability.

**Definition 2.7. Exponential Stability**<sup>5,13,26</sup>: *The equilibrium state  $\mathbf{x}_e$  is said to be exponentially stable if there exist  $\lambda$  and  $\epsilon$ , both strictly positive numbers, such that*

$$\|\mathbf{x}(t_0) - \mathbf{x}_e\| < \delta(\epsilon) \implies \|\mathbf{x}(t, t_0, \mathbf{x}_0) - \mathbf{x}_e\| < \epsilon e^{-\lambda(t-t_0)}, \quad \forall t \geq t_0. \quad (2.70)$$

In other words, if a system is exponentially stable, then the state vector converges to the equilibrium state at an exponential rate. The constant  $\lambda$  specifies the rate of exponential convergence. Defining a system as exponentially stable, allows one to place an explicit bound on the system state at any time<sup>13</sup>.

Definitions 2.4-2.7 characterize the local behavior of a system near an equilibrium state. In order to examine the behavior of the system when the initial state is not in close proximity to the equilibrium state, the concept of global stability is presented.

**Definition 2.8. Global Stability:** *The equilibrium state is said to be globally asymptotically stable if for any initial state  $\mathbf{x}(0)$  the solution is asymptotically stable. Similarly, if exponential stability holds for any initial state, then the equilibrium state is said to be globally exponentially stable. Global stability is also referred to as stability in the large.*

Finally, the concept of boundedness of state solutions is discussed. Suppose  $\mathbf{x}(t, t_0, \mathbf{x}_0)$  is the solution to the dynamical system  $\dot{\mathbf{x}} = f(\mathbf{x}, \mathbf{u}, t)$  with initial condition  $\mathbf{x}(t_0) = \mathbf{x}_0$ . Then, the solution  $\mathbf{x}(t, t_0, \mathbf{x}_0)$  is **uniform bounded** if there exists a number  $\beta \geq 0$ , independent of the initial conditions, such that  $\|\mathbf{x}(t, t_0, \mathbf{x}_0)\| \leq \beta$  for all time  $t \geq t_0$ . Furthermore, if there exists  $\beta > 0$  corresponding to any  $\alpha > 0$ , and the state originates within the ball  $\mathbf{B}_\alpha$ , while the corresponding solution trajectory stays within  $\mathbf{B}_\beta$  for all  $t \geq t_0 + T(\alpha)$ , then  $\mathbf{x}(t, t_0, \mathbf{x}_0)$  is said to be **uniform ultimate bounded**.

## 2.4 Vector Norms and $\mathcal{L}_p$ Spaces

In this section, the definitions and properties of vector norms and the function space  $\mathcal{L}_p$  are presented to allow the reader to follow extensive discussions on system stability in subsequent chapters. Vector norms provide an analog of the absolute value of a scalar, and allow arguments for scalar equations to be faithfully extended to vector equations.

Consider a vector signal,  $\mathbf{x}$ , restricted to positive real numbers ( $\mathbf{x} : \mathbb{R}^+ \rightarrow$

$\mathbb{R}^n$ ), then the  $p$ -vector norm is defined as

$$\|\mathbf{x}\|_p = \left[ \sum_{k=1}^n |x_k|^p \right]^{1/p}, \quad (2.71)$$

where  $p \in [1, \infty)$  is any integer<sup>27</sup>. The following three vector norms constitute the most common normed vector spaces:

1.  $\|\mathbf{x}\|_1 = \sum_{k=1}^n |x_k|$
2.  $\|\mathbf{x}\|_2 = \left[ \sum_{k=1}^n |x_k|^2 \right]^{\frac{1}{2}} = \sqrt{\mathbf{x}^T \mathbf{x}}$
3.  $\|\mathbf{x}\|_\infty = \max_k |x_k|$

The 2-vector norm is the standard Euclidean norm which defines the intuitive notion of length of the vector  $\mathbf{x}$ . All norms are equivalent in that they produce the same topology in the field of real or complex numbers. That is, for any two vector norms  $\|\cdot\|_\alpha$  and  $\|\cdot\|_\beta$

$$c_1 \|\mathbf{x}\|_\alpha \leq \|\mathbf{x}\|_\beta \leq c_2 \|\mathbf{x}\|_\alpha, \quad (2.72)$$

for some strictly positive numbers  $c_1$  and  $c_2$  and for all  $\mathbf{x} \in \mathbb{C}^n$ .

For vector functions of time, the  $\mathcal{L}_p$  norm is defined as<sup>28</sup>

$$\|\mathbf{x}\|_p = \left( \int_0^\infty \|\mathbf{x}\|^p dt \right)^{\frac{1}{p}}, \quad (2.73)$$

for  $p \in [1, \infty)$ . If the integral in Equation (2.73) exists and is finite, then  $\mathbf{x}$  is said to be in the  $\mathcal{L}_p$  space, that is  $\mathbf{x} \in \mathcal{L}_p$ . The  $\mathcal{L}_\infty$  norm is defined as

$$\|\mathbf{x}\|_\infty = \sup_{t \geq 0} \|\mathbf{x}(t)\|, \quad (2.74)$$

and  $\mathbf{x}$  is said to be in  $\mathcal{L}_\infty$  space when  $\|\mathbf{x}\|_\infty$  exists.

In the definitions above for  $\mathcal{L}_p$  and  $\mathcal{L}_\infty$  norms,  $\|\cdot\|$  denotes any vector norm in  $\mathbb{R}^n$ . If the definitions are applied to a scalar function of time,  $x(t)$ , then  $\|\cdot\|$  may simply be replaced by  $|\cdot|$ , denoting the absolute value<sup>28</sup>.

## 2.5 Summary

A dynamical model for the spacecraft tracking problem is developed. Rigid body kinematics are derived using an appropriate set of attitude coordinates to express the orientation of the spacecraft, while Euler's rotational equations of motion are developed starting from the basic concept of rigid body angular momentum. A brief overview of stability concepts, definitions of vector norms, and properties of  $\mathcal{L}_p$  function space are also provided to allow the reader to follow discussions of system stability in subsequent chapters.

## Chapter 3

### Linear Control Theory

In the previous chapter, the governing equations for the nanosatellite tracking problem were derived. The kinematic differential equations are determined to be highly coupled and nonlinear. In this chapter, a tracking controller is derived to stabilize the system for a broad class of trajectories. Linearization methods are implemented to obtain a time-varying linear model of the governing equations. Partial feedback linearization is employed to cancel known nonlinearities that are independent of state variables and the remaining dynamics are linearized using Jacobian linearization. The linearized dynamics are stabilized using full state feedback control for certain “slowly time-varying” reference trajectories. The total nonlinear control law has mixed feedback and feedforward components.

#### 3.1 Tracking Control

In general, a tracking controller,  $\mathbf{u}$ , may be characterized as the composition of

$$\mathbf{u} = \mathbf{u}_{ff} + \mathbf{u}_{fb}, \quad (3.1)$$

where  $\mathbf{u}_{ff}$  and  $\mathbf{u}_{fb}$  are the feedforward and feedback components, respectively, of the tracking control system. The feedforward compensator<sup>7,13</sup> provides the necessary inputs to track the prescribed trajectory while canceling the effects of disturbances

that arise from unknown signals. The feedback action then stabilizes the remaining tracking error dynamics. Whereas feedback control might be model independent, feedforward action always requires information about the structure of the plant in order to provide the necessary anticipative action for accomplishing the tracking tasks<sup>13</sup>.

Full-state feedback control assumes that, at any given instant, the measured updates of all the state signals are available to the control law. The feedback control law attempts to minimize the error between the current and desired state by providing a corrective action to adequately adjust the state variables. A proportional derivative (PD) controller is based on the notion of feedback and consists of two separate parameters: a proportional value that determines corrective action that is proportional to the error, and a derivative term that calculates correction that is proportional to the rate of change of the error.

For the application of spacecraft attitude tracking, the proportional feedback action is provided in terms of the quaternion error vector, while the derivative feedback action is in terms of the angular velocity error vector. PD-type controllers, with and without feedforward compensation, have been extensively studied for attitude control for many years<sup>6,7,9,11</sup>. A special class of tracking maneuvers known as setpoint regulation, in which the final desired angular velocity is zero, has also been extensively studied<sup>5</sup>. In this case, pure PD control that is model-independent has been shown to be globally stabilizing and naturally robust to parametric uncertainties and unknown disturbances.

The PD control law in Wen et al.<sup>7</sup> is presented as a generalization of the



setpoint control law to a class of desired trajectories with nonzero final angular velocity. In this controller, tracking performance is dependent on the availability of high feedback gains. For fast slewing operation, nonzero transient tracking error might be incurred if high feedback gains are not possible due to actuator constraints. Such a scenario is undesirable for spacecraft missions that demand high precision tracking performance without the availability of high control gains. In such cases, the model dependent feedforward action becomes critical in delivering zero transient tracking error.

### 3.2 Control Design Based on Feedback Linearization

Feedback linearization is a commonly used tool in nonlinear control design. The basic concept is to algebraically transform the nonlinear model of a system to an equivalent model of simpler form<sup>13</sup>. In its simplest form, feedback linearization is achieved by canceling the nonlinear dynamics of a system and imposing desirable linear terms that can be handled using linear control techniques. This method can be applied to nonlinear systems that appear in the controllability companion form<sup>13</sup> represented by

$$\mathbf{x}^{(n)} = \mathbf{f}(\mathbf{x}) + \mathbf{b}(\mathbf{x})\mathbf{u}, \quad (3.2)$$

where  $\mathbf{x} = [\mathbf{x}, \dot{\mathbf{x}}, \dots, \mathbf{x}^{(n-1)}]$  is the state vector,  $\mathbf{u}$  is the vector control input, and  $\mathbf{f}$  and  $\mathbf{b}$  are vector functions. The controllability companion form is unique because only derivatives of the state, and not the control input, appear in Equation (3.2).

For the spacecraft attitude tracking problem, partial feedback linearization is applied in order to simplify the highly nonlinear dynamics of the tracking error

equations. The transformed dynamics are then analyzed through linear approximation by Taylor series expansion.

The tracking error dynamics for spacecraft attitude tracking derived in Chapter 2 are

$$\mathbf{J}\dot{\boldsymbol{\omega}}_e = -\boldsymbol{\omega} \times \mathbf{J}\boldsymbol{\omega} + \mathbf{u} - \mathbf{J}\left[\mathbf{C}(\mathbf{q}_e)\dot{\boldsymbol{\omega}}_r - \boldsymbol{\omega}_e \times \mathbf{C}(\mathbf{q}_e)\boldsymbol{\omega}_r\right], \quad (3.3a)$$

$$\dot{\mathbf{q}}_e = \frac{1}{2}\mathbf{E}(\mathbf{q}_e)\boldsymbol{\omega}_e. \quad (3.3b)$$

Recall that the current spacecraft trajectory,  $\boldsymbol{\omega}$ , can be described in terms of  $\boldsymbol{\omega}_e$  and  $\boldsymbol{\omega}_r$  as

$$\boldsymbol{\omega} = \boldsymbol{\omega}_e + \mathbf{C}(\mathbf{q}_e)\boldsymbol{\omega}_r. \quad (3.4)$$

Substituting Equation (3.4) into Equation (3.3a) yields the expanded form

$$\begin{aligned} \mathbf{J}\dot{\boldsymbol{\omega}}_e = & -(\boldsymbol{\omega}_e + \mathbf{C}(\mathbf{q}_e)\boldsymbol{\omega}_r) \times \mathbf{J}(\boldsymbol{\omega}_e + \mathbf{C}(\mathbf{q}_e)\boldsymbol{\omega}_r) \\ & - \mathbf{J}\left[\mathbf{C}(\mathbf{q}_e)\dot{\boldsymbol{\omega}}_r - \boldsymbol{\omega}_e \times \mathbf{C}(\mathbf{q}_e)\boldsymbol{\omega}_r\right] + \mathbf{u}. \end{aligned} \quad (3.5)$$

Observe that in Equation (3.5), the terms  $\mathbf{C}(\mathbf{q}_e)\boldsymbol{\omega}_r \times \mathbf{J}\mathbf{C}(\mathbf{q}_e)\boldsymbol{\omega}_r$  and  $\mathbf{J}\mathbf{C}(\mathbf{q}_e)\dot{\boldsymbol{\omega}}_r$  are not explicitly dependent on the state signal  $\boldsymbol{\omega}_e$ . Based on Equation (3.1),  $\mathbf{u}$  is expressed in terms of a feedforward and feedback compensator as

$$\mathbf{u} = \underbrace{\mathbf{u}_r}_{\text{feedforward}} + \underbrace{\boldsymbol{\nu}}_{\text{feedback}}. \quad (3.6)$$

The feedforward compensation is selected to directly cancel known nonlinearities that are dependent on the plant structure and the reference trajectory but are not explicitly dependent on the state  $\boldsymbol{\omega}_e$ . This approach amounts to performing partial feedback linearization to cancel undesirable nonlinearities in the nonlinear system<sup>13</sup>.

The anticipative nonlinear feedforward control  $\mathbf{u}_r$  is given by

$$\mathbf{u}_r = \mathbf{C}(\mathbf{q}_e)\boldsymbol{\omega}_r \times \mathbf{J} \mathbf{C}(\mathbf{q}_e)\boldsymbol{\omega}_r + \mathbf{J} \mathbf{C}(\mathbf{q}_e)\dot{\boldsymbol{\omega}}_r. \quad (3.7)$$

Note that  $\mathbf{u}_r$  is composed of terms that are linearly parameterized in terms of the plant parameter  $\mathbf{J}$ . Substituting Equation (3.7) into Equation (3.5) results in term cancellation. The remaining angular velocity error dynamics are

$$\begin{aligned} \mathbf{J}\dot{\boldsymbol{\omega}}_e &= -\boldsymbol{\omega}_e \times \mathbf{J}(\boldsymbol{\omega}_e + \mathbf{C}(\mathbf{q}_e)\boldsymbol{\omega}_r) - \mathbf{C}(\mathbf{q}_e)\boldsymbol{\omega}_r \times \mathbf{J}\boldsymbol{\omega}_e \\ &+ \mathbf{J}\boldsymbol{\omega}_e \times \mathbf{C}(\mathbf{q}_e)\boldsymbol{\omega}_r + \boldsymbol{\nu}. \end{aligned} \quad (3.8)$$

Note that, every term in Equation (3.8) is dependent on both state signals  $\boldsymbol{\omega}_e$  and  $\mathbf{q}_e$ . Partial feedback linearization, performed through the control algorithm in Equation (3.7), allows one to obtain a more manageable form of the system dynamics by canceling some of the highly nonlinear terms. The stability of the transformed dynamics of Equation (3.8) is treated in the next section.

### 3.3 Lyapunov's Indirect Method

Linear control theory is a well developed subject that has been long prevalent in engineering due to its broad applications and powerful tools. In analyzing nonlinear systems and designing control systems to satisfy specific performance requirements, a common practice is to linearize the system about a nominal or equilibrium point. The method of linearization permits one to obtain a linear model that approximates a nonlinear model about the operating point. Subsequently, linear control methods can be used to stabilize the nonlinear system when the range of motion is assumed to be within the vicinity of the operating point. However,

inherent in that assumption is the fact that linear control methods are likely to perform well only in the region near the operating point. Further away, linear control techniques may break down as the system nonlinearities become significant, rendering the linear control method ineffective. Thus, for a nonlinear system designed to operate over a large range of motion, linear control methods may become unstable. Nevertheless, linearization is a useful tool in the analysis of a nonlinear system, as it offers the engineer a better understanding of how the system behaves and where the linear approximation breaks down.

The procedure for obtaining a linear approximation to an autonomous nonlinear system is discussed. The method of linearizing the equations of motion about a nominal state known as Lyapunov's indirect method or Jacobian linearization, is presented. In essence, a linear approximation is obtained through a Taylor Series expansion. An extension of Lyapunov's indirect method is also discussed for non-autonomous systems.

### 3.3.1 Linearization of Autonomous Systems

Consider a nonlinear autonomous system with inputs  $\mathbf{x} \in \mathbb{R}^n$ , outputs  $\mathbf{u} \in \mathbb{R}^m$ , and closed loop dynamics described by

$$\dot{\mathbf{x}} = \mathbf{f}(\mathbf{x}, \mathbf{u}). \quad (3.9)$$

The first order Taylor series expansion applied to the displacement of  $\mathbf{f}(\mathbf{x}, \mathbf{u})$  from the nominal trajectories  $\mathbf{x}^*$ ,  $\mathbf{u}^*$  is

$$\mathbf{f}(\mathbf{x}, \mathbf{u}) \cong \mathbf{f}(\mathbf{x}^*, \mathbf{u}^*) + \left. \frac{\partial \mathbf{f}(\mathbf{x}, \mathbf{u})}{\partial \mathbf{x}} \right|_* \delta \mathbf{x} + \left. \frac{\partial \mathbf{f}(\mathbf{x}, \mathbf{u})}{\partial \mathbf{u}} \right|_* \delta \mathbf{u} + \text{h.o.t}, \quad (3.10)$$

where h.o.t denotes higher order terms in  $\mathbf{x}$  and  $\mathbf{u}$ . In Equation (3.10), let

$$\mathbf{A} = \left. \frac{\partial \mathbf{f}}{\partial \mathbf{x}} \right|^* \quad \text{and} \quad \mathbf{B} = \left. \frac{\partial \mathbf{f}}{\partial \mathbf{u}} \right|^*, \quad (3.11)$$

where,

$$\left. \frac{\partial \mathbf{f}}{\partial \mathbf{x}} \right|^* = \begin{bmatrix} \left. \frac{\partial f_1}{\partial x_1} \right|^* & \left. \frac{\partial f_1}{\partial x_2} \right|^* & \cdots & \left. \frac{\partial f_1}{\partial x_n} \right|^* \\ \left. \frac{\partial f_2}{\partial x_1} \right|^* & \left. \frac{\partial f_2}{\partial x_2} \right|^* & \cdots & \left. \frac{\partial f_2}{\partial x_n} \right|^* \\ \vdots & \vdots & \ddots & \vdots \\ \left. \frac{\partial f_n}{\partial x_1} \right|^* & \left. \frac{\partial f_n}{\partial x_2} \right|^* & \cdots & \left. \frac{\partial f_n}{\partial x_n} \right|^* \end{bmatrix} \quad (3.12a)$$

$$(3.12b)$$

$$\left. \frac{\partial \mathbf{f}}{\partial \mathbf{u}} \right|^* = \begin{bmatrix} \left. \frac{\partial f_1}{\partial u_1} \right|^* & \left. \frac{\partial f_1}{\partial u_2} \right|^* & \cdots & \left. \frac{\partial f_1}{\partial u_m} \right|^* \\ \left. \frac{\partial f_2}{\partial u_1} \right|^* & \left. \frac{\partial f_2}{\partial u_2} \right|^* & \cdots & \left. \frac{\partial f_2}{\partial u_m} \right|^* \\ \vdots & \vdots & \ddots & \vdots \\ \left. \frac{\partial f_n}{\partial u_1} \right|^* & \left. \frac{\partial f_n}{\partial u_2} \right|^* & \cdots & \left. \frac{\partial f_n}{\partial u_m} \right|^* \end{bmatrix}. \quad (3.12c)$$

The matrices  $\mathbf{A} \in \mathbb{R}^{n \times n}$  and  $\mathbf{B} \in \mathbb{R}^{n \times m}$  denote the constant Jacobian matrices of  $\mathbf{f}(\mathbf{x}, \mathbf{u})$  with respect to  $\mathbf{x}$  and  $\mathbf{u}$ , respectively. Subtracting the nominal solution from both sides of Equation (3.10), it is clear that

$$\delta \dot{\mathbf{x}} = \mathbf{f}(\mathbf{x}, \mathbf{u}) - \mathbf{f}(\mathbf{x}^*, \mathbf{u}^*), \quad (3.13)$$

and

$$\delta \dot{\mathbf{x}} \cong \mathbf{A} \delta \mathbf{x} + \mathbf{B} \delta \mathbf{u}. \quad (3.14)$$

### 3.3.2 Linearization of Non-Autonomous Systems

The extension of Lyapunov's indirect method to non-autonomous systems is provided here. Consider a nonlinear, non-autonomous system characterized by

$$\dot{\mathbf{x}} = \mathbf{f}(\mathbf{x}, \mathbf{u}, t), \quad (3.15)$$

where the vector function  $\mathbf{f}$  is continuously differentiable with respect to the state  $\mathbf{x}$ . Let the time-varying Jacobian matrices  $\mathbf{A}(t)$  and  $\mathbf{B}(t)$  be described as before by Equation (3.11). Then, for any fixed time  $t$  (that is,  $t$  is regarded as a parameter)<sup>13</sup>, a Taylor series expansion of  $\mathbf{f}$  about the nominal trajectories  $\mathbf{x}^*$  and  $\mathbf{u}^*$  is given by

$$\delta\dot{\mathbf{x}} \cong \mathbf{A}(t)\delta\mathbf{x} + \mathbf{B}(t)\delta\mathbf{u} + \text{h.o.t.}, \quad (3.16)$$

where the higher order terms in  $\mathbf{x}$  and  $\mathbf{u}$  can have explicit dependence on time  $t$ . Let the function  $\mathbf{g}_1(\mathbf{x}, t)$  contain all higher order terms in  $\mathbf{x}$  and let  $\mathbf{g}_2(\mathbf{u}, t)$  contain all higher order terms in  $\mathbf{u}$ . Suppose that

$$\lim_{\|\mathbf{x}\| \rightarrow \mathbf{x}^*} \sup \frac{\|\mathbf{g}_1(\mathbf{x}, t)\|}{\|\mathbf{x}\|} = 0, \quad \forall t \geq 0, \quad (3.17)$$

and

$$\lim_{\|\mathbf{u}\| \rightarrow \mathbf{u}^*} \sup \frac{\|\mathbf{g}_2(\mathbf{u}, t)\|}{\|\mathbf{u}\|} = 0, \quad \forall t \geq 0, \quad (3.18)$$

where “sup” indicates the supremum, or the least upper bound, then the non-autonomous system  $\mathbf{f}$  is well approximated by  $\mathbf{A}(t)\delta\mathbf{x} + \mathbf{B}(t)\delta\mathbf{u}$  for any time  $t$ . That is,

$$\delta\dot{\mathbf{x}} \cong \mathbf{A}(t)\delta\mathbf{x} + \mathbf{B}(t)\delta\mathbf{u} \quad (3.19)$$

represents the linearization of the nonlinear non-autonomous system about the nominal states  $(\mathbf{x}^*, \mathbf{u}^*)$ .

### 3.3.3 Stability Analysis Using Lyapunov’s Indirect Method

Lyapunov’s indirect method can be used to determine the precise relationship between the linearized model and the original nonlinear system if the original system

is autonomous. For example, consider a closed loop system linearized about the origin  $\mathbf{x} = \mathbf{0}$

$$\dot{\mathbf{x}} = \mathbf{A}\mathbf{x}. \quad (3.20)$$

When the eigenvalues of the  $\mathbf{A}$  matrix all have negative real parts, that is  $\text{Re}\{\lambda_i\} < 0$ ,  $\mathbf{A}$  is called a Hurwitz matrix<sup>27</sup>. Then, the closed-loop linear system is found to be strictly stable and the original nonlinear system itself is strictly stable near the equilibrium or nominal point. Similarly, if any of the eigenvalues lie on the right half of the complex plane, the linear system is unstable and the original nonlinear system is also unstable. This type of analysis permits the use of linear control methods to design a stable controller that locally guarantees the stability of the original nonlinear system. However, this standard approach does not generally apply to time-varying systems, and eigenvalue analysis cannot be forwarded in the same sense as the time-invariant case. For instance, consider the linear time varying (LTV) system modified from Slotine and Li<sup>13</sup>

$$\begin{bmatrix} \dot{x}_1 \\ \dot{x}_2 \end{bmatrix} = \begin{bmatrix} -1 & e^{5t} \\ 0 & -3 \end{bmatrix} \begin{bmatrix} x_1 \\ x_2 \end{bmatrix}. \quad (3.21)$$

At any time,  $t > t_o$ , the eigenvalues of  $\mathbf{A}(t)$  are constant values  $-1$  and  $-3$ . For a linear time-invariant (LTI) system, if all the eigenvalues have negative real parts, then the corresponding LTI system is asymptotically stable. However, upon solving the above system for  $x_1$  and  $x_2$ , one finds that

$$x_2 = x_2(0)e^{-3t}, \quad \dot{x}_1 + x_1 = x_2(0)e^{2t}. \quad (3.22)$$

Thus, the system is unstable since the second equation is a first-order differential equation with an unbounded input, that is,  $x_2(0)e^{2t} \rightarrow \infty$  as  $t \rightarrow \infty$ . Thus, the

stability of a an LTV system cannot be generally inferred from eigenvalue analysis of the  $\mathbf{A}$  matrix as it would be in the case of LTI systems.

### 3.3.4 Stability of Slowly Time-Varying Systems

For a specific class of LTV systems, global asymptotic stability may, however, show some relation to the eigenvalues of  $\mathbf{A}(t)$ , but it is not the only condition necessary to assess stability. Additional restrictions must be placed on the variation of the elements of  $\mathbf{A}(t)$ <sup>13,29</sup>. Specifically,  $\mathbf{A}(t)$  must satisfy the following conditions:

- $\mathbf{A}(t)$  is continuously differentiable
- The elements of  $\mathbf{A}(t)$  and their first time derivatives are uniformly bounded, that is,

$$\|\mathbf{A}(t)\| \leq \alpha, \quad \text{and} \quad \|\dot{\mathbf{A}}(t)\| \leq \delta, \quad \forall t \geq t_0. \quad (3.23)$$

In addition, if  $\mathbf{A}(t)$  is Hurwitz in  $t$ , such that, for every  $t > 0$  all the eigenvalues of  $\mathbf{A}(t)$  have negative real parts,

$$\text{Re}\{\lambda_k(\mathbf{A}(t))\} \leq -\sigma_s, \quad \forall t \geq t_0, \quad k = 1, 2, \dots, n, \quad \sigma_s > 0, \quad (3.24)$$

then the system is guaranteed to be asymptotically stable. The value of  $\delta$  is system specific and can be prohibitively small for practical applications. The underlying notion of a slowly time-varying system is that the system responds much faster to changes in initial conditions than it does to time-varying parameters. Thus, if the additional smoothness conditions on  $\mathbf{A}(t)$  are met, for a specific value of  $\delta$  (to be determined) the stability of the system can still be analyzed through Lyapunov's indirect method.



### 3.4 Control Design Based on Lyapunov's Indirect Method

Consider the remaining angular velocity error dynamics after partial feedback linearization as described by Equation (3.8), and the attitude error dynamics described by Equation (3.3b). In order to linearize the nonlinear, non-autonomous system, the nominal values of  $\mathbf{x}^*$ ,  $\boldsymbol{\nu}^*$  are selected to be at the current trajectory of the spacecraft; that is,  $\mathbf{x}^* = \mathbf{x}(t)$  and  $\boldsymbol{\nu}^* = \boldsymbol{\nu}(t)$ . Then, in order to obtain a linear model, the nonlinear equations are expanded in terms of displacements,  $\delta\mathbf{x}$  and  $\delta\boldsymbol{\nu}$ , measured relative to the current spacecraft state.

Equation (3.3b) is written in long hand form for each of the four Euler parameters as

$$f_1 \rightarrow \dot{q}_{e0} = \frac{1}{2}(-q_{e1}\omega_{e1} - q_{e2}\omega_{e2} - q_{e3}\omega_{e3}), \quad (3.25a)$$

$$f_2 \rightarrow \dot{q}_{e1} = \frac{1}{2}(q_{e0}\omega_{e1} - q_{e3}\omega_{e2} + q_{e2}\omega_{e3}), \quad (3.25b)$$

$$f_3 \rightarrow \dot{q}_{e2} = \frac{1}{2}(q_{e3}\omega_{e1} + q_{e0}\omega_{e2} - q_{e1}\omega_{e3}), \quad (3.25c)$$

$$f_4 \rightarrow \dot{q}_{e3} = \frac{1}{2}(-q_{e2}\omega_{e1} + q_{e1}\omega_{e2} + q_{e0}\omega_{e3}). \quad (3.25d)$$

Differential equations (3.25a)-(3.25d) are designated as equations  $f_1 - f_4$ . Since the body axes of the Texas 2 Step nanosatellite are assumed to be aligned with the principal axes, the products of inertia are zero and the rotational error equations described by Equation (3.3a) simplify to

$$f_5 \rightarrow \dot{\omega}_{e1} = \frac{J_2 - J_3}{J_1}(\omega_{e2}\omega_{e3} + \omega_{e2}\eta_3 + \omega_{e3}\eta_2) + \nu_1 - \omega_{e3}\eta_2 + \omega_{e2}\eta_3, \quad (3.26a)$$

$$f_6 \rightarrow \dot{\omega}_{e2} = \frac{J_3 - J_1}{J_2}(\omega_{e1}\omega_{e3} + \omega_{e1}\eta_3 + \omega_{e3}\eta_1) + \nu_2 + \omega_{e3}\eta_1 - \omega_{e1}\eta_3, \quad (3.26b)$$

$$f_7 \rightarrow \dot{\omega}_{e3} = \frac{J_1 - J_2}{J_3}(\omega_{e1}\omega_{e2} + \omega_{e1}\eta_2 + \omega_{e2}\eta_1) + \nu_3 - \omega_{e2}\eta_1 + \omega_{e1}\eta_2, \quad (3.26c)$$

where,

$$\eta_1 = C_{11}\omega_{r_1} + C_{12}\omega_{r_2} + C_{13}\omega_{r_3},$$

$$\eta_2 = C_{21}\omega_{r_1} + C_{22}\omega_{r_2} + C_{23}\omega_{r_3},$$

$$\eta_3 = C_{31}\omega_{r_1} + C_{32}\omega_{r_2} + C_{33}\omega_{r_3}.$$

Differential equations (3.26a)-(3.26c) are designated as dynamical equations  $f_5$  -  $f_7$  respectively. The direction cosine matrix,  $\mathbf{C}(\mathbf{q}_e) \equiv [C_{ij}]$ , associated with  $\mathbf{q}_e$ , transforms a quaternion in the commanded reference frame to the body reference frame. Also, the principal moments of inertia of the spacecraft along the symmetric  $\hat{b}_1$ ,  $\hat{b}_2$ , and  $\hat{b}_3$  axes are defined as  $J_1$ ,  $J_2$ , and  $J_3$  respectively. Recall from Chapter 2, that the direction cosine matrix  $\mathbf{C}(\mathbf{q}_e)$ , parameterized in terms of  $\mathbf{q}_e$ , is expressed as

$$\mathbf{C}(\mathbf{q}_e) = (q_{e_0}^2 - \mathbf{q}_{e_v}^T \mathbf{q}_{e_v})\mathbf{I} + 2\mathbf{q}_{e_v} \mathbf{q}_{e_v}^T - 2[\mathbf{q}_{e_v} \times]. \quad (3.27)$$

Equation (3.27) is written longhand as follows:

$$\mathbf{C}(\mathbf{q}_e) = \begin{bmatrix} q_{e_0}^2 + q_{e_1}^2 - q_{e_2}^2 - q_{e_3}^2 & 2(q_{e_1}q_{e_2} + q_{e_0}q_{e_3}) & 2(q_{e_1}q_{e_3} - q_{e_0}q_{e_2}) \\ 2(q_{e_1}q_{e_2} - q_{e_0}q_{e_3}) & q_{e_0}^2 - q_{e_1}^2 + q_{e_2}^2 - q_{e_3}^2 & 2(q_{e_2}q_{e_3} + q_{e_0}q_{e_1}) \\ 2(q_{e_1}q_{e_3} + q_{e_0}q_{e_2}) & 2(q_{e_2}q_{e_3} - q_{e_0}q_{e_1}) & q_{e_0}^2 - q_{e_1}^2 - q_{e_2}^2 + q_{e_3}^2 \end{bmatrix}.$$

Let,

$$\mathbf{f}(\mathbf{x}, \boldsymbol{\nu}) = [f_1, f_2, f_3, f_4, f_5, f_6, f_7]^T. \quad (3.28)$$

The linear approximation of  $\mathbf{f}(\mathbf{x}, \boldsymbol{\nu})$  about  $(\mathbf{x}^*, \boldsymbol{\nu}^*)$  for any fixed time  $t$  is given by

$$\delta \dot{\mathbf{x}} \cong \mathbf{A}(t)\delta \mathbf{x} + \mathbf{B}\delta \boldsymbol{\nu}, \quad (3.29)$$

where  $\delta \mathbf{x} = [ \delta \mathbf{q}_e, \delta \boldsymbol{\omega}_e ]^T$  is the displacement vector of the state  $\mathbf{x}$ , and  $\mathbf{A}(t) \in \mathbb{R}^{7 \times 7}$  and  $\mathbf{B} \in \mathbb{R}^{7 \times 3}$  are the corresponding Jacobian matrices. The elements of the time varying matrix  $\mathbf{A}$ , are computed as follows

$$\mathbf{A} = \begin{bmatrix} 0 & -\frac{1}{2}\omega_{e1} & -\frac{1}{2}\omega_{e2} & -\frac{1}{2}\omega_{e3} & -\frac{1}{2}q_{e1} & -\frac{1}{2}q_{e2} & -\frac{1}{2}q_{e3} \\ \frac{1}{2}\omega_{e1} & 0 & \frac{1}{2}\omega_{e3} & -\frac{1}{2}\omega_{e2} & \frac{1}{2}q_{e0} & -\frac{1}{2}q_{e3} & \frac{1}{2}q_{e2} \\ \frac{1}{2}\omega_{e2} & -\frac{1}{2}\omega_{e3} & 0 & -\frac{1}{2}\omega_{e1} & \frac{1}{2}q_{e3} & \frac{1}{2}q_{e0} & -\frac{1}{2}q_{e1} \\ \frac{1}{2}\omega_{e3} & \frac{1}{2}\omega_{e2} & -\frac{1}{2}\omega_{e1} & 0 & -\frac{1}{2}q_{e1} & -\frac{1}{2}q_{e2} & -\frac{1}{2}q_{e3} \\ a_{51} & a_{52} & a_{53} & a_{54} & 0 & a_{56} & a_{57} \\ a_{61} & a_{62} & a_{63} & a_{64} & a_{65} & 0 & a_{67} \\ a_{71} & a_{72} & a_{73} & a_{74} & a_{75} & a_{76} & 0 \end{bmatrix}, \quad (3.30)$$

where the elements in the top left quadrant of  $\mathbf{A}$  are the partial derivatives of  $f_1 - f_4$  with respect to  $\mathbf{q}_e$  and the elements in the top right quadrant are the partial derivatives of  $f_1 - f_4$  with respect to  $\boldsymbol{\omega}_e$ . Similarly, the elements in the bottom left quadrant of  $\mathbf{A}$  are the partial derivatives of  $f_5 - f_7$  with respect to  $\mathbf{q}_e$ . These are computed as follows:

$$\begin{aligned} a_{5i} &= \omega_{e2} \frac{\partial \eta_3}{\partial q_{e_j}} \left( \frac{J_2 - J_3}{J_1} + 1 \right) + \omega_{e3} \frac{\partial \eta_2}{\partial q_{e_j}} \left( \frac{J_2 - J_3}{J_1} - 1 \right), \\ a_{6i} &= \omega_{e1} \frac{\partial \eta_3}{\partial q_{e_j}} \left( \frac{J_3 - J_1}{J_2} - 1 \right) + \omega_{e3} \frac{\partial \eta_1}{\partial q_{e_j}} \left( \frac{J_3 - J_1}{J_2} + 1 \right), \\ a_{7i} &= \omega_{e1} \frac{\partial \eta_2}{\partial q_{e_j}} \left( \frac{J_1 - J_2}{J_3} + 1 \right) + \omega_{e2} \frac{\partial \eta_1}{\partial q_{e_j}} \left( \frac{J_1 - J_2}{J_3} - 1 \right), \end{aligned}$$

for  $i = 1, 2, 3, 4$  and  $j = i - 1$ . In the above equations, the partial derivatives are defined as

$$\begin{aligned} \frac{\partial \eta_1}{\partial q_{e_0}} &= 2(q_{e_0}\omega_{r_1} + q_{e_3}\omega_{r_2} - q_{e_2}\omega_{r_3}), & \frac{\partial \eta_1}{\partial q_{e_1}} &= 2(q_{e_1}\omega_{r_1} + q_{e_2}\omega_{r_2} + q_{e_3}\omega_{r_3}), \\ \frac{\partial \eta_1}{\partial q_{e_2}} &= 2(-q_{e_2}\omega_{r_1} + q_{e_1}\omega_{r_2} - q_{e_0}\omega_{r_3}), & \frac{\partial \eta_1}{\partial q_{e_3}} &= 2(-q_{e_3}\omega_{r_1} + q_{e_0}\omega_{r_2} + q_{e_1}\omega_{r_3}), \\ \frac{\partial \eta_2}{\partial q_{e_0}} &= 2(-q_{e_3}\omega_{r_1} + q_{e_0}\omega_{r_2} + q_{e_1}\omega_{r_3}), & \frac{\partial \eta_2}{\partial q_{e_1}} &= 2(q_{e_2}\omega_{r_1} - q_{e_1}\omega_{r_2} + q_{e_0}\omega_{r_3}), \end{aligned}$$

$$\begin{aligned}
\frac{\partial \eta_2}{\partial q_{e_2}} &= 2(q_{e_1}\omega_{r_1} + q_{e_2}\omega_{r_2} + q_{e_3}\omega_{r_3}), & \frac{\partial \eta_2}{\partial q_{e_3}} &= 2(-q_{e_0}\omega_{r_1} - q_{e_3}\omega_{r_2} + q_{e_2}\omega_{r_3}), \\
\frac{\partial \eta_3}{\partial q_{e_0}} &= 2(q_{e_2}\omega_{r_1} - q_{e_1}\omega_{r_2} + q_{e_0}\omega_{r_3}), & \frac{\partial \eta_3}{\partial q_{e_1}} &= 2(q_{e_3}\omega_{r_1} + q_{e_2}\omega_{r_2} - q_{e_1}\omega_{r_3}), \\
\frac{\partial \eta_3}{\partial q_{e_2}} &= 2(q_{e_0}\omega_{r_1} + q_{e_3}\omega_{r_2} - q_{e_2}\omega_{r_3}), & \frac{\partial \eta_3}{\partial q_{e_3}} &= 2(q_{e_1}\omega_{r_1} + q_{e_2}\omega_{r_2} + q_{e_3}\omega_{r_3}).
\end{aligned}$$

The bottom right quadrant of  $\mathbf{A}$  corresponds to partial derivatives of  $f_5 - f_7$  with respect to  $\omega_e$ . These are computed as follows:

$$\begin{aligned}
a_{56} &= \frac{J_2 - J_3}{J_1}(\omega_{e_3} + \eta_3) + \eta_3, & a_{57} &= \frac{J_2 - J_3}{J_1}(\omega_{e_2} + \eta_2) - \eta_2, \\
a_{65} &= \frac{J_3 - J_1}{J_2}(\omega_{e_3} + \eta_3) - \eta_3, & a_{67} &= \frac{J_3 - J_1}{J_2}(\omega_{e_1} + \eta_1) + \eta_1, \\
a_{75} &= \frac{J_1 - J_2}{J_3}(\omega_{e_2} + \eta_2) + \eta_2, & a_{76} &= \frac{J_1 - J_2}{J_3}(\omega_{e_1} + \eta_1) - \eta_1.
\end{aligned}$$

All the elements of  $\mathbf{A}$  in Equation (3.30) are evaluated along the reference values  $\mathbf{q}_e^*$ ,  $\omega_e^*$ , and  $\nu^*$ . The entries of  $\mathbf{B}$  can be compactly written as

$$\mathbf{B} = \begin{bmatrix} \mathbf{0}_{4 \times 3} \\ \mathbf{J}^{-1} \end{bmatrix}. \quad (3.31)$$

The Jacobian matrices characterizing the linearized system in Equation (3.29) have been defined. The next objective is to stabilize the linearized dynamics by using a feedback controller of the PD-form

$$\delta \nu = -k_p \delta \mathbf{q}_e - k_v \delta \omega_e, \quad (3.32)$$

where  $k_p > 0$  and  $k_v > 0$  are the scalar attitude and angular velocity feedback gains that are to be determined. The controller in Equation (3.32) can be equivalently written in terms of a gain matrix  $\mathbf{K} \in \mathbb{R}^{3 \times 7}$  as

$$\delta \nu = -\mathbf{K} \delta \mathbf{x}, \quad (3.33)$$

where,

$$\mathbf{K} = \begin{bmatrix} 0 & k_p & 0 & 0 & k_v & 0 & 0 \\ 0 & 0 & k_p & 0 & 0 & k_v & 0 \\ 0 & 0 & 0 & k_p & 0 & 0 & k_v \end{bmatrix}. \quad (3.34)$$

The linear closed loop system is now stated as

$$\delta\dot{\mathbf{x}} \cong \mathbf{A}(t)\delta\mathbf{x} - \mathbf{BK}\delta\mathbf{x}, \quad (3.35)$$

or in terms of an augmented matrix  $\tilde{\mathbf{A}}(t) = \mathbf{A}(t) - \mathbf{BK}$  such that

$$\delta\dot{\mathbf{x}} \cong \tilde{\mathbf{A}}(t)\delta\mathbf{x}. \quad (3.36)$$

Finally, it remains to find appropriate values for  $k_p$  and  $k_v$  so that the linearized system described by Equation (3.36) is closed-loop stable. Since Equation (3.36) is a linear time-varying system, the standard approach for analyzing the stability of linear time-invariant systems does not apply here. However, if the reference angular velocity is chosen such that  $\tilde{\mathbf{A}}(t)$  satisfies the sufficient conditions in Equation (3.23) and Equation (3.24), the system is guaranteed global exponential stability. This entails identifying a value for  $\delta$  in Equation (3.23) for which the system will remain stable.

Obtaining the analytical derivative of the matrix  $\tilde{\mathbf{A}}(t)$  is a nontrivial process. The derivative can be numerically approximated, however, by the finite difference method<sup>23</sup>. The forward difference of a function  $f(t)$  is typically expressed as

$$\dot{f}(t) = \lim_{\Delta t \rightarrow 0} \frac{f(t + \Delta t) - f(t)}{\Delta t} \approx \frac{f(t + \Delta t) - f(t)}{\Delta t}. \quad (3.37)$$

The approximation requires the selection of some arbitrarily small  $\Delta t$  to evaluate Equation (3.37). Errors are inherent in such an approximation since a very large

$\Delta t$  might not capture the behavior close to  $t$ . However, by choosing an appropriate size for  $\Delta t$ , the computational error can be minimized to within a user set tolerance. Since the time derivative of a matrix is equivalent to the derivative of every element of the matrix, the above definition can be easily implemented to obtain  $\dot{\tilde{\mathbf{A}}}(t)$ .

The equivalence of norms permits the use of the Frobenius norm in calculating  $\delta$ . The Frobenius norm of  $\dot{\tilde{\mathbf{A}}}(t)$  is given by

$$\|\dot{\tilde{\mathbf{A}}}(t)\|_F = \sqrt{\text{trace}\left(\dot{\tilde{\mathbf{A}}}(t)^T \dot{\tilde{\mathbf{A}}}(t)\right)}. \quad (3.38)$$

The Frobenius norm of  $\dot{\tilde{\mathbf{A}}}(t)$  is calculated for a series of reference trajectories. Through an empirical process, it is found that  $\delta \approx 0.72$ . Therefore, the system is considered slowly time-varying if

$$\|\dot{\tilde{\mathbf{A}}}(t)\| \leq 0.72. \quad (3.39)$$

This corresponds to tracking a reference angular velocity,  $\boldsymbol{\omega}_r(t)$ , that itself is slowly time-varying such that the constraint in Equation (3.39) is satisfied.

Since the system satisfies the condition in Equation (3.23)-(3.24) for  $\delta \approx 0.72$ , over this range it is possible to select the controller gains  $k_p$  and  $k_v$  to ensure asymptotic stability for the *linearized* closed-loop system. The gains  $k_p$  and  $k_v$  are selected such that at each time  $t$ , the matrix  $\tilde{\mathbf{A}}(t)$  is Hurwitz and satisfies condition (3.39). Now, based on Equation (3.32), the linear control that stabilizes the nonlinear system described by Equation (3.8) and Equation (3.3b) is

$$\boldsymbol{\nu} = -k_p \mathbf{q}_{e_v} - k_v \boldsymbol{\omega}_e, \quad (3.40)$$

where the gains  $k_p$  and  $k_v$  are the same as those calculated for the linear controller in Equation (3.32). The above controller is suitable for a slowly time-varying reference angular velocity profile that satisfies the smoothness constraints in Equation (3.39).

Recall that, the total tracking control input is composed of feedforward and feedback compensators, obtained in Equation (3.7) and Equation (3.40) respectively. Thus, the net desired nonlinear tracking control is expressed as

$$\mathbf{u}(t) = -k_q \mathbf{q}_{e_v} - k_v \boldsymbol{\omega}_e + \mathbf{C}(\mathbf{q}_e) \boldsymbol{\omega}_r \times \mathbf{J} \mathbf{C}(\mathbf{q}_e) \boldsymbol{\omega}_r + \mathbf{J} \mathbf{C}(\mathbf{q}_e) \dot{\boldsymbol{\omega}}_r. \quad (3.41)$$

In Equation (3.41),  $\mathbf{u}(t)$ , provides the net control effort required to achieve zero tracking error for a spacecraft tracking a slowly time-varying  $\boldsymbol{\omega}_r(t)$  that satisfies the condition in Equation (3.39).

Thus far, stability of the closed-loop system has been examined using Lyapunov indirect method. Using this method, the control system is shown to track certain slowly-varying reference trajectories that satisfy the smoothness constraints in Equation (3.39). However, the specified constraints may be relaxed using an alternative analysis approach known as Lyapunov's direct method. As shown in the next section, using Lyapunov's direct method allows one to obtain zero tracking error for any  $\boldsymbol{\omega}_r(t)$ .

### 3.5 Lyapunov's Direct Method

In the previous section, a nonlinear tracking control law is obtained using partial feedback linearization and Lyapunov's indirect method. However, since the linearized dynamics are time-varying, using Lyapunov's indirect method allows one

to deduce asymptotic stability for the system only when the spacecraft tracks  $\boldsymbol{\omega}_r(t)$  that is slowly time-varying. In this section, the slowly time-varying requirement on  $\boldsymbol{\omega}_r(t)$  is relaxed by examining the stability of the system using Lyapunov’s direct method. This method is based on the mathematical generalization of the physical property that if the total energy of a dynamical system is continually dissipated through the system’s own internal dynamics, or through some external force, then the system eventually stabilizes to a zero energy equilibrium point. Lyapunov’s direct method<sup>5,13</sup> allows one to deduce the stability of a complex nonlinear system through the examination of a scalar “energy-like” function.

The energy function for non-autonomous systems, denoted by  $V(\mathbf{x}(t))$  where  $\mathbf{x}$  is that state of the system, must satisfy certain properties in order to assert global asymptotic stability of a system. The first property<sup>13</sup> stems from physical considerations. Specifically, since the total energy of a function is always nonzero, the energy function has the property that it is positive definite, that is,  $V > 0 \forall t$ . The second condition<sup>13</sup> states that  $V(\mathbf{x})$  is monotonically decreasing along the system trajectory, that is,  $\dot{V} < 0$ . Since  $V$  is not explicitly dependent on time<sup>5</sup>, the derivative of  $V$  can be written as

$$\dot{V} = \frac{\partial V}{\partial \mathbf{x}} \dot{\mathbf{x}} = \frac{\partial V}{\partial \mathbf{x}} f(\mathbf{x}, t), \quad (3.42)$$

where the last substitution is valid since  $\mathbf{x}(t)$  satisfies the dynamical equation  $\dot{\mathbf{x}}(t) = f(\mathbf{x}, t)$ . In this way,  $\dot{V}$  can be thought of as the directional derivative of  $V$  along the state trajectory  $\mathbf{x}(t)$ . This idea is illustrated in Figure 3.1, where the bowl-shaped isosurface represents  $V(\mathbf{x}(t))$  over the state plane  $(x_1, x_2)$ . The projection



of the state trajectory  $\mathbf{x}(t)$  on the isosurface is seen to always point down, which corresponds to a lower and lower values of  $V$ .

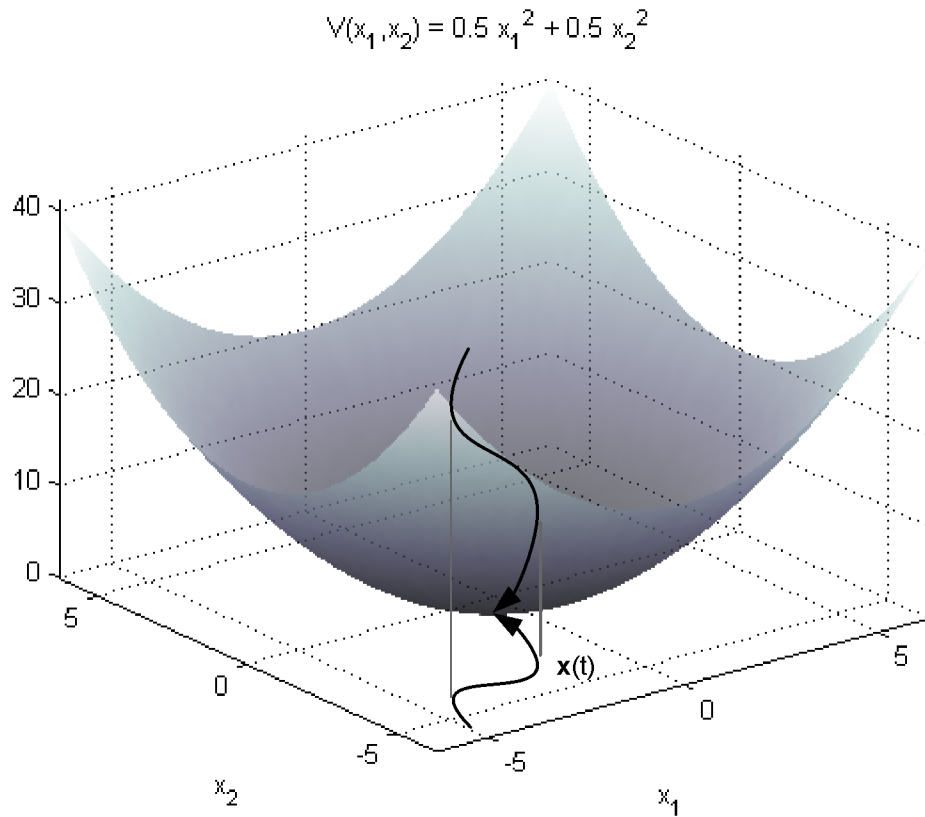


Figure 3.1: Illustration of a Lyapunov function.

If the conditions  $V > 0$  and  $\dot{V} < 0$  are satisfied, then the dynamical system is stable about the origin. In order to prove global stability, a third condition is required, which states that  $V(\mathbf{x})$  must be radially unbounded, that is  $V(\mathbf{x}) \rightarrow \infty$  as  $\mathbf{x}$  tends to infinity in any direction, that is  $\|\mathbf{x}\| \rightarrow \infty$ . For an autonomous system, these conditions are sufficient for concluding global asymptotic stability in the sense of Lyapunov. For non-autonomous systems, the scalar function must also

be decrescent; that is, it should always be upper bounded or dominated by a time-invariant positive definite function,  $V_1(\mathbf{x})$ . This condition is mathematically stated as

$$V(\mathbf{x}, t) \leq V_1(\mathbf{x}) \quad \text{and} \quad V(\mathbf{0}, t) = 0, \quad \forall t \geq 0. \quad (3.43)$$

If all of the above conditions are satisfied, then  $V(\mathbf{x}, t)$  is called a Lyapunov function and the equilibrium point at  $\mathbf{0}$  is globally uniformly asymptotically stable, that is,

$$\mathbf{x}(t) \rightarrow 0 \quad \text{as} \quad t \rightarrow \infty, \quad (3.44)$$

for any initial state values.

For a particular candidate Lyapunov function, it is possible that its derivative may not satisfy all the conditions previously stated. As it often happens,  $\dot{V}$  may only be negative *semi*-definite, i.e.  $\dot{V} \leq 0$ , rather than negative definite. If such a situation occurs in the context of autonomous systems, it is still possible to prove asymptotic stability by using La Salle's invariant set theorems<sup>13</sup>. However La Salle's invariant set theorems are not applicable to non-autonomous systems. Instead, an important mathematical result, known as Barbalat's Lemma, is invoked in order to prove asymptotic stability.

**Definition 3.1. Uniform Continuity**<sup>13,28</sup>: *A function  $f(t): \mathbb{R} \rightarrow \mathbb{R}^n$  is said to be uniformly continuous if for any given  $\epsilon > 0$ , there exists a  $\delta(\epsilon) \geq 0$  such that,*

$$\forall t, t_1 \geq 0, \quad |t - t_1| \leq \delta(\epsilon) \Rightarrow |f(t) - f(t_1)| \leq \epsilon. \quad (3.45)$$

Asserting uniform continuity of a function by using the above definition may not always be a convenient approach. A more direct approach is to examine

the function's derivative. Specifically, a sufficient condition for a function to be uniformly continuous is that its function derivative be bounded<sup>13</sup>.

**Lemma 3.1. (due to Barbalat)**<sup>13,28</sup>: *Let  $f(t): \mathbb{R} \rightarrow \mathbb{R}^n$  be differentiable and have a finite limit as  $t \rightarrow \infty$ . If  $\dot{f}(t)$  is uniformly continuous then  $\dot{f}(t) \rightarrow 0$  as  $t \rightarrow \infty$ .*

In order to apply Barbalat's lemma to the analysis of nonautonomous dynamics systems, the following immediate corollary is typically used<sup>13</sup>:

**Lemma 3.2. (Lyapunov-Like Lemma)**<sup>13,28</sup>: *If a scalar function  $V = V(\mathbf{x}, t)$  is such that*

1.  $V(\mathbf{x}, t)$  is lower bounded
2.  $\dot{V}(\mathbf{x}, t)$  is negative semi-definite
3.  $\dot{V}(\mathbf{x}, t)$  is uniformly continuous in time

*then  $\dot{V}(\mathbf{x}, t) \rightarrow 0$  as  $t \rightarrow \infty$ .*

The first two conditions imply that  $V(\mathbf{x}, t)$  approaches a finite limit. The last condition is satisfied if  $\ddot{V}$  exists and is finite. The above corollary then follows from Barbalat's lemma<sup>13</sup>. Stability analysis through Barbalat's lemma is referred to as Lyapunov-like analysis and the corresponding scalar function  $V$  is called a Lyapunov-like function. It differs from traditional Lyapunov analysis in the  $V(\mathbf{x}, t)$  is only required to be lower bounded, instead of positive definite, and  $\dot{V}$  must be negative or zero as well as uniformly continuous (i.e.,  $\ddot{V}$  exists and is bounded). Barbalat's lemma is a powerful result and is frequently used in proving asymptotic

stability of non-autonomous dynamic systems through Lyapunov-like analysis. It can also be formulated with respect to an integral of a function as shown below:

**Lemma 3.3. (due to Barbalat)**<sup>13,28</sup>: *Let  $f(t): \mathbb{R} \rightarrow \mathbb{R}^n$  be a uniformly continuous scalar or vector valued function. Suppose that  $\lim_{t \rightarrow \infty} \int_0^t f(\tau) d\tau$  exists and is finite, then  $\lim_{t \rightarrow \infty} f(t) = 0$ .*

Furthermore, an immediate and practical corollary to Barbalat's lemma stated above is given as follows:

**Corollary 3.1.** *If  $f(t)$  is bounded and absolutely integrable, that is  $f(t) \in \mathcal{L}_\infty \cap \mathcal{L}_p$  for some integer  $p \in [1, \infty)$ , and  $\dot{f} \in \mathcal{L}_\infty$  (bounded), then  $\lim_{t \rightarrow \infty} f(t) = 0$ .*

### 3.5.1 Stability Analysis using Lyapunov's Direct Method

Consider the original tracking error dynamics in the expanded form as described by Equation (3.5). In the interest of brevity, define  $\phi$  as

$$\phi = [\omega_e \times] \mathbf{J} (\omega_e + \mathbf{C}(\mathbf{q}_e) \omega_r) + \mathbf{C}(\mathbf{q}_e) [\omega_r \times] \mathbf{J} \omega_e - \mathbf{J} [\omega_e \times] \mathbf{C}(\mathbf{q}_e) \omega_r, \quad (3.46)$$

and  $\psi$  as

$$\psi = \mathbf{C}(\mathbf{q}_e) \omega_r \times \mathbf{J} \mathbf{C}(\mathbf{q}_e) \omega_r + \mathbf{J} \mathbf{C}(\mathbf{q}_e) \dot{\omega}_r. \quad (3.47)$$

Following an analysis approach to that presented in Bernstein et al.<sup>9</sup>, define a linear operator  $\mathbf{L}: \mathbb{R}^3 \rightarrow \mathbb{R}^{3 \times 6}$  acting on any vector  $\rho = [\rho_1 \ \rho_2 \ \rho_3]^T$  such that

$$\mathbf{L}(\rho) = \begin{bmatrix} \rho_1 & \rho_2 & \rho_3 & 0 & 0 & 0 \\ 0 & \rho_1 & 0 & \rho_2 & \rho_3 & 0 \\ 0 & 0 & \rho_1 & 0 & \rho_2 & \rho_3 \end{bmatrix}. \quad (3.48)$$

Furthermore, let  $\boldsymbol{\theta}$  be defined as  $6 \times 1$  vector that contains the six unique entries of the inertia-matrix,

$$\boldsymbol{\theta} = [ J_{11} \quad J_{12} \quad J_{13} \quad J_{22} \quad J_{23} \quad J_{33} ]. \quad (3.49)$$

Then,  $\boldsymbol{\psi}$  may be written as

$$\boldsymbol{\psi} = \mathbf{W}\boldsymbol{\theta}, \quad (3.50)$$

where

$$\mathbf{W} = \mathbf{C}(\mathbf{q}_e)[\boldsymbol{\omega}_r \times] \mathbf{L}(\mathbf{C}(\mathbf{q}_e)\boldsymbol{\omega}_r) + \mathbf{L}(\mathbf{C}(\mathbf{q}_e)\dot{\boldsymbol{\omega}}_r). \quad (3.51)$$

Using the definition of  $\boldsymbol{\phi}$  in Equation (3.46) and  $\boldsymbol{\psi}$  in (3.47), the tracking error dynamics in Equation ((3.5) can be expressed as

$$\mathbf{J}\dot{\boldsymbol{\omega}}_e = -\boldsymbol{\phi}(t) + \mathbf{W}\boldsymbol{\theta} + \mathbf{u}, \quad (3.52)$$

and the tracking control obtained in Equation (3.41) can be written as

$$\mathbf{u} = -k_q \mathbf{q}_{e_v} - k_v \boldsymbol{\omega}_e + \mathbf{W}\boldsymbol{\theta}. \quad (3.53)$$

Global asymptotic convergence for the control law described by Equation (3.53) is achieved using the following lower-bounded Lyapunov function candidate implemented in Wen et al.<sup>7</sup>

$$V(\boldsymbol{\omega}_e, \mathbf{q}_e) = \frac{1}{2} \boldsymbol{\omega}_e^T \mathbf{J} \boldsymbol{\omega}_e + k_p [\mathbf{q}_{e_v}^T \mathbf{q}_{e_v} + (q_{e_0} - 1)^2] - c \mathbf{q}_{e_v}^T \mathbf{J} \boldsymbol{\omega}_e, \quad (3.54)$$

where  $c$  is a scalar quantity that is chosen to be strictly negative in order to preserve the positive definiteness of  $V$ . Note that in Equation 3.54

$$k_p [\mathbf{q}_{e_v}^T \mathbf{q}_{e_v} + (q_{e_0} - 1)^2] = 2k_p [1 - q_{e_0}]. \quad (3.55)$$

The Lyapunov function candidate can be written as,

$$V = \frac{1}{2} \boldsymbol{\omega}_e^T \mathbf{J} \boldsymbol{\omega}_e + 2k_p [1 - q_{e0}] - c \mathbf{q}_{e_v}^T \mathbf{J} \boldsymbol{\omega}_e. \quad (3.56)$$

In this equation, the first term corresponds to the total error in kinetic energy as it is based on the angular velocity error signal. The second term represents the artificial error potential energy based on the vector part of the error quaternion. The last term is a product of the error angular velocity and error quaternion signals that is scaled by a constant  $c$  chosen negative so that the Lyapunov function candidate is positive definite<sup>7</sup>.

Using the results from Wen et al.<sup>7</sup>, the derivative of the Lyapunov function,  $V$  along the trajectories of the system is given by

$$\begin{aligned} \dot{V} &= \boldsymbol{\omega}_e^T \mathbf{J} \dot{\boldsymbol{\omega}}_e - 2k_p \dot{q}_{e0} - c \dot{\mathbf{q}}_{e_v}^T \mathbf{J} \boldsymbol{\omega}_e - c \mathbf{q}_{e_v}^T \mathbf{J} \dot{\boldsymbol{\omega}}_e, \\ &= \boldsymbol{\omega}_e^T (-\boldsymbol{\phi} + \mathbf{W}\boldsymbol{\theta} + \mathbf{u}) + k_p \mathbf{q}_{e_v}^T \boldsymbol{\omega}_e \\ &\quad - \left( \frac{c}{2} (q_{e0} \mathbf{I} + [\mathbf{q}_{e_v} \times]) \boldsymbol{\omega}_e \right)^T \mathbf{J} \boldsymbol{\omega}_e - c \mathbf{q}_{e_v}^T (-\boldsymbol{\phi} + \mathbf{W}\boldsymbol{\theta} + \mathbf{u}). \end{aligned} \quad (3.57)$$

Substituting the control law yields

$$\begin{aligned} \dot{V} &= \boldsymbol{\omega}_e^T (-\boldsymbol{\phi} - k_p \mathbf{q}_{e_v} - k_v \boldsymbol{\omega}_e) + k_p \mathbf{q}_{e_v}^T \boldsymbol{\omega}_e - \frac{c}{2} q_{e0} \boldsymbol{\omega}_e^T \mathbf{J} \boldsymbol{\omega}_e \\ &\quad - \frac{c}{2} (\mathbf{q}_{e_v} \times \boldsymbol{\omega}_e)^T \mathbf{J} \boldsymbol{\omega}_e - c \mathbf{q}_{e_v}^T (-\boldsymbol{\phi}(t) - k_p \mathbf{q}_{e_v} - k_v \boldsymbol{\omega}_e), \\ &= -k_v \boldsymbol{\omega}_e^T \boldsymbol{\omega}_e + c k_p \mathbf{q}_{e_v}^T \mathbf{q}_{e_v} - (\boldsymbol{\omega}_e - c \mathbf{q}_{e_v})^T \boldsymbol{\phi} + c k_v \mathbf{q}_{e_v}^T \boldsymbol{\omega}_e \\ &\quad - \frac{c}{2} q_{e0} \boldsymbol{\omega}_e^T \mathbf{J} \boldsymbol{\omega}_e - \frac{c}{2} (\mathbf{q}_{e_v} \times \boldsymbol{\omega}_e)^T \mathbf{J} \boldsymbol{\omega}_e, \\ &\leq c k_p \|\mathbf{q}_{e_v}\|^2 - (k_v - \gamma_J \gamma_d - \gamma_J c) \|\boldsymbol{\omega}\|^2, \end{aligned} \quad (3.58)$$

where,

$$\gamma_J \triangleq \|\mathbf{J}\|, \quad (3.59)$$

$$\gamma_d \triangleq \sup_{t \geq 0} \|\mathbf{C}(\mathbf{q}_e) \boldsymbol{\omega}_r(t)\|. \quad (3.60)$$

If  $k_v$  satisfies the condition

$$k_v > \gamma_J \gamma_d, \quad (3.61)$$

and  $c$  is chosen such that

$$c < 0, \quad (3.62)$$

then  $\dot{V} \leq 0$ . As  $c$  does not appear in the control law, it can be arbitrarily chosen to satisfy the condition in Equation (3.62) and for the property  $V > 0$  to hold. With the above assumptions, it can be shown<sup>7</sup> that  $\mathbf{q}_{e_v}$  and  $\boldsymbol{\omega}_e$  are uniformly bounded, and hence  $V$  is uniformly bounded. Furthermore, it can be shown that  $\mathbf{q}_{e_v}$  and  $\boldsymbol{\omega}_e$  are uniformly continuous<sup>7</sup> since  $\dot{\mathbf{q}}_{e_v}$  and  $\dot{\boldsymbol{\omega}}_e$  are also uniformly bounded (from the differential equations of motion). Then by using Barbalat's theorem, it follows that

$$\lim_{t \rightarrow \infty} \begin{bmatrix} \mathbf{q}_e(t) \\ \boldsymbol{\omega}_e(t) \end{bmatrix} = 0. \quad (3.63)$$

### 3.5.2 Robustness to Plant Perturbations

In this section, the robustness of the inertia parameters to small perturbations is analyzed. As shown in Wen et al.<sup>7</sup>, an additional condition can be imposed to ensure exponential convergence of  $V$  to zero. Specifically,

$$\frac{1}{2} \boldsymbol{\omega}_e^T(0) \mathbf{J} \boldsymbol{\omega}_e(0) < 2k_p(1 + q_0(0)). \quad (3.64)$$

The exponential convergence of  $V$  leads to robustness to variations in the inertia matrix. If the inertia  $\mathbf{J}$  in the control law is perturbed from its true value, that is,

$$\mathbf{J} = \mathbf{J}_{true} + \Delta \mathbf{J}, \quad (3.65)$$

the system remains uniformly ultimate bounded<sup>7</sup> where the bound is linear in the size of the normed inertia error.

### 3.6 Control Magnitude Constraints

The feedback control law in Equation (3.41) was developed without consideration of control magnitude constraints. Actuation devices such as thrusters and reaction wheels, are subject to physical limitations and constraints. When the actuation device is operating at its maximum capacity, it is said to be saturated<sup>5</sup>. This section augments the existing tracking control law to incorporate saturation constraints while ensuring global asymptotic stability.

The problem of control torque saturation can be solved in essentially two different ways. The first is to use conventional gain scheduling and deadband methods to reduce the feedback gains such that all control torques remain in the unsaturated range. However, a major practical limitation of this method is that it introduces discontinuities in the control history, leading to a degraded overall performance of the feedback control law. An alternate method, known as Lyapunov optimal control, allows individual control devices to become saturated while others are within the saturation bounds. The saturated control law is said to be Lyapunov optimal because it makes the derivative of the Lyapunov function as negative as possible for periods when at least one control device is saturated<sup>5</sup>.

The unsaturated control law that stabilizes the error states is given by

$$\mathbf{u} = -k_q \mathbf{q}_{e_v} - k_v \boldsymbol{\omega}_e + \mathbf{C}(\mathbf{q}_e) \boldsymbol{\omega}_r \times \mathbf{J} \mathbf{C}(\mathbf{q}_e) \boldsymbol{\omega}_r + \mathbf{J} \mathbf{C}(\mathbf{q}_e) \dot{\boldsymbol{\omega}}_r. \quad (3.66)$$



The derivative of the corresponding Lyapunov function can be expressed as

$$\begin{aligned} \dot{V} = & \boldsymbol{\omega}_e^T \left( -\boldsymbol{\phi}(t) + \mathbf{W}\boldsymbol{\theta} + \mathbf{u} + k_p \mathbf{q}_{e_v} - \frac{c}{2} \mathbf{J}\boldsymbol{\omega}_e^T (q_0 \mathbf{I} + [\mathbf{q}_{e_v} \times]) \right) - \\ & c \mathbf{q}_{e_v}^T (-\boldsymbol{\phi} + \mathbf{W}\boldsymbol{\theta} + \mathbf{u}) - \beta \left( \frac{1}{2} q_0^T \boldsymbol{\omega}_e + \mathbf{q}_{e_v} \times \boldsymbol{\omega}_e \right)^T \mathbf{J}\boldsymbol{\omega}_e \\ & - c \mathbf{q}_{e_v}^T (-\boldsymbol{\phi}(t) + \mathbf{W}\boldsymbol{\theta} + \mathbf{u}). \end{aligned} \quad (3.67)$$

Assume that the control authority exerted about the  $i^{\text{th}}$  body axis has an upper bound  $|u_i(t)| < u_{\max_i}$ . Under the above assumption, the unsaturated control law  $\mathbf{u}$  can be modified to account for saturation with a Lyapunov optimal saturated term as shown by Robinett et al<sup>5,30</sup>. The modified control law  $\mathcal{S}(\mathbf{u}(t))$  for  $i = 1, 2, 3$  is

$$\mathcal{S}(u_i) = \begin{cases} u_i & \text{for } |u_i| \leq u_{\max_i} \\ u_{\max_i} \cdot \text{sgn}(u_i) & \text{for } |u_i(t)| > u_{\max_i} \end{cases}. \quad (3.68)$$

The “sgn” denotes the mathematical signum function that extracts the sign of a real number and is defined by

$$\text{sgn}(x) = \begin{cases} -1 & \text{if } x < 0 \\ 0 & \text{if } x = 0 \\ 1 & \text{if } x > 0 \end{cases}. \quad (3.69)$$

A useful feature of the saturation control logic in Equation (3.68) is that it allows some elements of the control vector to become saturated while others remain in the unsaturated range. This feature differs from conventional gain scheduling<sup>5</sup> where the feedback gains are adjusted so that all elements of the control vector operate in the unsaturated region. Note that if the optimal saturated term  $u_{\max_i} \cdot \text{sgn}[u_i(t)]$  is implemented directly, then the resulting control law would have a bang-bang characteristic which produces a discontinuity at the origin as shown in Figure (3.2). Such a discontinuity is highly undesirable as it induces chattering at  $u_i(t) = 0$ <sup>5,30</sup>. However, a limitation of the saturation control in Equation (3.68) is that it retains

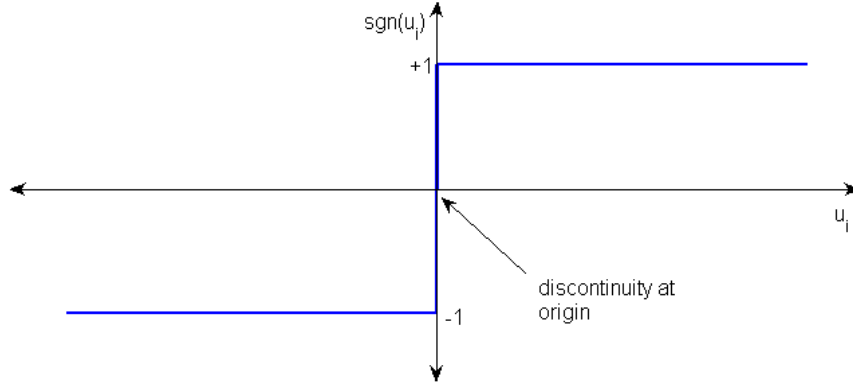


Figure 3.2: Direct implementation of the optimal saturated term  $u_{\max_i} \cdot \text{sgn}[u_i(t)]$  results in band-bang characteristics.

a sharp corner when  $|u_i| = u_{\max_i}$ , which leads to non-uniqueness of the control rate  $\dot{\mathbf{u}}$ . In order to smooth the transition across the saturation boundary, the hyperbolic tangent function,  $\tanh$ , can be implemented to approximate the saturated control profile<sup>20</sup>. The range of the  $\tanh$  function is  $[-1, 1]$  on the domain  $(-\infty, \infty)$ . As illustrated in Figure 3.3, the  $\tanh$  function takes on the values

$$\begin{aligned} \tanh(x) &\approx -1, & \forall x < -2, \\ \tanh(x) &\approx 1, & \forall x > 2, \end{aligned}$$

with a maximum approximation error of  $\pm 0.036$  near  $x = \pm 2$ , and has a slope of 1 at the origin<sup>20</sup>. Using the  $\tanh$  function, the saturated control law can be expressed as

$$\mathcal{S}(u_i) = u_{\max_i} \cdot \tanh\left(\frac{u_i}{u_{\max_i}}\right), \quad \text{for } i = 1, 2, 3, \quad (3.70)$$

where the scaling factor  $1/u_{\max_i}$  is needed to appropriately track the signum function<sup>20</sup>.

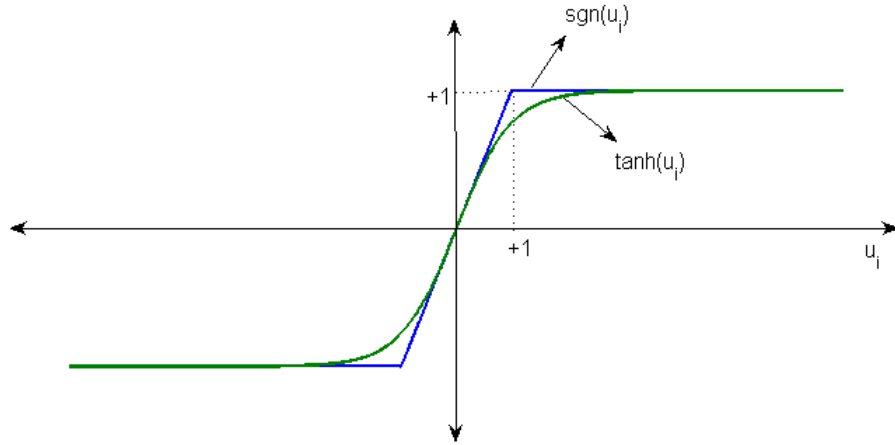


Figure 3.3: Using the hyperbolic tangent function to smooth the transition across saturation boundary.

An inherent assumption for saturated control development is that the problem must be feasible. In other words, there must be enough control authority to track the desired trajectory motion. From the Lyapunov function derivative, a sufficient condition to ensure feasibility (and stability) is found to be

$$\max \left( \|\phi(t) - \mathbf{W}\theta - k_p \mathbf{q}_{e_v} + \frac{c}{2} \mathbf{J}\boldsymbol{\omega}_e^T (q_{0_e} \mathbf{I} + [\mathbf{q}_{e_v} \times])\|, \|\phi - \mathbf{W}\theta\| \right) \leq u_{\max_i}. \quad (3.71)$$

The feasibility constraint may be overly conservative for a higher-dimensional systems such as the spacecraft tracking problem. It is clear, then, that the condition is immediately violated if any body axis fails to satisfy the strict equality. As demonstrated in the numerical simulation in Section 3.7, having  $u_{\max_i}$  less than the sufficient feasibility condition may still lead to asymptotically stable closed-loop behavior. The stability condition in Equation (3.71) might be locally violated, making

$\dot{V} > 0$  for brief periods of time without affecting overall global stability.

### 3.7 Design Examples

In this section, various attitude maneuver simulations are presented to demonstrate the capabilities of the control law developed in Section 3.2-3.6. All simulations were conducted using MATLAB Simulation Software. Runge-Kutta 4(5) numerical integrator, ODE45, was used to propagate the differential equations with both the absolute and relative tolerances set to  $10^{-6}$ .

#### Spacecraft Initial Conditions

The numerical model for the attitude tracking control system is based on the system parameters of FASTRAC. The inertia matrix,  $\mathbf{J}$ , that approximates the nanosatellite is given by,

$$\mathbf{J} = \begin{bmatrix} 0.656 & 0 & 0 \\ 0 & 0.656 & 0 \\ 0 & 0 & 0.986 \end{bmatrix} \text{ kg}\cdot\text{m}^2. \quad (3.72)$$

The spacecraft is assumed to be initially at rest. The spacecraft initial conditions are

$$\begin{aligned} \mathbf{q}(0) &= [ 0.9487, 0.1826, 0.1826, 0.18268, ]^T, \\ \boldsymbol{\omega}(0) &= [ 0, 0, 0 ]^T \text{ rad/s.} \end{aligned}$$

The thruster actuation system is assumed to be upper bound in each body-axis by  $u_{\max_i} = 0.5 \text{ N}\cdot\text{m}$  for  $i = 1, 2, 3$ .

## Simulation Parameters

The reference initial quaternion is

$$\mathbf{q}_r(0) = [ 1, 0, 0, 0 ]^T. \quad (3.73)$$

and the reference angular velocity profile is updated at each simulation time. The controller gains are set to  $k_p = 5$  and  $k_v = 8$ .

Each set of simulations is performed for two types of attitude trajectories: one that is periodic and has large variations in its angular velocity profile, and another that contains exponentially decaying terms that attenuate the amount of variation in the signal. The signal with large variation is referred to as a persistently exciting (PE) signal, whereas the signal with little variation is referred to as a non-persistently exciting (non-PE) signal. Generally speaking, a PE signal is one that produces enough excitation in a system to uniquely identify the system's parameters. PE signals will be formally defined in the context of adaptive control in Chapter 5, where their implication in unique system identifiability plays a crucial role in parameter estimation. For now, the terms "PE" and "non-PE" are simply used to distinguish between the two angular velocity profiles. The exponentially decaying reference angular velocity signal is referred to as a non-PE signal for the system.

Numerical simulations are performed for the following scenarios:

1. Ideal, no saturation and no inertia perturbations
2. Control saturation
3. Control saturation and inertia perturbations

The first scenario is used as the nominal case for comparison. The simulation period is 40 seconds for each attitude tracking scenario. For the second scenario, torque limits are imposed on the control profile, limiting the output to

$$u_{\max_i} = 0.5 \text{ N} \cdot \text{m} \quad i = 1, 2, 3, \quad (3.74)$$

and the system is simulated using the saturated control law described in Equation (3.70). Finally, the inertia  $\mathbf{J}$  in the control law is perturbed from its true value, that is,

$$\mathbf{J} = \mathbf{J}_{true} + \Delta\mathbf{J}, \quad (3.75)$$

and the system is simulated again with torque limits imposed. The performance of the controller is examined for  $\Delta\mathbf{J} = 0.3 \mathbf{J}_{true}$ ; that is, a 30% deviation from the inertia parameters under control torque limits. The control gains and spacecraft initial conditions are kept the same for all three simulation scenarios.

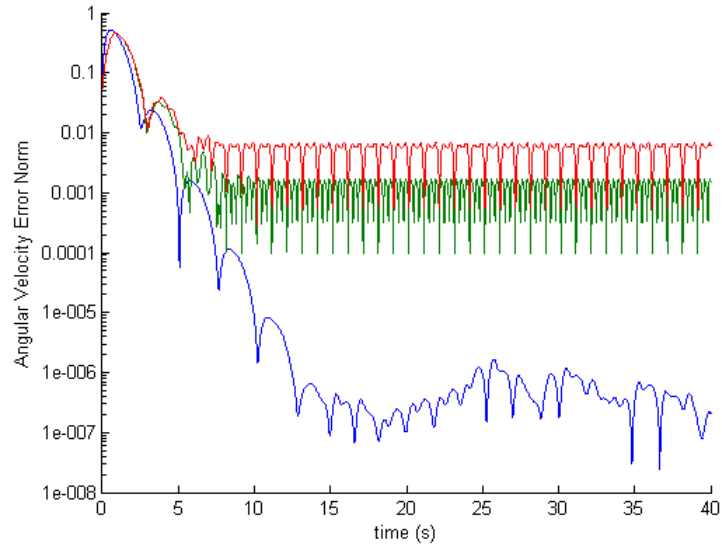
### PE Trajectory

For the first set of simulations, the PE signal is considered, where the reference angular velocity profile is generated by

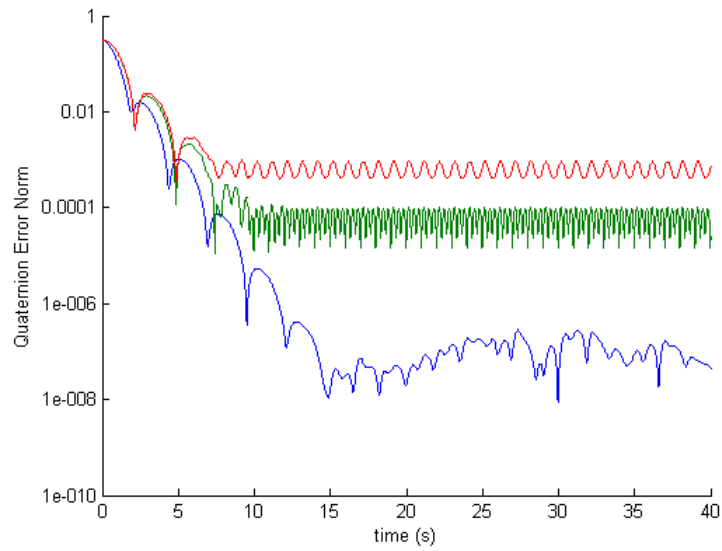
$$\boldsymbol{\omega}_r = 0.02 \left[ \cos(\pi t), \cos(2\pi t), \cos(3\pi t) \right]^T \text{ rad/s}. \quad (3.76)$$

The spacecraft initial conditions, reference quaternion and control gains are as stated previously. Figure 3.4a and Figure 3.4b illustrate the evolution of the error states, wherein the ideal response is indicated by the blue line, the saturated control response by the green line, and the performance of the system with inertia perturbations and torque constraints is indicated by the red line. The color identity is

consistent for Figures 3.4c - 3.4f. Starting from an initial angular velocity error of about 2 deg/s the saturated control law is able to drive the errors below 0.0573 deg/s when there is no disturbance in the plant parameters. As illustrated by Figure 3.4f, the maximum torque value  $u_{\max_i} = 0.5$  does not satisfy the stability condition in Equation (3.71), thus violating the requirement of  $\dot{V}$  being negative semi-definite for finite periods of time. There is noticeable performance degradation when the controller faces uncertainty in the plant inertia parameters. The error states remain bounded near 0.6 deg/s, indicating that the closed-loop performance is offset by almost 30% from the case of the saturated control law with no uncertainty. The settling time for both cases is approximately 5-6 seconds.



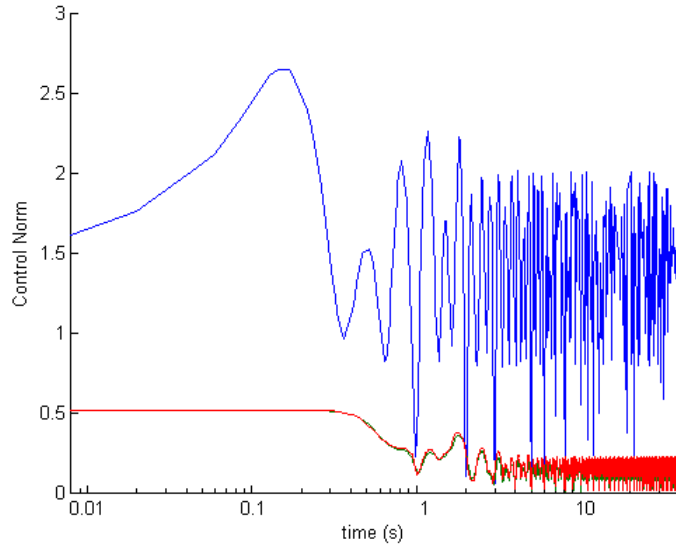
(a) Norm of the angular velocity error vector  $\|\omega_e\|$ .



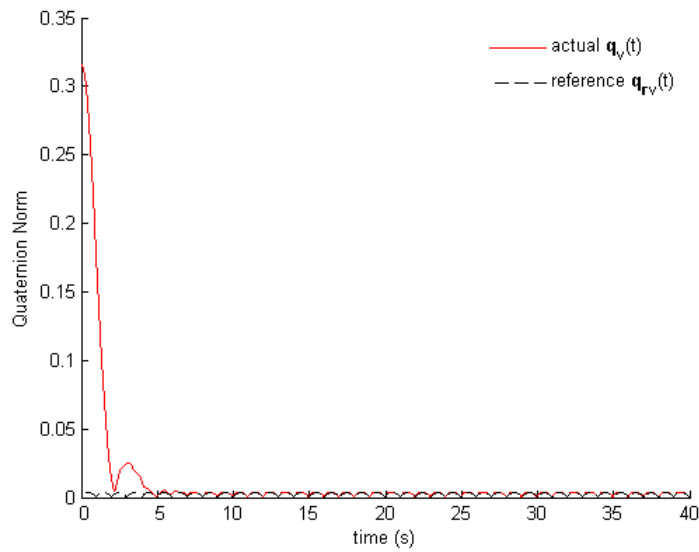
(b) Norm of the quaternion error vector  $\|\mathbf{q}_{e_v}\|$ .

Figure 3.4



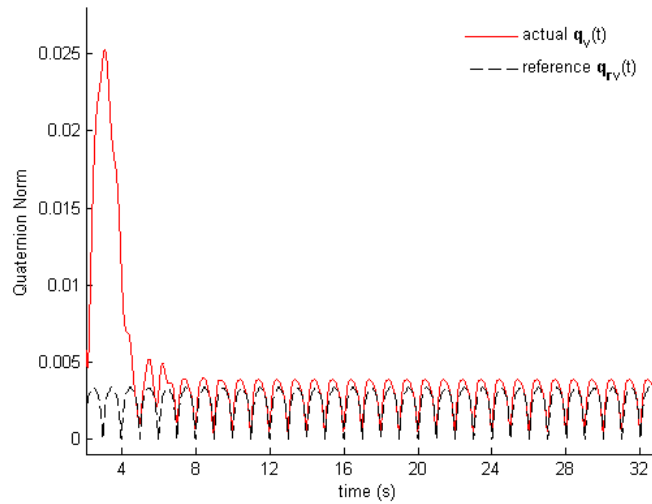


(c) Norm of the control vector  $\|\mathbf{u}\|$  in N·m

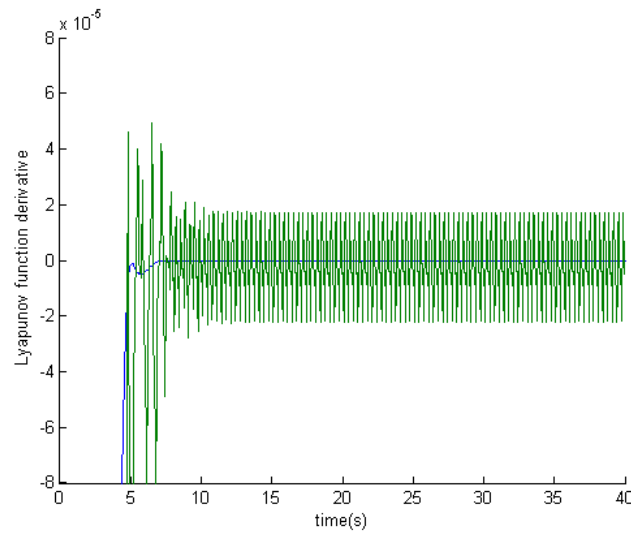


(d) Reference attitude trajectory following of perturbed plant with (30%) uncertainty in inertia parameters.

Figure 3.4



(e) Zoomed-in view of Figure 3.2d



(f) Lyapunov function derivative of saturated control system (green) indicating finite time periods where the stability condition in Equation (3.71) is violated.

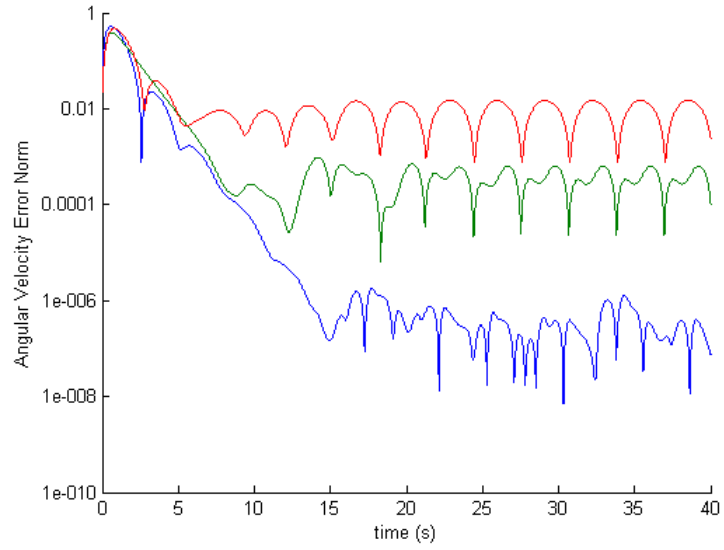
Figure 3.4: Nonlinear tracking control law simulation for a PE reference trajectory. Simulations demonstrate ideal system response (blue), system response with torque constraints (green), and system response with torque constraints and inertia perturbations (red).

## Non-PE Trajectory

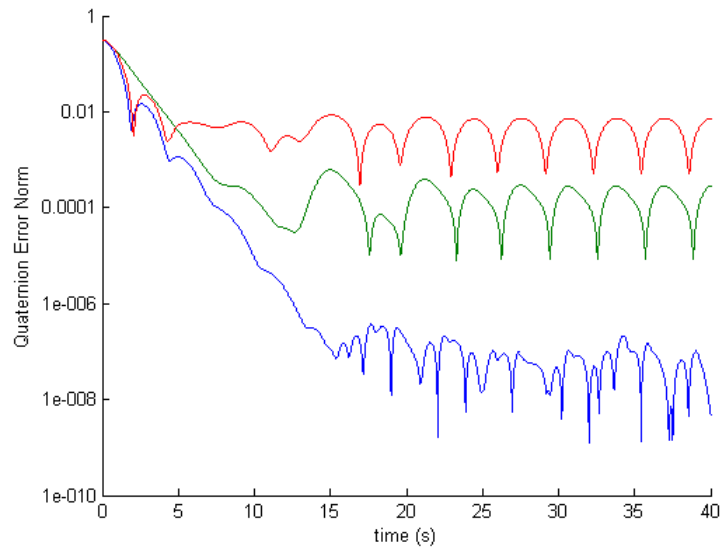
Next, the system is simulated to track a non-PE reference trajectory that has an angular velocity profile described by

$$\boldsymbol{\omega}_r = 0.1 \cos(t)(1 - e^{0.01t^2}) + (0.08\pi + 0.006 \sin(t))te^{-0.01t^2} [ 1, 1, 1, ]^T \text{ rad/s} \quad (3.77)$$

The same initial controller and estimator gain values as the non-decaying reference trajectory are used. As before, the ideal response is indicated by the blue line, the saturated control response by the green line, and the response of the system with inertia perturbations and torque constraints is indicated by the red line. Figures 3.5a and 3.5b show that the error states have slower convergence than the PE-trajectory tracking case, settling at approximately 12-13 seconds. As before, there is noticeable performance degradation when there is uncertainty in the inertia parameters. As illustrated in Figure 3.5c, the initial transient of the control history indicates that the saturated control operates at the saturation boundary for roughly 0.5 seconds, beyond which its profile is matched with the ideal case. Figure 3.5d indicates that the saturated control system is once again operating below the feasibility (stability) requirement, thereby violating the requirement of  $\dot{V}$  being negative semi-definite.

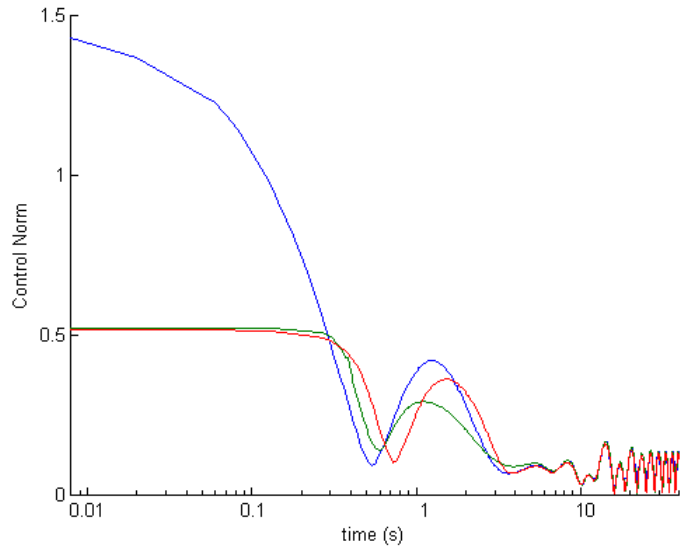


(a) Norm of Angular velocity error vector  $\|\omega_e\|$

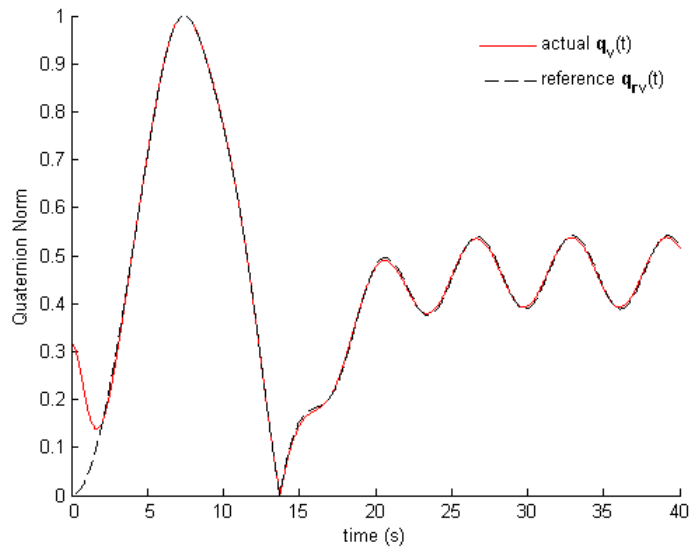


(b) Norm of quaternion error vector  $\|q_{e_v}\|$

Figure 3.5

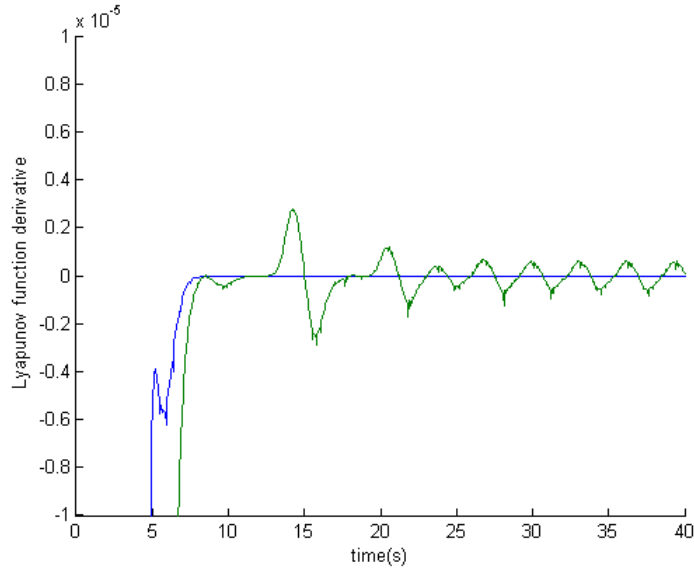


(c) Norm of control vector  $\|\mathbf{u}\|$  in N·m



(d) Reference attitude trajectory following of perturbed plant with (30%) uncertainty in inertia parameters.

Figure 3.5



(e) Lyapunov function derivative of saturated control system (green) indicating finite time periods where the stability condition in Equation (3.71) is violated.

Figure 3.5: Nonlinear tracking control law simulation for a non-PE reference trajectory. Simulations demonstrate ideal system response (blue), system response with torque constraints (green), and system response with torque constraints and inertia perturbations (red).

### 3.8 Summary

A nonlinear control law is obtained for spacecraft attitude tracking maneuvers using partial feedback linearization and Jacobian linearization concepts from linear control theory. Stability analysis using Lyapunov’s indirect method is found to be limiting for the spacecraft error dynamics due to the strong nonlinearities inherent in the system. The limitations leads to the analysis of the system using Lyapunov’s direct method and Barbalat’s lemma, which is not restricted to small motions around equilibrium points. Using this approach, the nonlinear control law

is found to be globally stabilizing without the previous restrictions on the class of reference trajectories.

Additional sufficient conditions are imposed on the feedback gains to make the system naturally robust to perturbations in the inertia parameter. Control torque limitations are taken into consideration. The unsaturated control design is augmented with a Lyapunov optimal term so that the modified control law continuously transitions across the saturation boundary. MATLAB simulations are provided to demonstrate the performance of the unsaturated and saturated control design with and without perturbations in the inertia parameter. The overall performance of the saturated controller begins to degrade undesirably when the inertia parameters are perturbed more than 30% from their true values. For a PnP satellite environment, where arbitrarily large inertia uncertainties are a practical design consideration, performance degradation of the control law formulation due to small inertia perturbations is highly undesirable. The results suggest the need for an adaptive control law formulation that can adjust to uncertain or unknown parameters and maintain consistent performance of the spacecraft system.

## Chapter 4

### Nonlinear Control Design Based on Lyapunov's Direct Method

In the previous chapter, a Lyapunov direct method was introduced as a tool to assess the stability of the nonlinear system to some prespecified model-dependent stabilizing control. In this chapter, a Lyapunov direct method is applied in the design of a globally stabilizing controller for the spacecraft tracking error dynamics. In addition, filter state variables are introduced in aiding the design of the control system. The filter control design is introduced in this chapter as it will be implemented in Chapter 5 as well. The resulting control law is dependent on the model structure and delivers high tracking performance. Torque constraints are incorporated using a similar construction as shown in Chapter 3.

#### 4.1 Nonlinear Tracking Control Using Filter Variables

Consider the spacecraft tracking error equations of motion derived in Chapter 2 and described by

$$\mathbf{J}\dot{\boldsymbol{\omega}}_e = -\boldsymbol{\omega} \times \mathbf{J}\boldsymbol{\omega} + \mathbf{u} - \mathbf{J}[\mathbf{C}(\mathbf{q}_e)\dot{\boldsymbol{\omega}}_r - \boldsymbol{\omega}_e \times \mathbf{C}(\mathbf{q}_e)\boldsymbol{\omega}_r], \quad (4.1a)$$

$$\dot{\mathbf{q}}_e = \frac{1}{2}\mathbf{E}(\mathbf{q}_e)\boldsymbol{\omega}_e. \quad (4.1b)$$



Equation (4.1a) can be rearranged such that

$$\dot{\boldsymbol{\omega}}_e = \mathbf{J}^{-1}[\mathbf{u} - [\boldsymbol{\omega} \times] \mathbf{J} \boldsymbol{\omega} - \mathbf{J} \boldsymbol{\phi}], \quad (4.2)$$

where the quantity  $\boldsymbol{\phi}(t)$  is given by

$$\boldsymbol{\phi}(t) = (\mathbf{C}(\mathbf{q}_e) \dot{\boldsymbol{\omega}}_r - [\boldsymbol{\omega}_e \times] \mathbf{C}(\mathbf{q}_e) \boldsymbol{\omega}_r). \quad (4.3)$$

For the sake of brevity, Equation (4.2) is stated in terms of the vector  $\boldsymbol{\nu}$  as

$$\dot{\boldsymbol{\omega}}_e = \mathbf{J}^{-1} \boldsymbol{\nu}, \quad (4.4)$$

where  $\boldsymbol{\nu}$  is characterized by

$$\boldsymbol{\nu} = \mathbf{u} - [\boldsymbol{\omega} \times] \mathbf{J} \boldsymbol{\omega} - \mathbf{J} \boldsymbol{\phi}. \quad (4.5)$$

Define the following first order filter variables<sup>28</sup>

$$\dot{\boldsymbol{\omega}}_{e_f} = -\beta \boldsymbol{\omega}_{e_f} + \boldsymbol{\omega}_e, \quad (4.6)$$

$$\dot{\boldsymbol{\nu}}_f = -\beta \boldsymbol{\nu}_f + \boldsymbol{\nu}, \quad (4.7)$$

where  $\beta$  is a filter gain that regulates the response of the filter to the state variables. The initial values of the filter states,  $\boldsymbol{\omega}_{e_f}(0)$  and  $\boldsymbol{\nu}_f(0)$  are selected arbitrarily. Differentiating the filter dynamics in Equation (4.6), and making appropriate substitutions for  $\dot{\boldsymbol{\omega}}_e$  and  $\boldsymbol{\nu}$  along Equation (4.4) and Equation (4.7) one obtains

$$\begin{aligned} \ddot{\boldsymbol{\omega}}_{e_f} &= -\beta \dot{\boldsymbol{\omega}}_{e_f} + \dot{\boldsymbol{\omega}}_e, \\ &= -\beta \dot{\boldsymbol{\omega}}_{e_f} + \mathbf{J}^{-1} \boldsymbol{\nu}, \\ &= -\beta \dot{\boldsymbol{\omega}}_{e_f} + \mathbf{J}^{-1} (\dot{\boldsymbol{\nu}}_f + \beta \boldsymbol{\nu}_f). \end{aligned} \quad (4.8)$$

The above expression can be further rearranged so that the following perfectly integrable first order differential equation is established

$$\frac{d}{dt}[\dot{\boldsymbol{\omega}}_{e_f} - \mathbf{J}^{-1}\boldsymbol{\nu}_f] = -\beta(\dot{\boldsymbol{\omega}}_{e_f} - \mathbf{J}^{-1}\boldsymbol{\nu}_f). \quad (4.9)$$

The solution to the Equation (4.9) is obtained by separating and integrating both sides to obtain

$$\dot{\boldsymbol{\omega}}_{e_f} = \mathbf{J}^{-1}\boldsymbol{\nu}_f + \boldsymbol{\varepsilon}e^{-\beta t}, \quad (4.10)$$

where the coefficient,  $\boldsymbol{\varepsilon}$ , of the exponentially decaying term  $\boldsymbol{\varepsilon}e^{-\beta t}$  is characterized by the initial conditions of the filtered signals

$$\boldsymbol{\varepsilon} = \dot{\boldsymbol{\omega}}_{e_f}(0) - \mathbf{J}^{-1}\boldsymbol{\nu}_f(0). \quad (4.11)$$

Since the initial conditions of the filtered states may be arbitrarily chosen, Equation (4.10) is simplified by setting  $\boldsymbol{\varepsilon} = 0$ . Thus,

$$\dot{\boldsymbol{\omega}}_{e_f} = \mathbf{J}^{-1}\boldsymbol{\nu}_f \quad (4.12)$$

represents the transformation of the tracking error dynamics of Equation (4.2) using the filter state variables in Equation (4.6). The stability characteristics of  $\boldsymbol{\omega}_e$  are conserved in  $\boldsymbol{\omega}_{e_f}$  in that both signals have an identical construction and converge to zero as  $t \rightarrow \infty$ . Since the additional terms introduced due to the filtering are exponentially decaying, they may simply be ignored in the analysis of the system stability.

Suppose the filtered signal,  $\boldsymbol{\nu}_f$ , and its corresponding dynamics are described

as follows

$$\boldsymbol{\nu}_f = -\mathbf{J} [k_p \mathbf{q}_{e_v} + k_v \boldsymbol{\omega}_{e_f}], \quad (4.13)$$

$$\dot{\boldsymbol{\nu}}_f = -\mathbf{J} [k_p \dot{\mathbf{q}}_{e_v} + k_v \dot{\boldsymbol{\omega}}_{e_f}], \quad (4.14)$$

where  $k_p$  and  $k_v$  are any positive scalars. Substituting Equation (4.13) into the filter dynamics of Equation (4.10) yields

$$\dot{\boldsymbol{\omega}}_{e_f} = \mathbf{J}^{-1} \mathbf{J} [-k_p \mathbf{q}_{e_v} - k_v \boldsymbol{\omega}_{e_f}] = -k_p \mathbf{q}_{e_v} - k_v \boldsymbol{\omega}_{e_f}. \quad (4.15)$$

The stability of the system in Equation (4.15) can be examined through Lyapunov direct method. Consider the following strict (radially unbounded and decrescent) Lyapunov function candidate

$$V = \frac{1}{2} \boldsymbol{\omega}_{e_f}^T \boldsymbol{\omega}_{e_f} + [\mathbf{q}_{e_v}^T \mathbf{q}_{e_v} + (q_{e_0} - 1)^2]. \quad (4.16)$$

Recall from Chapter 3 that

$$[\mathbf{q}_{e_v}^T \mathbf{q}_{e_v} + (q_{e_0} - 1)^2] = 2[1 - q_{e_0}],$$

which can be substituted into Equation (4.16) to obtain

$$V = \frac{1}{2} \boldsymbol{\omega}_{e_f}^T \boldsymbol{\omega}_{e_f} + 2[1 - q_{e_0}]. \quad (4.17)$$

Recall from Chapter 2 that

$$\dot{q}_{e_0} = -\frac{1}{2} \mathbf{q}_{e_v}^T \boldsymbol{\omega},$$

which can be used to express the derivative of  $V$  as

$$\begin{aligned} \dot{V} &= \boldsymbol{\omega}_{e_f}^T \dot{\boldsymbol{\omega}}_{e_f} + \mathbf{q}_{e_v}^T \boldsymbol{\omega}_e, \\ &= \boldsymbol{\omega}_{e_f}^T \dot{\boldsymbol{\omega}}_{e_f} + \mathbf{q}_{e_v}^T (\dot{\boldsymbol{\omega}}_{e_f} + \beta \boldsymbol{\omega}_{e_f}). \end{aligned} \quad (4.18)$$

Substituting Equation (4.15) into Equation (4.18) results in

$$\dot{V} = \beta \mathbf{q}_{e_v}^T \boldsymbol{\omega}_{e_f} - k_v \boldsymbol{\omega}_{e_f}^T \boldsymbol{\omega}_{e_f} - k_p \mathbf{q}_{e_v}^T \mathbf{q}_{e_v} - (k_p + k_v) \mathbf{q}_{e_v}^T \boldsymbol{\omega}_{e_f}. \quad (4.19)$$

Choosing  $\beta = k_p + k_v$  allows the above expression to be simplified through term cancellation, thus yielding

$$\dot{V} = -k_v \|\boldsymbol{\omega}_{e_f}\| - k_p \|\mathbf{q}_{e_v}\| \leq 0, \quad (4.20)$$

which is strictly negative definite. Thus, from Lyapunov analysis it can be shown that  $\boldsymbol{\omega}_{e_f} \rightarrow 0$  and  $\mathbf{q}_{e_v} \rightarrow 0$  as  $t \rightarrow 0$ . Since  $\boldsymbol{\omega}_{e_f}$  is related to  $\boldsymbol{\omega}_e$  through a stable first order filter, one may conclude that  $\boldsymbol{\omega}_{e_f} \rightarrow 0$  indicates that  $\boldsymbol{\omega}_e \rightarrow 0$ .

The dynamics of the original controller  $\mathbf{u}$  can now be recovered from Equation (4.5). The control is described by

$$\mathbf{u} = \boldsymbol{\nu} + [\boldsymbol{\omega} \times] \mathbf{J} \boldsymbol{\omega} - \mathbf{J} \boldsymbol{\phi}. \quad (4.21)$$

Rewriting  $\boldsymbol{\nu}$  in terms of its filter states as described in Equation (4.7), and performing the appropriate substitutions for  $\boldsymbol{\nu}_f$  and  $\dot{\boldsymbol{\nu}}_f$  in terms of Equation (4.13), the expression above can be stated as

$$\begin{aligned} \mathbf{u} &= \dot{\boldsymbol{\nu}}_f + \beta \boldsymbol{\nu}_f + [\boldsymbol{\omega} \times] \mathbf{J} \boldsymbol{\omega} - \mathbf{J} \boldsymbol{\phi}, \\ &= -\mathbf{J}[k_p \dot{\mathbf{q}}_{e_v} + k_v \dot{\boldsymbol{\omega}}_{e_f}] - \beta \mathbf{J}[k_p \mathbf{q}_{e_v} + k_v \boldsymbol{\omega}_{e_f}] + [\boldsymbol{\omega} \times] \mathbf{J} \boldsymbol{\omega} - \mathbf{J} \boldsymbol{\phi}, \\ &= -k_p \mathbf{J} \dot{\mathbf{q}}_{e_v} - \mathbf{J} k_v (-\beta \boldsymbol{\omega}_{e_f} + \boldsymbol{\omega}_e) - \beta \mathbf{J}(k_p \mathbf{q}_{e_v} \\ &\quad + k_v \boldsymbol{\omega}_{e_f}) + [\boldsymbol{\omega} \times] \mathbf{J} \boldsymbol{\omega} - \mathbf{J} \boldsymbol{\phi}. \end{aligned} \quad (4.22)$$

Recognizing once again that  $\dot{\mathbf{q}}_{e_v} = \frac{1}{2} q_{0e} \mathbf{I} + [\mathbf{q}_{e_v} \times]$ , and performing term expansion results in

$$\begin{aligned} \mathbf{u} &= \frac{-k_p \mathbf{J}}{2} (q_{0e}^T \mathbf{I} + [\mathbf{q}_{e_v} \times]) \boldsymbol{\omega}_e + \mathbf{J} k_v \beta \boldsymbol{\omega}_{e_f} - \mathbf{J} k_v \boldsymbol{\omega}_e \\ &\quad - \beta \mathbf{J} k_p \mathbf{q}_{e_v} - \mathbf{J} k_v \beta \boldsymbol{\omega}_{e_f} + [\boldsymbol{\omega} \times] \mathbf{J} \boldsymbol{\omega} - \mathbf{J} \boldsymbol{\phi}. \end{aligned} \quad (4.23)$$

In the equation above, the second and fifth terms cancel and the control torque is recovered in terms of the state variables as

$$\mathbf{u} = \frac{-k_p \mathbf{J}}{2} (q_{0e}^T \mathbf{I} + [\mathbf{q}_{e_v} \times]) \boldsymbol{\omega}_e - \mathbf{J} k_v \boldsymbol{\omega}_e - \beta \mathbf{J} k_p \mathbf{q}_{e_v} + [\boldsymbol{\omega} \times] \mathbf{J} \boldsymbol{\omega} + \mathbf{J} \boldsymbol{\phi}. \quad (4.24)$$

The control torque in Equation (4.24) is clearly dependent on the model structure, that is, the unknown inertia parameters.

## 4.2 Control Magnitude Constraints

Let the control law derived in Equation (4.24) be denoted as  $\mathbf{u}_{\text{us}}$ , indicating that it is the unsaturated control law.

$$\mathbf{u}_{\text{us}} = \frac{-k_p \mathbf{J}}{2} (q_{0e}^T \mathbf{I} + [\mathbf{q}_{e_v} \times]) \boldsymbol{\omega}_e - \mathbf{J} k_v \boldsymbol{\omega}_e - \beta \mathbf{J} k_p \mathbf{q}_{e_v} + [\boldsymbol{\omega} \times] \mathbf{J} \boldsymbol{\omega} + \mathbf{J} \boldsymbol{\phi}. \quad (4.25)$$

As shown in Chapter 3, the unsaturated control law  $\mathbf{u}_{\text{us}}$  can be modified to account for saturation using the tanh function. The modified control law  $\mathbf{u}(t)$  is

$$S(u_i) = u_{\max_i} \cdot \tanh\left(\frac{u_i}{u_{\max_i}}\right), \quad \text{for } i = 1, 2, 3. \quad (4.26)$$

## 4.3 Design Examples

In this section, attitude maneuver simulations are presented to demonstrate the capabilities of the control law developed in Section 4.1 and Section 4.2.

### Spacecraft Initial Conditions

The numerical model for the attitude tracking control system is based on the system parameters of FASTRAC. The inertia matrix,  $\mathbf{J}$ , that approximates the

nanosatellite is given by,

$$\mathbf{J} = \begin{bmatrix} 0.656 & 0 & 0 \\ 0 & 0.656 & 0 \\ 0 & 0 & 0.986 \end{bmatrix} \text{ kg}\cdot\text{m}^2. \quad (4.27)$$

The spacecraft is assumed to be initially at rest. The spacecraft initial conditions are

$$\begin{aligned} \mathbf{q}(0) &= [ 0.9487, 0.1826, 0.1826, 0.18268 ]^T, \\ \boldsymbol{\omega}(0) &= [ 0, 0, 0 ]^T \text{ rad/s.} \end{aligned}$$

The thruster actuation system is assumed to be upper bound in each body-axis by  $u_{\max_i} = 0.5 \text{ N}\cdot\text{m}$  for  $i = 1, 2, 3$ .

### Simulation Parameters

The reference initial quaternion is

$$\mathbf{q}_r(0) = [ 1, 0, 0, 0 ]^T, \quad (4.28)$$

and the reference angular velocity profile is updated at each simulation time. The controller gains are set to  $k_p = 5$  and  $k_v = 8$ .

As in the design examples in Chapter 3, each simulation is performed for two types of trajectories: persistently exciting (PE) and non-persistently exciting (non-PE). Simulations are obtained for the following scenarios:

1. Ideal, no saturation and no inertia perturbations
2. Control saturation

### 3. Control saturation and inertia perturbations

The first scenario is used as the nominal case for comparison. The simulation period is 40 seconds for each attitude tracking scenario. Next, control saturation limits are imposed on the control profile, limiting the output to

$$u_{\max_i} = 0.5 \text{ N} \cdot \text{m}, \quad \text{for } i = 1, 2, 3. \quad (4.29)$$

Finally, the inertia  $\mathbf{J}$  in the control law is perturbed from its true value, that is,

$$\mathbf{J} = \mathbf{J}_{true} + \Delta\mathbf{J}. \quad (4.30)$$

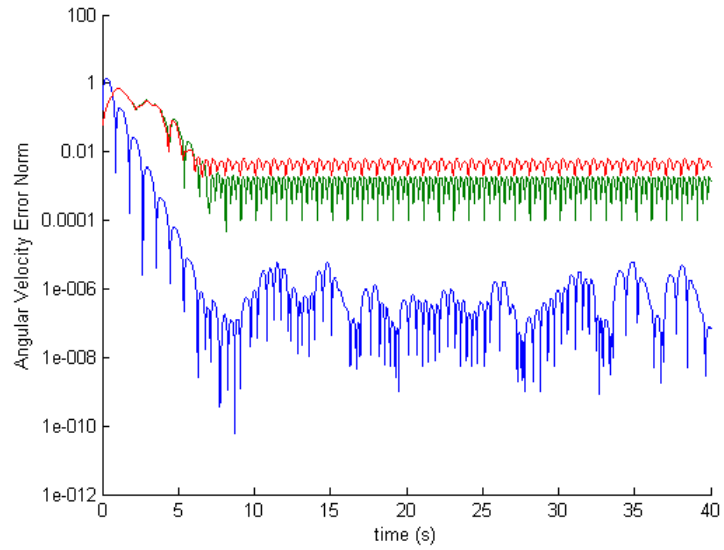
The performance of the controller is examined for  $\Delta\mathbf{J} = 0.3 \mathbf{J}_{true}$ , that is, 30% deviation from the inertia parameters, under control torque limits. The control gains and spacecraft initial conditions are kept the same.

#### **PE Trajectory**

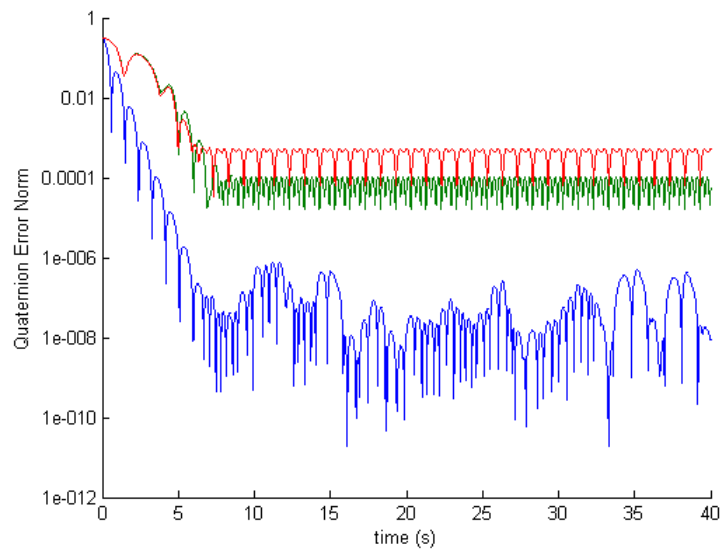
For the first set of simulations, a PE trajectory is considered, where the reference angular velocity profile is generated by

$$\boldsymbol{\omega}_r = 0.02 \left[ \cos(\pi t), \cos(2\pi t), \cos(3\pi t) \right]^T \text{ rad/s}. \quad (4.31)$$

The spacecraft initial conditions, reference quaternion and control gains are as stated in the previous section.



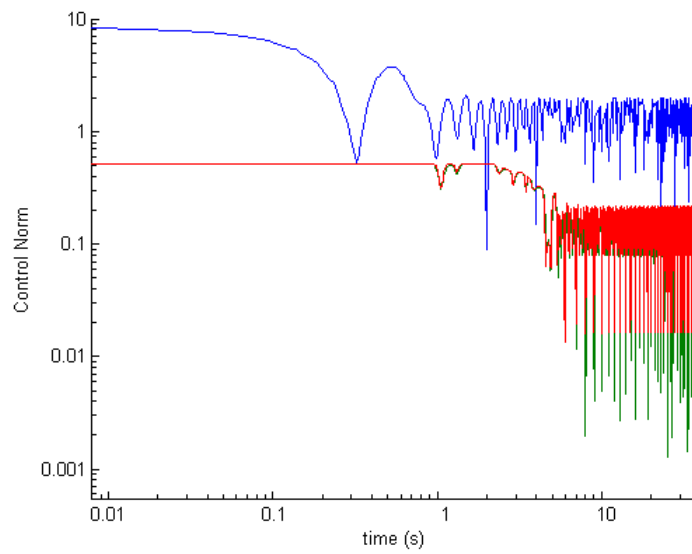
(a) Norm of Angular velocity error vector  $\|\omega_e\|$



(b) Norm of quaternion error vector  $\|q_{e_v}\|$

Figure 4.1





(c) Norm of control vector  $\|\mathbf{u}\|$

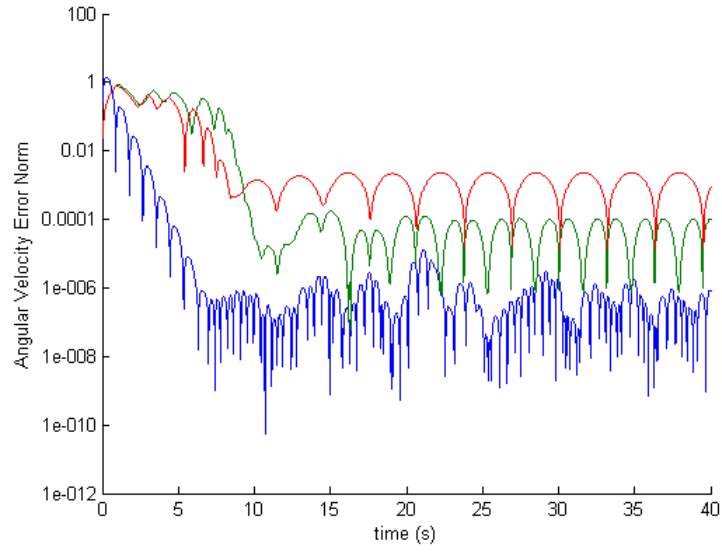
Figure 4.1: PE reference trajectory simulation for a Lyapunov controller formulation obtained via filter construction. Simulations demonstrate ideal system response (blue), system response with torque constraints (green), and system response with torque constraints and inertia perturbations (red).

### Non-PE Trajectory

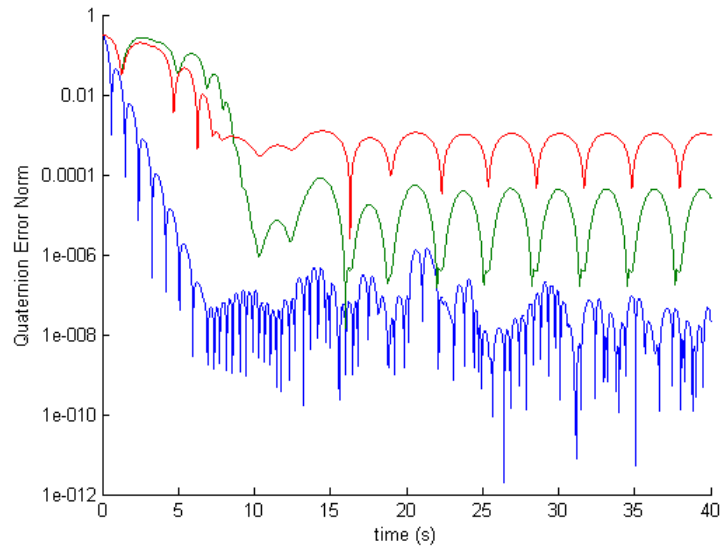
Next, the system is simulated to track a non-PE reference trajectory that has a decaying angular velocity profile described by

$$\boldsymbol{\omega}_r = 0.1 \cos(t)(1 - e^{0.01t^2}) + (0.08\pi + 0.006 \sin(t))te^{-0.01t^2} [ 1 \ 1 \ 1 ]^T \text{ rad/s.} \quad (4.32)$$

The same initial controller and estimator gain values as the non-decaying reference trajectory are used.

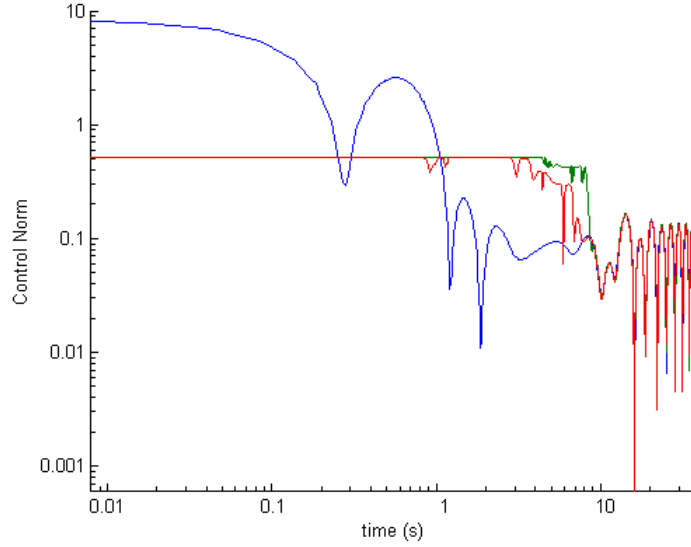


(a) Norm of Angular velocity error vector  $\|\omega_e\|$



(b) Norm of quaternion error vector  $\|q_{e_v}\|$

Figure 4.2



(c) Norm of control vector  $\|\mathbf{u}\|$

Figure 4.2: Non-PE reference trajectory simulation for a Lyapunov controller formulation obtained via filter construction. Simulations demonstrate ideal system response (blue), system response with torque constraints (green), and system response with torque constraints and inertia perturbations (red).

#### 4.4 Summary

A nonlinear model-dependent control law is obtained for spacecraft attitude tracking maneuvers through filter state construction. Global stability of the controller formulation is rigorously proved through a strict Lyapunov function candidate. Control saturation is imposed with the aid of the tanh saturation function described in Chapter 3. Numerical simulations are provided to demonstrate the performance of the unsaturated and saturated control design with and without perturbations in the inertia parameter. The error states converge to zero using the saturated controller solution with a slightly degraded closed-loop performance.

However, the saturated controller is sensitive to changes in the inertia matrix resulting in degraded closed-loop performance. It is clear that an online adaptation technique is essential in order to reduce parametric uncertainty and maintain the accuracy of the controller.

## Chapter 5

### Nonlinear Adaptive Control Design

As indicated by the results in Chapter 3 and 4, precise attitude tracking without the expense of high feedback gains can only be accomplished when the control law is dependent on the model structure. However, as is often the case, spacecraft mass properties may not be completely determined in the course of pre-flight testing. This results in dynamic uncertainty with regard to attitude controller performance as the inertia parameters cannot be reliably determined. Unless uncertainty in the inertia parameters is minimized with some estimation or adaptation technique, the controller might become inaccurate or unstable.

For applications where there is sufficient time for estimation before control, it might be preferable to perform the estimation off-line, that is, before system operation. Several estimation techniques exist in the literature including minimum variance, least squares, batch estimation and sequential batch estimation<sup>31</sup>. However, if there is insufficient time for estimation before control as is the case in nanosatellite reference attitude tracking application, on-line estimation or adaptation is a more suitable technique.

In this chapter, an adaptive controller is designed to maintain consistent performance of the nanosatellite with high uncertainty in its inertia parameters. An adaptive controller is essentially a control law coupled with an online estimator. The

online estimator updates the inertia values based on measured state signals. The particular choice of adaptive control is based on the results of Seo and Akella<sup>11</sup> which delivers superior performance compared to conventional adaptive control techniques.

## **5.1 Introduction to Adaptive Control**

Adaptive control adjusts to unknown system parameters by updating its controller parameters online using measured signals, and does so while maintaining stability and consistent performance of the system. Conventional adaptive control can be classified into two main categories. One is the direct adaptive control method, also known as model reference adaptive control (MRAC). The other is indirect adaptive control, or the so-called self-tuning regulator. A third approach to designing adaptive controllers is called immersion and invariance (I&I) control<sup>10</sup>.

### **5.1.1 Direct Adaptive Control**

Direct adaptive control, or MRAC, is schematically represented by Figure 5.1. MRAC consists of a single unit composed of the plant, reference model, feedback control law, and an adaptation law. The unit performs control parameter adaptation as well as system control simultaneously. The plant has a known dynamic model with uncertain or unknown parameters. The reference model captures the ideal response of the adaptive control system, thereby dictating the goal of the adaptation mechanism. The controller is parameterized in terms of adjustable parameters which are updated using the adaptation algorithm.

The design process begins with a deterministic control design that delivers

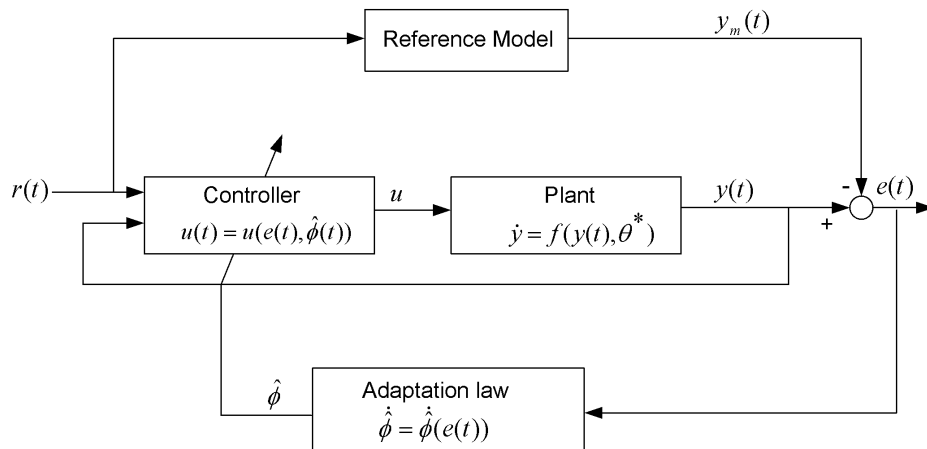


Figure 5.1: A model reference adaptive control system. <sup>12,13</sup>

perfect tracking capability. That is, when the plant parameters are assumed to be exactly known, the controller parameters,  $\phi^*$ , should produce the ideal response (identical to the reference model). When the plant parameters are not known, the adaptation mechanism updates the controller parameters,  $\phi^*$ , in such a way that the tracking error asymptotically converges to zero. The controller parameters are computed from the estimated plant parameters as if they were the true plant parameters. Essentially, the structure of the control when parameters are known is used to construct an equivalent adaptive controller when parameters are unknown by using their estimated values. This is known as the *certainty equivalence principle*. Thus, the adaptation mechanism is driven by the tracking error and is unconcerned with the plant parameter estimation error. Whether the parameter estimate converges to its true values and how quickly this occurs depends entirely on the richness of the reference signal. If the reference signal satisfies suitable persistence of excitation conditions, that means it has certain variation and does not decay to a constant



value, then the parameter estimates have better convergence performance.

A simple example is provided here to illustrate the design and analysis of the MRAC scheme. Consider the following scalar, linear, time-invariant plant modified from

$$\dot{x}(t) = \theta^* x(t) + bu(t); \quad x(0) = x_0 \quad (5.1)$$

where  $u(t)$  is the control variable scaled by an unknown non-zero constant  $b$ ,  $x(t)$  is the measured output, and  $\theta^*$  is the constant unknown parameter of the plant. Assume that the sign of  $b$  is known. Consider the ideal closed-loop system response given by the reference model

$$\dot{x}_m(t) = -\theta_m x_m(t) + b_m u_m(t), \quad (5.2)$$

where  $\theta_m > 0$  and  $b_m$  are chosen to specify the system performance specifications. The signal  $u_m(t)$  in Equation (5.2) is the bounded reference input, while the reference model output  $x_m(t)$  is the ideal output of the control system. The control objective is to design  $u(t)$  so that  $x(t)$  asymptotically converges to  $x_m(t)$ . Introduce the tracking error signal  $e(t)$  as

$$e(t) = x(t) - x_m(t). \quad (5.3)$$

If the plant parameters  $\theta^*$  and  $b$  are known exactly, the control input  $u(t)$  that stabilizes the system is given by

$$u(t) = -\frac{\theta^*}{b}x(t) + \frac{1}{b}(-\theta_m x(t) + b_m u_m(t)). \quad (5.4)$$

The control input in Equation (5.4) may be written as

$$u(t) = \phi_1^* x(t) + \phi_2^* (-\theta_m x(t) + b_m u_m(t)), \quad (5.5)$$

where the  $\phi_1^*$  and  $\phi_2^*$  are the known controller parameters defined by

$$\phi_1^* = -\frac{\theta^*}{b} \quad \text{and} \quad \phi_2^* = \frac{1}{b}. \quad (5.6)$$

If the control parameters are unknown (due to  $\theta^*$  and  $b$  being unknown), then the adaptive controller is written in terms of their parameter estimates  $\hat{\phi}_1(t)$  and  $\hat{\phi}_2(t)$ .

Similar to the known case, the adaptive controller has the structure

$$u_a(t) = \hat{\phi}_1(t)x(t) + \hat{\phi}_2(t)(-\theta_m x(t) + b_m u_m(t)). \quad (5.7)$$

The update for the estimates are selected using the gradient estimation law<sup>13</sup>

$$\dot{\hat{\phi}}_1 = -\lambda_1 x(t) \text{sgn}(b) e(t), \quad (5.8)$$

$$\dot{\hat{\phi}}_2 = -\lambda_2 (-\theta_m x(t) + b_m u_m(t)) \text{sgn}(b) e(t). \quad (5.9)$$

where  $\lambda_1$  and  $\lambda_2$  are strictly positive constant adaptation gains. Now, define the estimation error vectors  $\tilde{\phi}_1$  and  $\tilde{\phi}_2$  as

$$\tilde{\phi}_1 = \hat{\phi}_1 - \phi_1^*, \quad (5.10)$$

$$\tilde{\phi}_2 = \hat{\phi}_2 - \phi_2^*. \quad (5.11)$$

Note that since  $\phi_1^*$  and  $\phi_2^*$  are constant parameters,  $\dot{\tilde{\phi}}_1 = \dot{\hat{\phi}}_1$  and likewise  $\dot{\tilde{\phi}}_2 = \dot{\hat{\phi}}_2$ . In order to analyze the stability of the control law described by Equation (5.7), consider the scalar function in terms of the tracking error signal  $e(t)$  and the estimation error vectors  $\tilde{\phi}_1$  and  $\tilde{\phi}_2$

$$V = \frac{1}{2}e^2 + \frac{|b|}{2\lambda_1}\tilde{\phi}_1^2 + \frac{|b|}{2\lambda_2}\tilde{\phi}_2^2. \quad (5.12)$$

Taking the derivative of  $V$  along system trajectories and substituting Equation (5.1), Equation (5.2), and Equation (5.7) yields

$$\begin{aligned}
\dot{V} &= e\dot{e} + \frac{|b|}{\lambda_1}\tilde{\phi}_1\dot{\hat{\phi}}_1 + \frac{|b|}{\lambda_2}\tilde{\phi}_2\dot{\hat{\phi}}_2 \\
&= e(\dot{x} - \dot{x}_m) + \frac{|b|}{\lambda_1}\tilde{\phi}_1\dot{\hat{\phi}}_1 + \frac{|b|}{\lambda_2}\tilde{\phi}_2\dot{\hat{\phi}}_2 \\
&= e(\theta^*x + bu_a + \theta_mx_m - b_mu_m) + \frac{|b|}{\lambda_1}\tilde{\phi}_1\dot{\hat{\phi}}_1 + \frac{|b|}{\lambda_2}\tilde{\phi}_2\dot{\hat{\phi}}_2 \\
&= e\left(\theta^*x + b\left(\hat{\phi}_1x + \hat{\phi}_2(-\theta_mx + b_mu_m)\right) + \theta_mx_m - b_mu_m\right) \\
&\quad + \frac{|b|}{\lambda_1}\tilde{\phi}_1\dot{\hat{\phi}}_1 + \frac{|b|}{\lambda_2}\tilde{\phi}_2\dot{\hat{\phi}}_2.
\end{aligned} \tag{5.13}$$

By adding and subtracting the terms  $eb(-\hat{\phi}_1^*x - \hat{\phi}_2^*(-\theta_mx + b_mu_m))$  to Equation (5.13) and performing minor algebraic manipulations and term cancellations, one obtains

$$\begin{aligned}
\dot{V} &= e\left(-\theta_m(x - x_m) + b\tilde{\phi}_1x + b\tilde{\phi}_2(-\theta_mx + b_mu_m)\right) + \\
&\quad \frac{|b|}{\lambda_1}\tilde{\phi}_1\dot{\hat{\phi}}_1 + \frac{|b|}{\lambda_2}\tilde{\phi}_2\dot{\hat{\phi}}_2 \\
&= e\left(-\theta_me + b\tilde{\phi}_1x + b\tilde{\phi}_2(-\theta_mx + b_mu_m)\right) \\
&\quad + \frac{|b|}{\lambda_1}\tilde{\phi}_1\dot{\hat{\phi}}_1 + \frac{|b|}{\lambda_2}\tilde{\phi}_2\dot{\hat{\phi}}_2.
\end{aligned} \tag{5.14}$$

Substituting Equation (5.8) and Equation (5.9) into Equation (5.14) results in term cancellations, which yields a negative semi-definite function derivative

$$\dot{V} = -\theta_me^2. \tag{5.15}$$

Using Lyapunov-like analysis, one can easily show that since  $V \geq 0$  and  $\dot{V} \leq 0$ , then  $\lim_{t \rightarrow \infty} V(t) = V_\infty$  exists and is finite. Since  $\dot{V} \leq 0$  implies that  $V(t) \leq V(0)$ , every signal that comprises  $V(t)$  is bounded, that is,  $e \in \mathcal{L}_\infty$ ,  $\tilde{\phi}_1 \in \mathcal{L}_\infty$ , and  $\tilde{\phi}_2 \in \mathcal{L}_\infty$ . In addition,  $e \in \mathcal{L}_2 \cap \mathcal{L}_\infty$  since  $\int_0^\infty V(\tau) d\tau = V_\infty - V(0)$  and  $\dot{e} \in \mathcal{L}_\infty$  since  $\dot{x}$  and

$\dot{x}_m$  are defined as bounded signals. Then using Barbalat's lemma in Chapter 3, it follows that the trajectory error vector  $e \rightarrow 0$  as  $t \rightarrow \infty$ , which implies that  $x(t)$  adequately tracks the reference model trajectory  $x_m(t)$ .

By the application of Barbalat's lemma to Equation (5.15), it is shown that the tracking error  $e(t)$  approaches zero asymptotically. As for the parameter estimation error  $\tilde{\phi}_1$  and  $\tilde{\phi}_2$ , the only guarantee that has been provided so far is that the signals  $\tilde{\phi}_1$  and  $\tilde{\phi}_2$  are bounded. Naturally, the convergence of parameter estimates to their true values is desired so that, as the system reaches steady-state, its closed-loop transfer function truly matches that of the reference model<sup>27</sup>. In order to achieve zero parameter estimation error, the underlying reference trajectory,  $u_m(t)$ , must satisfy an important condition known as *persistence of excitation*. This property and its central role in the analysis of system identification and adaptive control systems is discussed in the next section.

### 5.1.2 Persistence of Excitation

The features of a reference signal play an important role in parameter convergence. For the plant described by Equation (5.1) tracking the reference model in Equation (5.2), the estimated signals will converge to their true values, that is  $\hat{\phi}_1 \rightarrow \phi_1^*$  and  $\hat{\phi}_2 \rightarrow \phi_2^*$ , provided that the underlying reference signal  $u_m(t)$  is complex enough to produce rich excitation in the system for high quality estimation data. The reference signal that is able to uniquely identify the parameters of a system is said to be persistently exciting. Specifically,  $u_m(t)$  is said to be persistently

exciting if there exist positive constants  $\alpha$ , and  $T$  such that

$$\int_t^{t+T} u_m^2(\tau) d\tau \geq \alpha, \quad \forall t \geq 0. \quad (5.16)$$

The definition of persistence of excitation given in Equation (5.16) can be generalized for a vector signal  $\mathbf{u}_m$  as<sup>13</sup>

$$\int_t^{t+T} \mathbf{u}_m(\tau) \mathbf{u}_m^T(\tau) d\tau \geq \alpha \mathbf{I}, \quad \forall t \geq 0, \quad (5.17)$$

where  $\mathbf{I}$  is the  $3 \times 3$  identity matrix.

The importance of persistence of excitation in parameter identification is demonstrated by simulating the model reference adaptive controller in the previous example. Let a stable first-order plant be described as

$$\dot{x}(t) = -2x(t) + 3u(t); \quad x(0) = x_0, \quad (5.18)$$

where the unknown plant parameters are  $\theta^* = -2$  and  $b = 3$ . The plant is to be controlled by the model reference adaptive control derived in the previous section. The reference model is given by

$$\dot{x}_m(t) = -4x_m(t) + 5u_m(t), \quad (5.19)$$

where the  $\theta_m = 4$  and  $b_m = 5$ . The adaptation gains  $\lambda_1$  and  $\lambda_2$  are chosen to be equal to 4 and 3 respectively. Initial conditions for the plant and reference model are set to zero, and no *a priori* knowledge is assumed for the unknown control parameters ( $\hat{\phi}_1(0) = \hat{\phi}_2(0) = 0$ ).

The system is simulated using two types of signals for the reference input:

- $u_m(t) = 1$ . The system response to this signal is illustrated in Figure 5.2. The tracking error is driven to zero but only one parameter converges to its true value.
- $u_m(t) = \sin(6t)$ . The system response to this signal is illustrated in Figure 5.3. The tracking error and the parameter estimation error for both signals converges to zero.

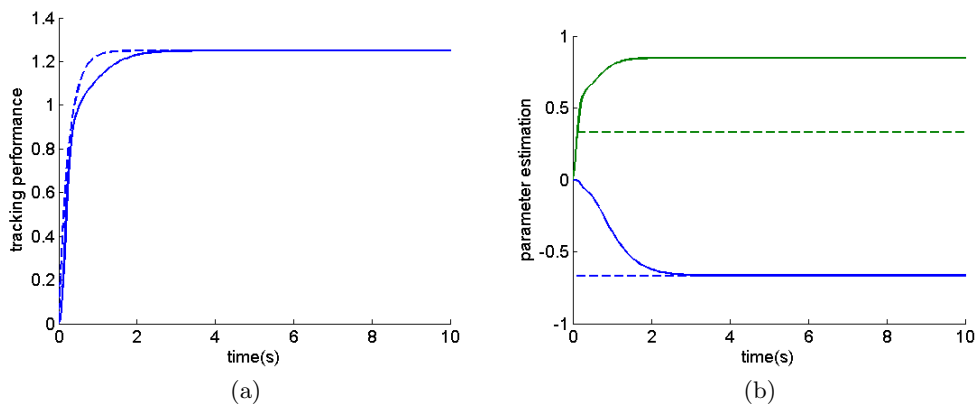


Figure 5.2: Simulation of the model reference adaptive controller with constant reference input  $u_m(t) = 1$ . Reference trajectory in (a) and ideal parameter values in (b) are indicated by dashed lines.

It is clear in the above demonstration that the reference input characterized by the sinusoidal function is the PE signal for this linear time invariant system. The constant reference input is very simple to track which leads to controller parameters that are non-ideal but fit the input-output relation and consequently drive the tracking error to zero. In other words, the estimated parameters are not the ideal values but they get the job done. From these observations, one can conclude that the constant reference input is a non-PE signal for the system as it does not achieve

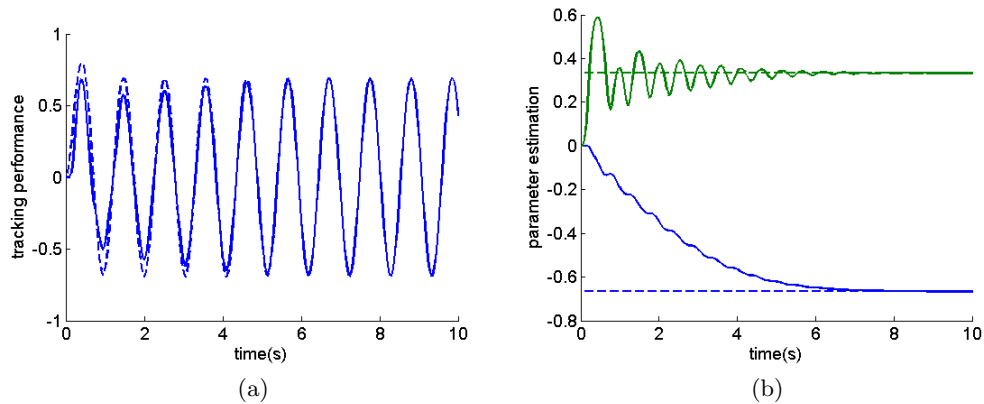


Figure 5.3: Simulation of the model reference adaptive controller with non-constant reference input  $u_m(t) = \sin(6t)$ . Reference trajectory in (a) and ideal parameter values in (b) are indicated by dashed lines.

unique identification of the estimated parameters.

In general, for a linear system, estimation of  $m$  parameters with zero estimation error necessitates at least  $m/2$  sinusoids in the perturbing (reference) signal. For a nonlinear system this relation does not hold as nonlinearities may naturally introduce more frequencies into the system that drive the estimates to their true or ideal values<sup>13,14</sup>.

### 5.1.3 Indirect Adaptive Control

An indirect adaptive control system is composed of two loops: an inner loop that consists of the plant and a feedback controller, and an outer loop that adjusts the control parameters based on the estimates provided by an online estimation technique. The operation of an indirect adaptive controller (also known as self-tuning controller) is illustrated by Figure 5.4.

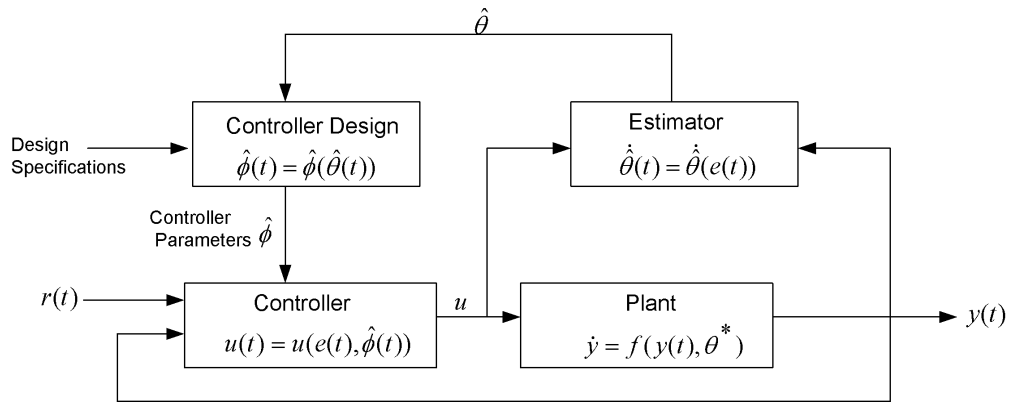


Figure 5.4: An indirect adaptive control system.<sup>12,13</sup>

At each time  $t$ , the estimator calculates the plant parameter estimates,  $\hat{\theta}$ , by essentially performing a linear fit of past values of the input  $u$  and plant output  $y$ . The estimated parameters are fed into the controller, which accepts the estimates as truth and computes the corresponding control torques for that sampled time. Hence, the certainty equivalence principle is applied in both direct and indirect adaptive control. Certainty equivalence requires that the unknown parameters appear linearly in the governing equations, that is, the governing equations must have affine parameterization.

The control torques computed in this way are used to produce new plant output that is in turn used to update the current parameter estimate. The cycle repeats itself for each sampled time. In this way, indirect adaptive control differs from MRAC in that the unknown plant parameter is estimated explicitly rather than through its implicit relation to controller parameters. As with MRAC, the convergence of estimation parameters to their true values depends heavily on It is also possible to adjust the loops so that the updates for the parameter estimates



occur at a different frequency from the control.

A simple example is shown here to demonstrate construction of an adaptive control law. Consider the following scalar non-autonomous nonlinear system

$$\dot{x}(t) = \theta^* f(x, t) + u(t); \quad x(0) = x_0, \quad (5.20)$$

where  $x(t) \in \mathbb{R}$ ,  $f(x, t)$  is a nonlinear and non-autonomous function,  $\theta^*$  is a constant parameter of the system, and  $u(t)$  is the control signal to be determined in terms of the measured state signal. The control objective is to design  $u(t)$  such that the state  $x(t)$  can track a prescribed reference signal  $r(t)$  that is assumed to be smooth, bounded, and have bounded derivatives. Thus, a control input  $u(t)$  must be obtained so that

$$\lim_{t \rightarrow \infty} [x(t) - r(t)] = 0, \quad (5.21)$$

while ensuring that  $x(t)$  remains bounded. Define a tracking error signal  $e(t)$  as

$$e(t) = x(t) - r(t). \quad (5.22)$$

The tracking error dynamics can be written as

$$\dot{e}(t) = \dot{x}(t) - \dot{r}(t) = \theta^* f(x, t) + u - \dot{r}(t). \quad (5.23)$$

To begin with, it is assumed that the plant parameter  $\theta^*$  is exactly known. Using feedback linearization,  $u(t)$  is chosen as

$$u(t) = -\theta^* f(x, t) + \dot{r}(t) + \nu, \quad (5.24)$$

with  $\nu$  being an "equivalent input" to be specified, the resulting error dynamics is linear

$$\dot{e}(t) = \nu. \quad (5.25)$$

Choosing  $\nu$  as

$$\nu = -ke(t), \quad (5.26)$$

with  $k$  being a positive scalar constant, the resulting stable closed loop dynamics is

$$\dot{e}(t) = -ke(t). \quad (5.27)$$

The solution to the above equation is

$$e(t) = e^{-kt}e(0), \quad (5.28)$$

which implies that  $e(t) \rightarrow 0$  as  $t \rightarrow \infty$ .

Now, consider the case when the plant parameter  $\theta^*$  is unknown. Using the certainty equivalence principle, the structure of the controller for the known case is used to synthesize an adaptive control law for the unknown parameters by implementing an online estimation technique. Let  $\hat{\theta}(t)$  denote the time-varying estimate of the unknown parameter  $\theta^*$ . The corresponding parameter estimation error  $\tilde{\theta}$  is given by

$$\tilde{\theta}(t) = \hat{\theta}(t) - \theta^*. \quad (5.29)$$

The adaptive control is

$$u(t) = -\hat{\theta}f(x, t) + \dot{r}(t) - ke(t), \quad (5.30)$$

which results in the closed loop dynamics

$$e(t) = -(\hat{\theta} - \theta^*)f(x, t) - ke(t). \quad (5.31)$$

It remains to find an update law for the parameter estimate  $\hat{\theta}(t)$ . Consider the following radially unbounded, decrescent scalar function

$$V(e, \tilde{\theta}) = \frac{1}{2}e^2 + \frac{1}{2}\tilde{\theta}^2. \quad (5.32)$$

The derivative of the function along system trajectories is

$$\begin{aligned} \dot{V} &= e\dot{e} + \tilde{\theta}\dot{\tilde{\theta}} \\ &= -ke^2 - \tilde{\theta}ef(x, t) + \tilde{\theta}\dot{\tilde{\theta}} \\ &= -ke^2 - \tilde{\theta}(ef(x, t) - \dot{\tilde{\theta}}), \end{aligned} \quad (5.33)$$

where the substitution  $\dot{\tilde{\theta}} = \dot{\hat{\theta}}$  is valid since  $\theta^*$  is assumed to be a constant parameter in Equation (5.29). If  $\dot{\hat{\theta}}$  is chosen as

$$\dot{\hat{\theta}} = ef(x, t), \quad (5.34)$$

then  $\dot{V}$  becomes

$$\dot{V} = -ke^2, \quad (5.35)$$

which is negative semi-definite. Then using Lyapunov-like analysis it can be easily shown that  $e \in \mathcal{L}_2 \cap \mathcal{L}_1$  and from the dynamic equation,  $\dot{x}$  is also uniformly bounded. It follows from Barbalat's lemma that  $e(t) \rightarrow 0$  as  $t \rightarrow \infty$ .

Thus, the nonlinear system

$$\dot{e}(t) = \dot{x}(t) - \dot{r}(t) = \theta^* f(x, t) + u - \dot{r}(t), \quad (5.36)$$

with unknown parameter  $\theta^*$  is stabilized by the adaptive control law

$$u_a(t) = -\hat{\theta}f(x, t) + \dot{r}(t) - ke(t), \quad (5.37)$$

$$\dot{\hat{\theta}} = ef(x, t) \quad (5.38)$$

wherein  $k > 0$  is any scalar constant.

### 5.1.4 Non-Certainty Equivalence Adaptive Control

Adaptive control methods based on the certainty equivalence (CE) principle have certain limiting factors.

1. The adaptation law does not seek to minimize the plant parameter estimation error but rather is driven by the tracking error of the system. Parameter updates stop as soon as tracking errors have converged to zero even if the plant parameter estimates are not at the true values. Conversely, parameter update continues even when the parameters have converged to true values, thereby causing the parameter estimates to drift from truth.
2. Adaptive control system based on the CE principle can never recover the ideal system dynamics unless the estimated parameters converge to their deterministic (no uncertainty) values. However, this can only occur if the reference signal satisfies suitable persistence of excitation conditions<sup>11</sup> that ensure fast convergence rates for parameter estimates. Practical considerations don't always guarantee reference signals that will satisfy PE constraints. Thus, there is always a residual disturbance in the adaptive control system that might result in a non-smooth control history profile.

Non-certainty equivalence adaptive control, based on immersion and invariance adaptive control theory<sup>10</sup>, is a recent formulation by Seo and Akella<sup>11</sup> that overcomes the performance limitations arising from CE-based methods. One of the main advantages of non-CE adaptive control is that it recovers the deterministic closed loop system performance without imposing any additional PE constraints on

the reference signal. Another novel contribution of this controller is that, unlike conventional CE-based adaptive methods, once the parameter estimates lock on to the true parameter values, the adaptation mechanism automatically stops. The non-CE adaptive controller does not guarantee parameter estimation error convergence; rather, it ensures that if the parameters happen to coincide with their true values, they will remain there for the remainder of the system operation.

## 5.2 Non-CE Adaptive Control Design for Spacecraft Tracking

In previous chapters, reference tracking controllers for a nanosatellite were developed using Lyapunov stability theory. The tracking controllers showed performance degradation due to small perturbations in the inertia parameters of the system. In this section, a novel form of adaptive control known as noncertainty equivalence adaptive control is implemented to handle the unknown inertia parameters by combining an online estimation technique that estimates the unknown values.

Recall the dynamics of the error angular velocity

$$\dot{\boldsymbol{\omega}}_e = \mathbf{J}^{-1} (\mathbf{u} - [\boldsymbol{\omega} \times] \mathbf{J} \boldsymbol{\omega} - \mathbf{J} \boldsymbol{\phi}), \quad (5.39)$$

where

$$\boldsymbol{\phi}(t) = \mathbf{C}(\mathbf{q}_e) \dot{\boldsymbol{\omega}}_r - [\boldsymbol{\omega}_e \times] \mathbf{C}(\mathbf{q}_e) \boldsymbol{\omega}_r. \quad (5.40)$$

Upon examining Equation (5.41), one recognizes that certain terms in the dynamical expression have a nonlinear dependence on  $\mathbf{J}$ . Recall that in the estimation of unknown plant parameters, the principle of certainty equivalence is applicable only when the unknown parameters appear linearly in the governing equation. It is

precisely due to this nonlinear dependence on the unknown inertia parameters that non-certainty equivalence adaptive control is implemented for the given problem<sup>11</sup>.

In its current state, Equation (5.41) does not have an integrable form. Therefore, some new terms are added and simultaneously subtracted while preserving the original dynamics of Equation (5.41)<sup>11</sup>

$$\begin{aligned} \dot{\boldsymbol{\omega}}_e = & \underbrace{-k_p\beta\mathbf{q}_{e_v} - k_p\dot{\mathbf{q}}_{e_v} - k_v\boldsymbol{\omega}_e}_{\text{subtracted term}} \\ & + \mathbf{J}^{-1} \left( \mathbf{u} - [\boldsymbol{\omega} \times] \mathbf{J} \boldsymbol{\omega} - \mathbf{J} \boldsymbol{\phi} + \mathbf{J} \underbrace{(k_p\beta\mathbf{q}_{e_v} + k_p\dot{\mathbf{q}}_{e_v} + k_v\boldsymbol{\omega}_e)}_{\text{added term}} \right), \end{aligned} \quad (5.41)$$

for any  $k_p, k_v > 0$  and  $\beta = k_p + k_v$ . Later, it will be evident that the added terms make the  $\dot{\boldsymbol{\omega}}_e$  equation perfectly integrable. Note that the newly added term is linearly parameterized with respect to  $\mathbf{J}$ .

Next, a regression matrix,  $\mathbf{W}(\cdot) \in \mathbb{R}^{3 \times 6}$  is formed that has the structure,

$$\mathbf{W}\boldsymbol{\theta}^* = [\boldsymbol{\omega} \times] \mathbf{J} \boldsymbol{\omega} + \mathbf{J} \boldsymbol{\phi} - \mathbf{J} (k_p\beta\mathbf{q}_{e_v} + k_p\dot{\mathbf{q}}_{e_v} + k_v\boldsymbol{\omega}_e), \quad (5.42)$$

where  $\boldsymbol{\theta}^*$  is described similarly to Equation (3.49). The entries of  $\mathbf{W}$  are computed as

$$\begin{aligned} \mathbf{W} = & -[\boldsymbol{\omega} \times] \mathbf{L}(\boldsymbol{\omega}) + \mathbf{L}([\boldsymbol{\omega} \times] \mathbf{C}(\mathbf{q}_e) \boldsymbol{\omega}_r - \mathbf{C}(\mathbf{q}_e) \dot{\boldsymbol{\omega}}_r) \\ & + \mathbf{L}(k_v\boldsymbol{\omega}_e + k_p\dot{\mathbf{q}}_e + \beta k_p \mathbf{q}_e), \end{aligned} \quad (5.43)$$

where  $\mathbf{L} : \mathbb{R}^3 \rightarrow \mathbb{R}^{3 \times 6}$  is the linear operator defined in Section 3.5.1. Equation (5.41) can now be written in terms of the regression matrix as follows:

$$\dot{\boldsymbol{\omega}}_e = -k_p\beta\mathbf{q}_{e_v} - k_p\dot{\mathbf{q}}_{e_v} - k_v\boldsymbol{\omega}_e + \mathbf{J}^{-1} (\mathbf{u} - \mathbf{W}\boldsymbol{\theta}^*). \quad (5.44)$$

As shown in Chapter 4, filter construction is used to transform the tracking error dynamics by filtering the signals  $\boldsymbol{\omega}_e$  and  $\mathbf{W}$  through stable linear filters having the following first-order dynamics

$$\dot{\boldsymbol{\omega}}_{e_f} = -\beta\boldsymbol{\omega}_{e_f} + \boldsymbol{\omega}_e, \quad (5.45)$$

$$\dot{\mathbf{W}}_f = -\beta\mathbf{W}_f + \mathbf{W}, \quad (5.46)$$

where Equation (5.45) is a vector quantity whereas Equation (5.46) is a matrix quantity. In addition to the filter signals defined above, a third signal  $\mathbf{u}_f$  is introduced with similar dynamics

$$\dot{\mathbf{u}}_f = -\beta\mathbf{u}_f + \mathbf{u}. \quad (5.47)$$

As shown previously in Chapter 4, the transformed dynamics have the same structure as Equation (5.44). Differentiating both sides of the filter dynamics in Equation (5.45) and making appropriate substitutions of Equation (5.44) yields

$$\begin{aligned} \ddot{\boldsymbol{\omega}}_{e_f} &= -\beta\dot{\boldsymbol{\omega}}_{e_f} + \dot{\boldsymbol{\omega}}_e, \\ &= -\beta\dot{\boldsymbol{\omega}}_{e_f} - k_p\beta\mathbf{q}_{e_v} - k_p\dot{\mathbf{q}}_{e_v} - k_v\boldsymbol{\omega}_e + \mathbf{J}^{-1}(\mathbf{u} - \mathbf{W}\boldsymbol{\theta}^*). \end{aligned} \quad (5.48)$$

The signals  $\boldsymbol{\omega}_e$ ,  $\mathbf{u}$ , and  $\mathbf{W}$  are rewritten in terms of their filtered counterparts as

$$\begin{aligned} \ddot{\boldsymbol{\omega}}_{e_f} &= -\beta\dot{\boldsymbol{\omega}}_{e_f} - k_p\beta\mathbf{q}_{e_v} - k_p\dot{\mathbf{q}}_{e_v} - k_v(\dot{\boldsymbol{\omega}}_{e_f} + \beta\boldsymbol{\omega}_{e_f}) \\ &\quad + \mathbf{J}^{-1}(\dot{\mathbf{u}}_f + \beta\mathbf{u}_f - \dot{\mathbf{W}}_f\boldsymbol{\theta}^* + \beta\mathbf{W}_f\boldsymbol{\theta}^*). \end{aligned} \quad (5.49)$$

Upon examining the above expression, note that every term is scaled by the constant  $\beta$  and is accompanied by its corresponding derivative. The expression is rearranged so that the derivatives are on the left hand side of the equation. Then, Equation (5.49) can be written as a perfect differential, that is,

$$\begin{aligned} \frac{d}{dt} \left[ \dot{\boldsymbol{\omega}}_{e_f} + k_p\mathbf{q}_{e_v} + k_v\boldsymbol{\omega}_{e_f} - \mathbf{J}^{-1}\mathbf{u}_f + \mathbf{J}^{-1}\mathbf{W}_f\boldsymbol{\theta}^* \right] \\ = -\beta \left( \dot{\boldsymbol{\omega}}_{e_f} + k_p\mathbf{q}_{e_v} + k_v\boldsymbol{\omega}_{e_f} - \mathbf{J}^{-1}\mathbf{u}_f + \mathbf{J}^{-1}\mathbf{W}_f\boldsymbol{\theta}^* \right). \end{aligned} \quad (5.50)$$

The algebraic manipulations performed by adding and subtracting terms earlier in Equation (5.41) is what allows one to create the perfectly differentiable form of Equation (5.50). The solution to Equation (5.50) is given by

$$\dot{\boldsymbol{\omega}}_{e_f} + k_p \mathbf{q}_{e_v} + k_v \boldsymbol{\omega}_{e_f} - \mathbf{J}^{-1} (\mathbf{u}_f - \mathbf{W}_f \boldsymbol{\theta}^*) = \boldsymbol{\varepsilon} e^{-\beta t}, \quad (5.51)$$

where  $\boldsymbol{\varepsilon}$  encompasses the initial conditions of all integrable terms

$$\boldsymbol{\varepsilon} = \dot{\boldsymbol{\omega}}_{e_f}(0) + k_p \mathbf{q}_{e_v}(0) + k_v \boldsymbol{\omega}_{e_f}(0) - \mathbf{J}^{-1} (\mathbf{u}_f(0) - \mathbf{W}_f(0) \boldsymbol{\theta}^*). \quad (5.52)$$

The initial conditions are chosen such that  $\boldsymbol{\varepsilon} = 0$ . This can be accomplished if  $\mathbf{W}_f(0) = 0$  and

$$\dot{\boldsymbol{\omega}}_{e_f}(0) + k_p \mathbf{q}_{e_v}(0) + k_v \boldsymbol{\omega}_{e_f}(0) = 0. \quad (5.53)$$

The above condition is achieved by adding and subtracting the term  $k_p \boldsymbol{\omega}_{e_f}(0)$  and recognizing that  $\beta = k_p + k_v$ , that is,

$$\dot{\boldsymbol{\omega}}_{e_f}(0) + \beta \boldsymbol{\omega}_{e_f}(0) + k_p \mathbf{q}_{e_v}(0) - k_p \boldsymbol{\omega}_{e_f}(0) = 0. \quad (5.54)$$

The first two terms in the above equation are recognized as  $\boldsymbol{\omega}_e(0)$  from the filter dynamics. Thus, Equation (5.54) can be simplified to

$$\boldsymbol{\omega}_{e_f}(0) = \frac{\boldsymbol{\omega}_e(0) + k_p \mathbf{q}_{e_v}(0)}{k_p}. \quad (5.55)$$

Thus setting  $\boldsymbol{\varepsilon} = 0$ , Equation (5.51) is expressed as

$$\dot{\boldsymbol{\omega}}_{e_f} = -k_p \mathbf{q}_{e_v} - k_v \boldsymbol{\omega}_{e_f} + \mathbf{J}^{-1} [\mathbf{u}_f - \mathbf{W}_f \boldsymbol{\theta}^*]. \quad (5.56)$$

The parameter estimation error,  $\tilde{\boldsymbol{\theta}}$ , is given by

$$\tilde{\boldsymbol{\theta}} = \hat{\boldsymbol{\theta}} - \boldsymbol{\theta}^*, \quad (5.57)$$



where  $\boldsymbol{\theta}^*$  is the unknown constant parameter, that is, the six unique terms of the positive definite spacecraft inertia matrix, and  $\hat{\boldsymbol{\theta}}$  is the estimated parameter. If the certainty equivalence principle is employed, the corresponding adaptive control law would be stated as  $\mathbf{u}_f = \mathbf{W}_f \hat{\boldsymbol{\theta}}$ , where the estimated parameters would be treated as the true values and an estimation law would be found to continuously update the parameter estimates<sup>14</sup>.

However, in this study, the non-certainty equivalence adaptive control approach is employed. An additional signal,  $\boldsymbol{\delta}(t) \in \mathbb{R}^6$ , is introduced that estimates the unknown inertia in conjunction with  $\hat{\boldsymbol{\theta}}$ . In other words, the online estimates for the unknown  $\boldsymbol{\theta}^*$  vector are now generated by the combined signal  $\hat{\boldsymbol{\theta}} + \boldsymbol{\delta}$ . The control law can now be stated as

$$\mathbf{u}_f = \mathbf{W}_f (\hat{\boldsymbol{\theta}} + \boldsymbol{\delta}), \quad (5.58)$$

where  $\boldsymbol{\delta}(t)$  is chosen as

$$\boldsymbol{\delta} = \mathbf{W}_f^T \boldsymbol{\omega}_{e_f}. \quad (5.59)$$

Combining Equation (5.56) and Equation (5.58), the dynamical equation for the filter signal,  $\boldsymbol{\omega}_{e_f}$  is given by

$$\dot{\boldsymbol{\omega}}_{e_f} = -k_p \mathbf{q}_{e_v} - k_v \boldsymbol{\omega}_{e_f} + \mathbf{J}^{-1} \mathbf{W}_f (\hat{\boldsymbol{\theta}} + \boldsymbol{\delta} - \boldsymbol{\theta}^*). \quad (5.60)$$

In Equation (5.60), let  $\mathbf{z} = \hat{\boldsymbol{\theta}} + \boldsymbol{\delta} - \boldsymbol{\theta}^*$ , which now plays the role of the estimator for the adaptive control problem as it gives the difference between the estimates,  $\hat{\boldsymbol{\theta}} + \boldsymbol{\delta}$ ,

and the true values,  $\boldsymbol{\theta}^*$ . The dynamical equation for  $\mathbf{z}$  is given by

$$\begin{aligned}\dot{\mathbf{z}} &= \dot{\hat{\boldsymbol{\theta}}} + \dot{\boldsymbol{\delta}} - \dot{\boldsymbol{\theta}}^*, \\ &= \dot{\hat{\boldsymbol{\theta}}} + \dot{\mathbf{W}}_f^T \boldsymbol{\omega}_{e_f} + \mathbf{W}_f^T \dot{\boldsymbol{\omega}}_{e_f}, \\ &= \dot{\hat{\boldsymbol{\theta}}} + (-\beta \mathbf{W}_f + \mathbf{W})^T \boldsymbol{\omega}_{e_f} + \mathbf{W}_f^T (-k_p \mathbf{q}_{e_v} - k_v \boldsymbol{\omega}_{e_f} + \mathbf{J}^{-1} \mathbf{W}_f \mathbf{z}).\end{aligned}\tag{5.61}$$

The parameter estimate update is chosen as a function of all the terms that are known, that is, terms independent of  $\mathbf{J}$  in Equation (5.61)

$$\dot{\hat{\boldsymbol{\theta}}} = (\beta \mathbf{W}_f - \mathbf{W})^T \boldsymbol{\omega}_{e_f} + \mathbf{W}_f^T (k_p \mathbf{q}_{e_v} + k_v \boldsymbol{\omega}_{e_f}).\tag{5.62}$$

Then, the remaining term in Equation 5.61 is a function of the unknown inertia matrix,  $\mathbf{J}$ , and is therefore the update for the estimator,  $\mathbf{z}$ . That is,

$$\dot{\mathbf{z}} = -\mathbf{W}_f^T \mathbf{J}^{-1} \mathbf{W}_f \mathbf{z}.\tag{5.63}$$

Finally, it remains to extract the actual controller  $\mathbf{u}$  from the filtered control signal  $\mathbf{u}_f$ . This can be done simply through the substitution

$$\mathbf{u} = \dot{\mathbf{u}}_f + \beta \mathbf{u}_f,\tag{5.64}$$

which can be expanded to form

$$\mathbf{u} = -\dot{\mathbf{W}}_f (\hat{\boldsymbol{\theta}} + \boldsymbol{\delta}) - \mathbf{W}_f (\dot{\hat{\boldsymbol{\theta}}} + \dot{\boldsymbol{\delta}}) + \beta \mathbf{u}_f.\tag{5.65}$$

The proof for stability properties is obtained through Lyapunov-like analysis.

### 5.2.1 Stability Analysis

The stability results are obtained from Seo and Akella<sup>11</sup>. Consider the following Lyapunov candidate function

$$V = \frac{1}{2} \boldsymbol{\omega}_{e_f}^T \boldsymbol{\omega}_{e_f} + [\mathbf{q}_{e_v}^T \mathbf{q}_{e_v} + (q_{0e} - 1)^2] + \frac{\lambda}{2} \mathbf{z}^T \mathbf{z},\tag{5.66}$$

where  $\lambda > 0$ . The derivative of  $V$  is given by

$$\begin{aligned}
\dot{V} &= \boldsymbol{\omega}_{e_f}^T \dot{\boldsymbol{\omega}}_{e_f} - 2q\dot{0}_e + \lambda \mathbf{z}^T \dot{\mathbf{z}}, \\
&= \boldsymbol{\omega}_{e_f}^T (-k_p \mathbf{q}_{e_v} - k_v \boldsymbol{\omega}_{e_f} + \mathbf{J}^{-1} \mathbf{W}_f \mathbf{z}) - 2 \left( -\frac{1}{2} \mathbf{q}_{e_v}^T \boldsymbol{\omega}_{e_f} \right) \\
&\quad + \lambda \mathbf{z}^T (-\mathbf{W}_f^T \mathbf{J}^{-1} \mathbf{W}_f \mathbf{z}), \\
&= \boldsymbol{\omega}_{e_f}^T (-k_p \mathbf{q}_{e_v} - k_v \boldsymbol{\omega}_{e_f}) + \mathbf{q}_{e_v}^T (\dot{\boldsymbol{\omega}}_{e_f} + \beta \boldsymbol{\omega}_{e_f}) - \lambda \mathbf{z}^T \mathbf{W}_f^T \mathbf{J}^{-1} \mathbf{W}_f \mathbf{z} \\
&\quad + \boldsymbol{\omega}_{e_f}^T \mathbf{J}^{-1} \mathbf{W}_f \mathbf{z}, \\
&= \boldsymbol{\omega}_{e_f}^T (-k_p \mathbf{q}_{e_v} - k_v \boldsymbol{\omega}_{e_f}) + \mathbf{q}_{e_v}^T (-k_p \mathbf{q}_{e_v} - k_v \boldsymbol{\omega}_{e_f} + \mathbf{J}^{-1} \mathbf{W}_f \mathbf{z} + \beta \boldsymbol{\omega}_{e_f}) \quad (5.67) \\
&\quad - \lambda \mathbf{z}^T \mathbf{W}_f^T \mathbf{J}^{-1} \mathbf{W}_f \mathbf{z} + \boldsymbol{\omega}_{e_f}^T \mathbf{J}^{-1} \mathbf{W}_f \mathbf{z}, \\
&= -k_p \|\mathbf{q}_{e_v}\|^2 - k_v \|\boldsymbol{\omega}_{e_f}\|^2 + (\beta - k_v - k_p) \mathbf{q}_{e_v}^T \boldsymbol{\omega}_{e_f} - \lambda \mathbf{z}^T \mathbf{W}_f^T \mathbf{J}^{-1} \mathbf{W}_f \mathbf{z} \\
&\quad + \mathbf{q}_{e_v}^T \mathbf{J}^{-1} \mathbf{W}_f \mathbf{z} + \boldsymbol{\omega}_{e_f}^T \mathbf{J}^{-1} \mathbf{W}_f \mathbf{z}, \\
&= -k_p \|\mathbf{q}_{e_v}\|^2 - k_v \|\boldsymbol{\omega}_{e_f}\|^2 - \lambda \|\mathbf{J}^{-\frac{1}{2}} \mathbf{W}_f \mathbf{z}\|^2 + \mathbf{q}_{e_v}^T \mathbf{J}^{-1} \mathbf{W}_f \mathbf{z} \\
&\quad + \boldsymbol{\omega}_{e_f}^T \mathbf{J}^{-1} \mathbf{W}_f \mathbf{z}.
\end{aligned}$$

In the above equation, it can be seen that

$$\mathbf{z}^T \mathbf{W}_f^T \mathbf{J}^{-1} \mathbf{W}_f \mathbf{z} \leq - (j^{-1})_{\min} \|\mathbf{W}_f \mathbf{z}\|^2, \quad (5.68)$$

where  $(j^{-1})_{\min}$  is the minimum eigenvalue of  $\mathbf{J}^{-1}$ . It can be also be stated as

$$(j^{-1})_{\min} = \frac{1}{j_{\max}}, \quad (5.69)$$

where  $j_{\max}$  is the maximum eigenvalue of  $\mathbf{J}$ . Thus,

$$\mathbf{z}^T \mathbf{W}_f^T \mathbf{J}^{-1} \mathbf{W}_f \mathbf{z} \leq \frac{-1}{j_{\max}} \|\mathbf{W}_f \mathbf{z}\|^2. \quad (5.70)$$

Similarly,

$$\mathbf{q}_{e_v}^T \mathbf{J}^{-1} \mathbf{W}_f \mathbf{z} \leq \frac{1}{j_{\min}} \|\mathbf{q}_{e_v}\| \|\mathbf{W}_f \mathbf{z}\|, \quad (5.71a)$$

$$\boldsymbol{\omega}_{e_f}^T \mathbf{J}^{-1} \mathbf{W}_f \mathbf{z} \leq \frac{1}{j_{\min}} \|\boldsymbol{\omega}_{e_f}\| \|\mathbf{W}_f \mathbf{z}\|. \quad (5.71b)$$

The time derivative of the Lyapunov candidate function can now be expressed as

$$\begin{aligned} \dot{V} &\leq -k_p \|\mathbf{q}_{e_v}\|^2 - k_v \|\boldsymbol{\omega}_{e_f}\|^2 - \frac{\lambda}{j_{\max}} \|\mathbf{W}_f \mathbf{z}\|^2 \\ &\quad + \frac{1}{j_{\min}} \|\mathbf{q}_{e_v}\| \|\mathbf{W}_f \mathbf{z}\| + \frac{1}{j_{\min}} \|\boldsymbol{\omega}_{e_f}\| \|\mathbf{W}_f \mathbf{z}\|. \end{aligned} \quad (5.72)$$

Using completion of squares and rearranging terms, Equation 5.72 can be written as

$$\begin{aligned} \dot{V} &\leq -\frac{k_p}{2} \|\mathbf{q}_{e_v}\|^2 - \frac{k_v}{2} \|\boldsymbol{\omega}_{e_f}\|^2 - \frac{\lambda}{2j_{\max}} \|\mathbf{W}_f \mathbf{z}\|^2 \\ &\quad - \left( \frac{\lambda}{2j_{\max}} - \frac{1}{2k_p j_{\min}^2} + \frac{1}{2k_v j_{\min}^2} \right) \|\mathbf{W}_f \mathbf{z}\|^2. \end{aligned} \quad (5.73)$$

For stability, the coefficient of the last term must satisfy the following condition

$$\frac{\lambda}{2j_{\max}} - \frac{1}{2k_p j_{\min}^2} + \frac{1}{2k_v j_{\min}^2} > 0. \quad (5.74)$$

Using the above equation,  $\lambda$  must satisfy the condition

$$\lambda > \frac{j_{\max} k_p + k_v}{j_{\min}^2 k_p k_v} > 0. \quad (5.75)$$

Choosing  $\lambda > 0$  that satisfies the above condition will lead to  $\boldsymbol{\omega}_{e_f}, \mathbf{q}_{e_v}, \mathbf{z} \in \mathcal{L}_\infty, \mathbf{q}_{e_v} \in \mathcal{L}_2 \cap \mathcal{L}_\infty, \boldsymbol{\omega}_{e_f} \in \mathcal{L}_2 \cap \mathcal{L}_\infty, \mathbf{W}_f \mathbf{z} \in \mathcal{L}_2 \cap \mathcal{L}_\infty, (\dot{\mathbf{q}}_{e_v}, \dot{\boldsymbol{\omega}}_{e_f}, \frac{d}{dt}(\mathbf{W}_f \mathbf{z})) \in \mathcal{L}_\infty$ , which permit the following conclusion

$$\lim_{t \rightarrow \infty} \begin{bmatrix} \mathbf{q}_e(t) \\ \boldsymbol{\omega}_{e_f}(t) \\ \mathbf{W}_f \mathbf{z}(t) \end{bmatrix} = 0. \quad (5.76)$$

### 5.3 Design Examples

The vector form of the unknown FASTRAC inertia parameters is  $\boldsymbol{\theta}^* = [0.656, 0, 0, 0.656, 0, 0.986]^T$ . The initial value of the parameter estimate is assumed to be at 30% deviation from the true value, that is,

$$\hat{\boldsymbol{\theta}}(0) + \boldsymbol{\delta}(0) = [0.8528, 0, 0, 0.8528, 0, 1.2818]^T. \quad (5.77)$$

The spacecraft initial conditions are

$$\begin{aligned} \mathbf{q}(0) &= [0.9487, 0.1826, 0.1826, 0.18268]^T, \\ \boldsymbol{\omega}(0) &= [0, 0, 0]^T \text{ rad/s}, \end{aligned}$$

and the reference initial quaternion is

$$\mathbf{q}_r(0) = [1, 0, 0, 0]^T. \quad (5.78)$$

The reference angular velocity profile is updated at each simulation time. In addition, the initial filter-states are as follows<sup>11</sup>

$$\mathbf{W}_f(0) = 0, \quad \boldsymbol{\omega}_f(0) = \frac{\boldsymbol{\omega}_e(0) + k_p \mathbf{q}_{v_e}(0)}{k_p}.$$

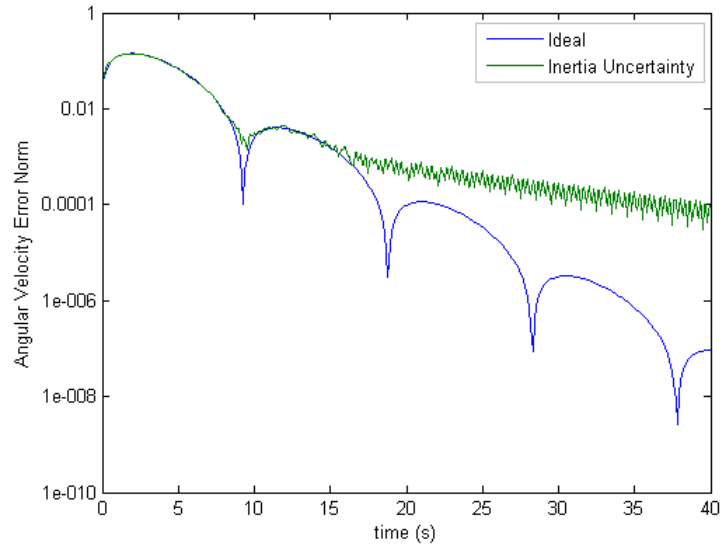
The control gains are chosen to be  $k_v = 0.5$ ,  $k_p = 0.5$ , and  $\gamma = 250$ . The simulations are performed for the PE and non-PE reference trajectories of the system. For each case, the ideal case performance is also plotted. The ideal case is when there is no uncertainty in the inertia parameters.

## PE Trajectory

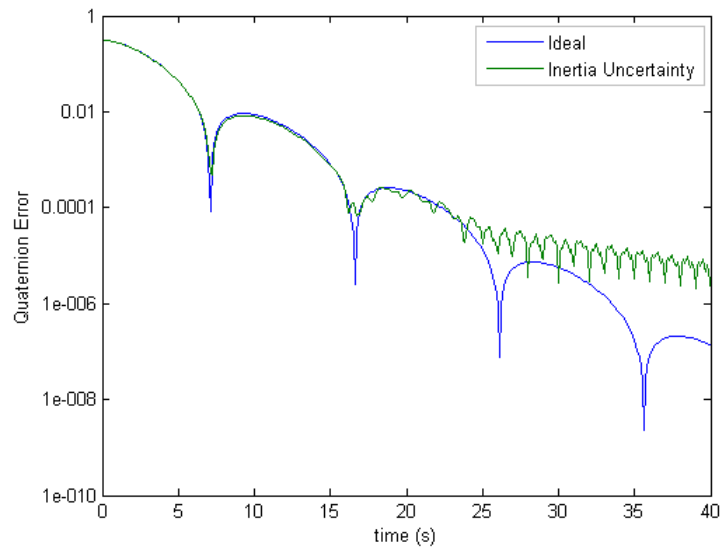
First, the PE trajectory is considered, where the reference angular velocity profile is generated by

$$\boldsymbol{\omega}_r = 0.02 [ \cos(\pi t), \cos(2\pi t), \cos(3\pi t) ]^T \text{ rad/s.} \quad (5.79)$$

The angular velocity and quaternion errors converge to zero, although the convergence is slower than the ideal case. The three inertia estimates converge to their true values. The control torque norms remain well below the total saturation constraint of approximately  $1 \text{ N} \cdot \text{m}$ .

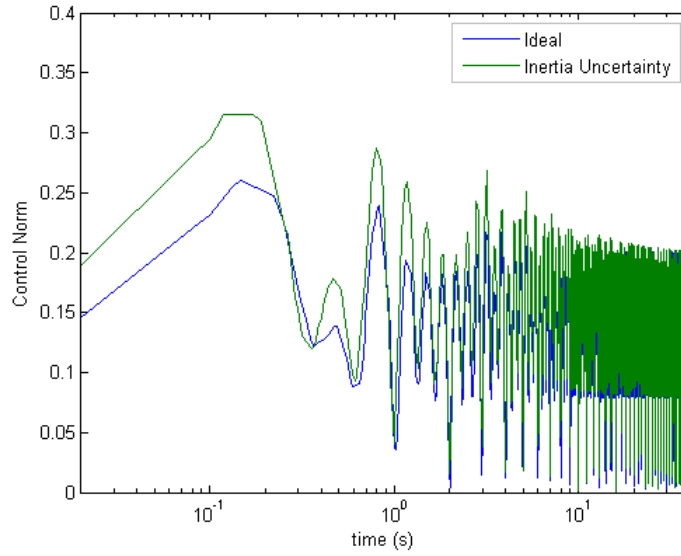


(a) Norm of Angular velocity error vector  $\|\omega_e\|$

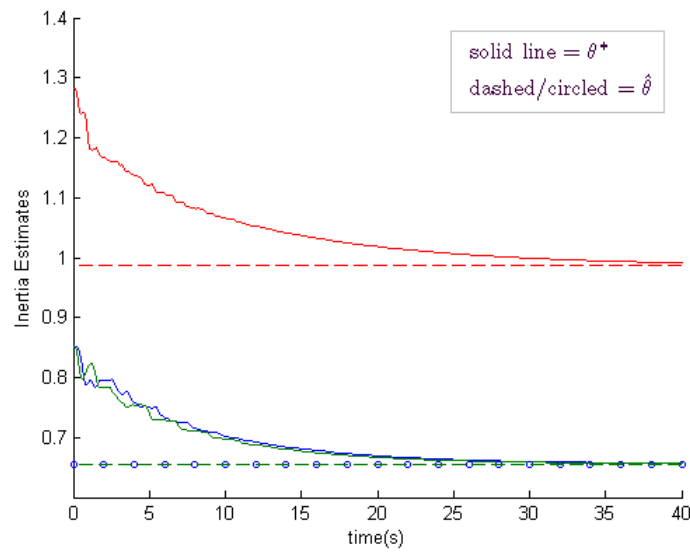


(b) Norm of quaternion error vector  $\|q_{e_v}\|$

Figure 5.5



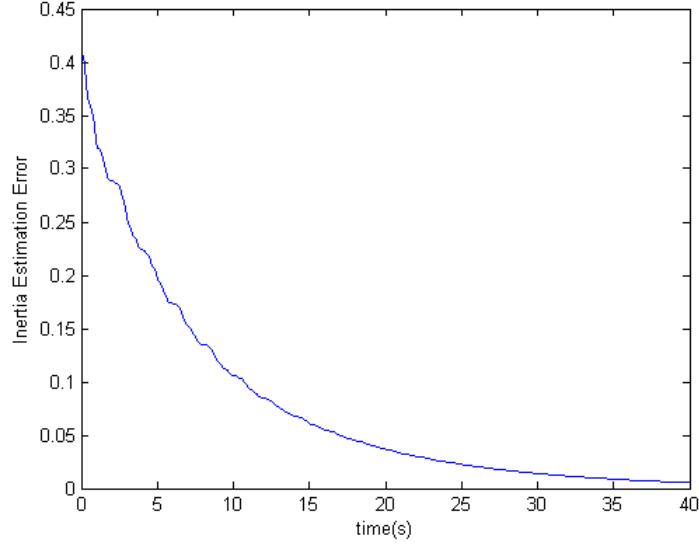
(c) Norm of control vector  $\|\mathbf{u}\|$



(d) Estimates for principle inertia parameters

Figure 5.5





(e) Norm of parameter estimation error  $\mathbf{z}$

Figure 5.5: Non-CE adaptive control law simulation for a PE reference trajectory.

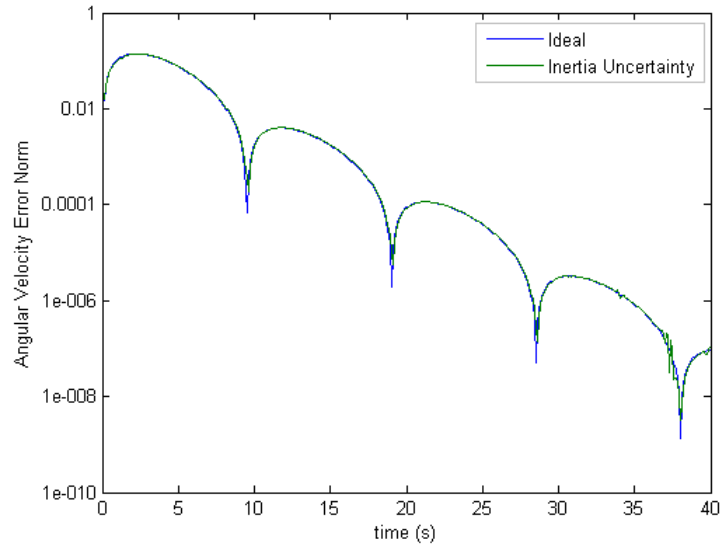
### Non-PE Trajectory

The second set of simulations is performed for a non-PE trajectory with angular velocity profile given by

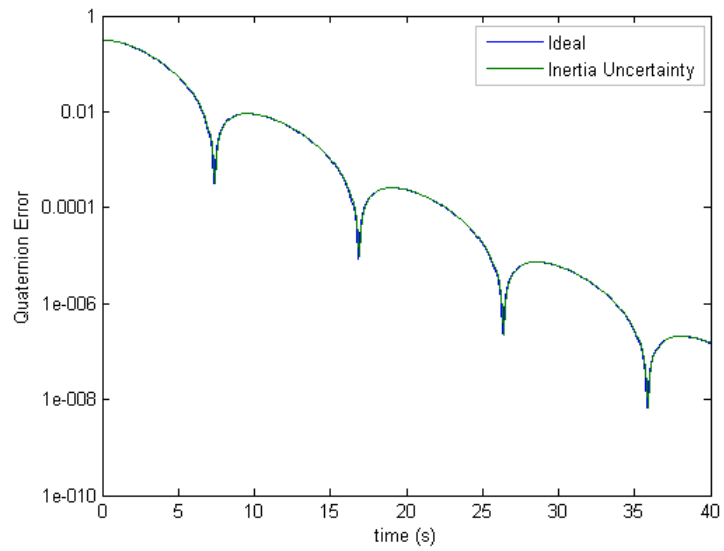
$$\boldsymbol{\omega}_r = 0.1 \cos(t)(1 - e^{0.01t^2}) + (0.08\pi + 0.006 \sin(t))te^{-0.01t^2} [ 1 \ 1 \ 1 ]^T \text{ rad/s.} \quad (5.80)$$

The same initial controller and estimator gain values as the PE trajectory are used. Figures 5.6a and 5.6b illustrated the performance of the error states when tracking the non-PE reference trajectory. The angular velocity and quaternion errors converge to zero and display closed-loop performance on par with the ideal case. As expected, the three inertia estimates do not converge to their true values as the underlying reference trajectory does not satisfy the PE conditions. This can be seen

in Figures 5.6d and 5.6e. As in the PE case, the control torque norms stay below the total saturation constraint of approximately  $1 \text{ N} \cdot \text{m}$ .

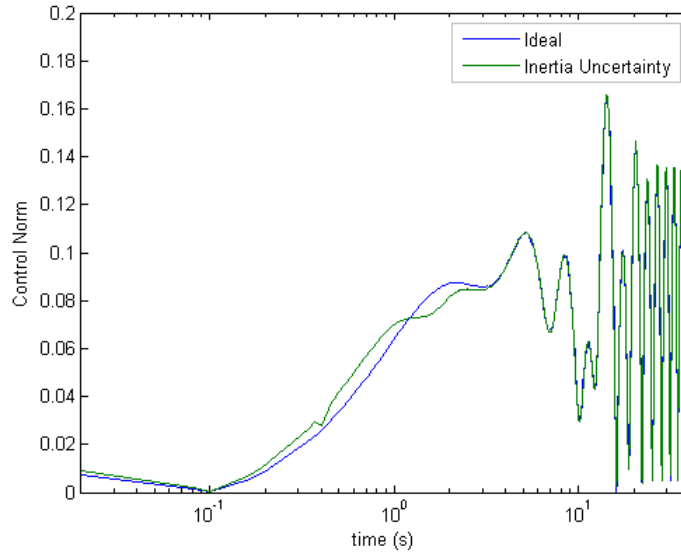


(a) Norm of Angular velocity error vector  $\|\omega_e\|$

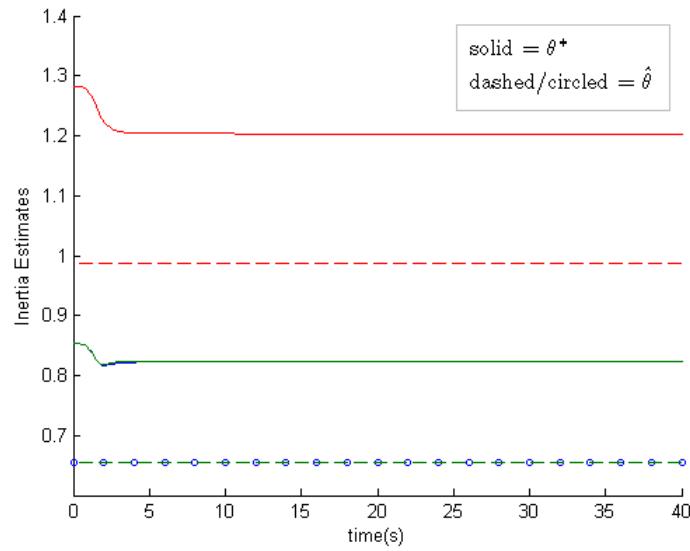


(b) Norm of quaternion error vector  $\|q_{e_v}\|$

Figure 5.6

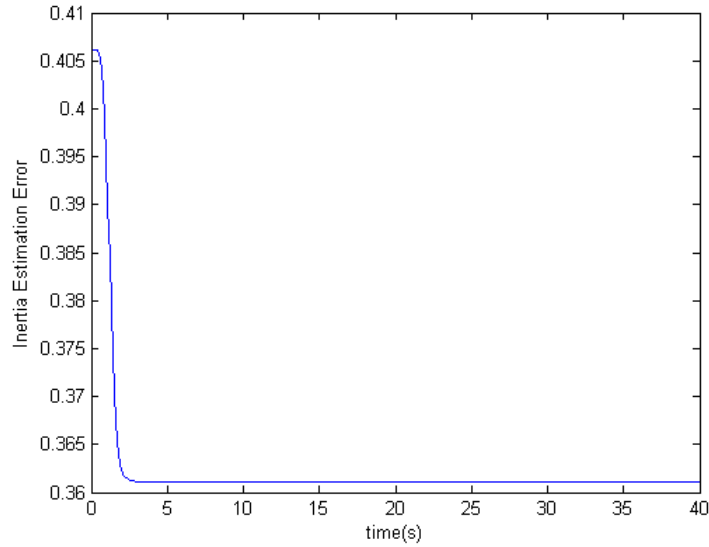


(c) Norm of control vector  $\|\mathbf{u}\|$



(d) Estimates for principle inertia parameters.

Figure 5.6



(e) Norm of parameter estimation error  $\mathbf{z}$

Figure 5.6: Non-CE adaptive control law simulation for a non-PE reference trajectory.

## 5.4 Summary

A noncertainty-equivalence adaptive control law is employed for spacecraft attitude tracking maneuvers in the presence of arbitrarily large inertia matrix uncertainties. Global stability and asymptotic convergence of angular velocity and quaternion errors to zero is shown using Lyapunov-like analysis. Numerical simulations for a PE reference trajectory demonstrate that the non-CE adaptive controller delivers fast convergence rates of tracking errors and convergence of parameter estimates to their true values. For a non-PE reference trajectory, the tracking errors converge to zero with fast convergence rate, although the parameter estimation errors do not converge to zero. The noncertainty-equivalence adaptive control delivers

precise tracking in the presence of inertia matrix uncertainties and is a far better alternative to non-adaptive controllers with mild robustness to inertia uncertainty. Control torque limits are not incorporated into the adaptive control regime due to unpredictable effects on the adaptation mechanism. An adaptation mechanism that explicitly accounts for control saturation is recommended as a future research direction.

## Chapter 6

### Conclusions

Often, it is the case that spacecraft mass properties are not completely determined in the course of pre-flight testing. Among other things, this results in dynamic uncertainty with regard to attitude controller performance in operation. In this study, several control regimes are analyzed for nanosatellite attitude and angular rate tracking in the presence of arbitrarily large inertia matrix uncertainty. The tracking controllers are designed using the University of Texas student nanosatellite, Texas 2 Step, as the experimental platform. The Texas 2 Step mission is to demonstrate autonomous rendezvous and proximity operations. The spacecraft is assumed to be equipped with cold-gas thruster actuation system that enables full three-axis control; that is, unrestricted control of rotation, precession and nutation motions.

A tracking controller is formulated using partial feedback linearization and Lyapunov's indirect method. In addition, a nonlinear tracking control law based on Lyapunov's direct method is developed. Control limits are incorporated into the non-adaptive controller formulations using a hyperbolic tangent saturation function. Numerical simulations are provided to demonstrate the performance of the unsaturated and saturated control design with and without uncertainties in the inertia parameter. Both control algorithms are robust to small inertia perturbations but

the performance subsequently degrades with large inertia uncertainty.

An adaptive control approach known as non-certainty equivalence adaptive control is implemented to maintain consistent performance of the nanosatellite in the face of inertia uncertainty of arbitrary magnitude. The adaptive control delivers high accuracy closed loop system performance and is a far better alternative to non-adaptive controllers that are only mildly robust to inertia uncertainty. Control torque limits are not incorporated into the adaptive control regime due to unpredictable effects on the adaptation mechanism. An adaptation mechanism that explicitly accounts for control saturation is recommended as a future research direction.



## Bibliography

- [1] P. Davies, D. Liddle, J. Paffett, M. Sweeting, A. da Silva Curiel, and S. Eves, “A Modular Design for Rapid Response Telecons and Navigation Missions,” in *AIAA 2nd Responsive Space Conference*, 2004.
- [2] P. McGuirk, G. Rakow, C. Kimmery, P. Jaffe, R. Klar, and A. Bertrand, “Spacewire Plug-and-Play (PnP),” in *AIAA Infotech Aerospace Conference and Exhibit*, 2007.
- [3] A. L. Kelly, “Development of Phase Plane Attitude Control Algorithms for Nanosatellite Rendezvous Applications,” Master’s thesis, The University of Texas at Austin, May 2007.
- [4] S. K. Scarritt, “Nonlinear Model Reference Adaptive Control for Satellite Attitude Tracking,” in *AIAA Guidance, Navigation and Control Conference and Exhibit*, 2008.
- [5] H. Schaub and J. Junkins, *Analytical Mechanics of Space Systems*. AIAA Education Series, 2003, ch. 3.
- [6] B. Wie and P. M. Barba, “Quaternion Feedback for Spacecraft Large Angle Maneuvers,” *Journal of Guidance and Control*, vol. 8, no. 3, pp. 360–365, 1985.
- [7] J. T. Wen and K. Kreutz-Delgado, “The Attitude Control Problem,” *IEEE Trans. on Automatic Control*, vol. 36, no. 10, pp. 1148–1162, 1991.

- [8] B. T. Costic, D. M. Dawson, M. S. de Queiroz, and V. Kapila, “Quaternion-Based Adaptive Attitude Tracking Controller Without Velocity Measurements,” *Journal of Guidance, Control, and Dynamics*, vol. 24, no. 6, pp. 1214–1222, 2001.
- [9] J. Ahmed and D. S. Bernstein, “Globally Convergent Adaptive Control of Spacecraft Angular Velocity Without Inertia Modeling,” *American Control Conference*, vol. 3, no. 1, pp. 1540–1544, 1999.
- [10] A. Astolfi and R. Ortega, “Immersion and Invariance: A New Tool for Stabilization and Adaptive Control of Nonlinear Systems,” *IEEE Trans. on Automatic Control*, vol. 48, no. 2, pp. 590–606, 2003.
- [11] D. Seo and M. R. Akella, “High-Performance Spacecraft Adaptive Attitude-Tracking Control Through Attracting-Manifold Design,” *Journal of Guidance, Control, and Dynamics*, vol. 31, no. 4, pp. 884–891, 2008.
- [12] D. E. Seo, “Noncertainty Equivalent Nonlinear Adaptive Control and its Application to Mechanical and Aerospace Systems,” Ph.D. dissertation, The University of Texas at Austin, August 2007.
- [13] J. J. E. Slotine and W. Li, *Applied Nonlinear Control*. Prentice-Hall, 1991.
- [14] K. J. Aström and B. Wittenmark, *Adaptive Control*. Addison-Wesley Publishing Co., Inc., 1995, ch. 3.
- [15] P. A. Ioannou and J. Sun, *Robust Adaptive Control*. Prentice-Hall, 1995, ch. 4.

- [16] J. D. Bösković, S. Li, and R. K. Mehra, “Robust Adaptive Variable Structure Control of Spacecraft Under Control Input Saturation,” *Journal of Guidance, Control, and Dynamics*, vol. 24, no. 1, pp. 14–22, 2001.
- [17] R. J. Wallsgrove and M. R. Akella, “Globally Stabilizing Saturated Attitude Control in the Presence of Bounded Unknown Disturbances,” *Journal of Guidance, Control, and Dynamics*, vol. 28, no. 5, pp. 957–963, 2005.
- [18] R. D. Robinett, G. D. Parker, H. Schaub, and J. L. Junkins, “Lyapunov Optimal Saturated Control for Nonlinear Systems,” *Journal of Guidance, Control, and Dynamics*, vol. 20, no. 6, pp. 1083–1088, 1997.
- [19] S. P. Kárason and A. M. Annaswamy, “Adaptive Control in the Presence of Input Constraints,” *IEEE Transactions on Automatic Control*, vol. 39, no. 11, pp. 2325–2330, 1994.
- [20] M. Tandale, K. Subbarao, J. Valasek, and M. R. Akella, “Structured Adaptive Model Inversion Control with Actuator Saturation Constraints Applied to Tracking Spacecraft Maneuvers,” in *Proceedings of the 2004 American Control Conference*, 2004.
- [21] A. Leonessa, W. M. Haddad, T. Hayakawa, and Y. Morel, “Adaptive Control for Nonlinear Uncertain Systems with Actuator Amplitude and Rate Saturation Constraints,” *International Journal of Adaptive Control and Signal Processing*, vol. 23, no. 1, pp. 73–96, 2009.

- [22] B. Wie, *Space Vehicle Dynamics and Control*. AIAA Education Series, 1998, ch. 7.
- [23] M. D. Bertsekas, *Advanced Engineering Mathematics*. Prentice Hall, 1998, ch. 8.
- [24] M. D. Shuster, “A Survey of Attitude Representation,” *The Journal of Astronautical Sciences*, vol. 41, no. 4, pp. 439–517, 1993.
- [25] W. S. Stanley, “Quaternion from Rotation Matrix,” *Journal of Guidance and Control*, vol. 1, no. 3, pp. 223–224, 1978.
- [26] P. J. Antsaklis and A. N. Michel, *Linear Systems*. Birkhäuser, 2006, ch. 6.
- [27] H. K. Khalil, *Nonlinear Systems*. Prentice-Hall, 1996, ch. 3.
- [28] P. A. Ioannou and J. Sun, *Robust Adaptive Control*. Prentice Hall, 1996.
- [29] A. Ilchmann, D. H. Owens, and D. Prätzel-Wolters, “Sufficient Conditions for Stability of Linear Time-varying Systems,” *Systems and Controls Letters*, vol. 9, no. 2, pp. 157–163, 1987.
- [30] R. D. Robinett, G. G. Parker, H. Schaub, and J. L. Junkins, “Lyapunov Optimal Saturated Control for Nonlinear Systems,” *Journal of Guidance and Control*, vol. 20, no. 6, pp. 1083–1088, 1997.
- [31] B. D. Tapley, B. E. Schutz, and G. H. Born, *Statistical Orbit Determination*. Elsevier Academic Press, 2004, ch. 3.

- [32] B. Wie and J. Lu, "Feedback Control Logic for Spacecraft Eigenaxis Rotations Under Slew Rate and Control Constraints," *Journal of Guidance, Control, and Dynamics*, vol. 18, no. 6, pp. 1372–9, 1995.
- [33] A. Bedford and W. Fowler, *Engineering Mechanics Dynamics*. Prentice Hall, 2002, ch. 20.
- [34] G. F. Franklin, J. D. Powell, and A. Emami-Naeini, *Feedback Control of Dynamic Systems*. Prentice Hall, 2002, ch. 2.
- [35] D. P. Bertsekas, *Nonlinear Programming*. Athena Scientific, 2003, ch. 1.

## Vita

Divya Thakur was born on June 21, 1985 in Karnataka, India, the daughter of Anita Thakur and Vijainder Kumar Thakur. She began her pursuit of aerospace engineering studies at the University of Texas in fall 2002, completing the program and receiving her Bachelor of Science with Honors in spring 2006. She continued on to the Graduate School at the University of Texas to study aerospace control systems. After receiving her Master of Science in Engineering in May 2009, Divya Thakur intends to continue to earn her Ph.D. at the University of Texas.

Permanent address: 4525 Avenue H Apt A  
Austin, Texas 78751

This thesis was typeset with  $\text{\LaTeX}^\dagger$  by the author.

---

<sup>†</sup> $\text{\LaTeX}$  is a document preparation system developed by Leslie Lamport as a special version of Donald Knuth's  $\text{\TeX}$  Program.